5-1965

A Study of the Structure of Shear Turbulence in Free Surface Flows

Maddineni Venkateswara Rao
Utah State University

A STUDY OF THE STRUCTURE OF SHEAR TURBULENCE IN FREE SURFACE FLOWS

by

Maddineni Venkateswara Rao

DISSERTATION

FOR

DOCTOR OF PHILOSOPHY

in

Fluid Mechanics

College of Engineering

UTAH STATE UNIVERSITY
Logan, Utah
September 1965

A STUDY OF THE STRUCTURE OF SHEAR TURBULENCE IN FREE SURFACE FLOWS

by

Maddineni Venkateswara Rao

A dissertation submitted in partial fulfillment
of the requirements for the degree

of

DOCTOR OF PHILOSOPHY

in

Fluid Mechanics

Approved:

Major Professor

Head of Department

Dean of Graduate Studies

UTAH STATE UNIVERSITY
Logan, Utah
1965

ACKNOWLEDGMENTS

This investigation could not have been accomplished successfully without the cooperation and help of many faculty members and employees of the College of Engineering.

At the outset the author wishes to single out the help rendered by Dr. C. G. Clyde, under whose supervision the research has been carried out. The author likes to take this opportunity to express his deepest sense of gratitude to him for his constant encouragement and constructive criticism in the course of the work, for his generosity in sparing considerable time to discuss every phase of the work, for his guidance in designing the equipment and valuable consultation in debugging the experimental equipment, and finally for his active interest in providing an environment conducive to research by acquiring necessary equipment in a short time.

The author extends his sincere thanks to the committee members Dr. A. A. Bishop, Dr. G. H. Flammer, Dr. G. Z. Watters, and Dr. R. K. Watkins for their advice and painstaking review of this dissertation.

Special thanks are due Dr. G. H. Flammer for permitting the author to conduct tests in the flume belonging to his project and to Professor L. S. Cole for permission to make use of the facilities of the anechoic chamber and to borrow various instruments from the stores of his department.

Since re thanks are offered to Professor C. N. Merkley for his help in constructing the tranducer probe, to Mr. Pat Buller and Professor D. G. Chadwick for their help in debugging the experimental equipment, and to my friend and colleague Mr. M. A. Abaza for extending his helping hand many a time ungrudgingly.

Thanks are due to Professor Elliot Rich of the Civil Engineering Department and Dr. V. E. Hansen of the Utah Water Research Laboratory for making available necessary funds.

Finally the author acknowledges with gratitude the financial aid supplied by the U. S. A. I. D. (TCM) scholarship and the study leave granted by the Madhya Pradesh Government, India.

Maddineni Venkateswara Rao

TABLE OF CONTENTS

LIST OF TABLES

LIST OF FIGURES

CHAPTER I

INTRODUCTION

Turbulence is a familiar phenomenon which gives rise to complicated problems in many branches of engineering. Hinze (1959, p. 1-2) has set forth the following definition for turbulence: "Turbulent fluid motion is an irregular condition of flow in which the various quantities show a random variation in time and space coordinates, so that statistically distinct average values can be discerned." Osborne Reynolds (1894) was the first to introduce the notion of statistical mean values into the study of turbulence. He visualized turbulent flow as the sum of mean and eddying motion. By introducing this sum of mean velocity and fluctuating velocity into the Navier-Stokes equations and with the aid of the continuity equation, he derived equations giving relationships between the various components of the fluctuating velocity. It was soon realized that before any further results could be obtained from a theoretical analysis of Reynold's equations of motion, a mechanism had to be postulated for the interaction of fluctuating velocity components at different points in the turbulent field. Consequently, three decades after Reynold's work, phenomenological theories of turbulence, such as the momentum-transfer theory of Prandtl (1926), the vorticity transport theory of Taylor (1932) and the similarity theory of Karman (1930) were introduced. Not only are they based on unrealistic physical models, but they do not

furnish any information beyond temporal-mean velocity distribution. A complete theory of turbulence should describe the mechanism of production of turbulence, its convection, diffusion, distribution, and eventual dissipation for any given boundary conditions.

A step towards this objective was undertaken by G. I. Taylor (1921, 1935, 1938) when he proposed a theory based on the statistical treatment of the random fluctuations of the properties of the turbulent velocity field assuming a stationary, homogeneous, isotropic turbulence. He introduced various concepts such as turbulence intensity, Lagrangian correlation coefficient, Eulerian time and double-velocity space-correlation coefficients, different scales of turbulence, and one-dimensional energy-spectrum function. These parameters would constitute what has come to be called the structure of turbulence. He further showed that the knowledge of the turbulence intensity and the Lagrangian correlation function alone would be sufficient to determine the laws of diffusion, independent of any physical model for mixing. Renewed interest was created among research workers in this field by his pioneering efforts; and subsequently many theoretical investigations have been made by Karman and Howarth (1938), Robertson (1940), Batchelor (1948), Kampé de Fériat (1948), and others. Progress in hot-wire annemometry and electronic instrumentation has made it possible to check the validity of the theory in flows of air in wind tunnels just downstream from screens which generate a homogeneous and near-isotropic turbulence. The most notable studies made in this connection are thoseof Dryden (1938) and Simmons and Salter (1938).

Although the concept of isotropy is essential for mathematical simplicity, it is not encountered in actuality. Nevertheless, the Fourier analysis of the equations of motion leads to some important clues pertaining to the mechanism of the production and dissipation of turbulent energy. From a Fourier transformation of the Reynolds equations there arise three distinct terms: (1) a term describing the production of turbulence and its convection and diffusion by the mean motion, (2) a term describing the interaction of eddies characterized by different wave numbers and the transfer of turbulent energy from one eddy to another of different wave number, and (3) a term describing the dissipation of turbulent energy by viscosity. From the form of these terms it can be inferred that the production term is important in the low wave-number region, the viscous dissipation term is important in the high wave-number region and the second term accounts for the transfer of energy between wave numbers throughout the spectrum.

Next the question arises regarding whether or not the transfer of turbulent energy and its dissipation by viscosity at high wave numbers is independent of the manner in which the turbulence is generated. An answer to this is found in Kolmogoroff's (1941) theory of local isotropy which states that the fine scale structure (high wave-number components) of actual turbulent shear flows at high Reynolds numbers is isotropic. The idea of local isotropy was put forward independently by Onsager (1945), and Obukoff (1941). Kolmogoroff derived spectral laws for the distribution of turbulent energy with wave number in the region of local isotropy or

equilibrium range. Various spectral laws for the equilibrium range have been put forward by Heisenberg (1948), Obukoff (1941), Karman (1948), Chandrasekhar (1949), Kovasznay (1948), and Tachen (1953) to bring the theory into closer agreement with experimental results.

As in the case of isotropic turbulence, dynamical equations either for the correlation function or for the spectrum function could not yet be developed for turbulent shear flows due to formidable mathematical difficulties. As a matter of fact, very little has been accomplished in the analytical study of the statistical theory of self-maintained shear turbulence such as occurs in fully-developed turbulent flow in pipes and open channels. To overcome these mathematical difficulties, perhaps new physical hypotheses might be required. Meanwhile, however, considerable insight into the mechanics of turbulent shear flows could be obtained by extensive experimental studies of the distribution of the intensity of turbulence, macro- and microscales of turbulence, double-velocity correlations and energy spectrums, since these parameters constitute the structure of turbulent shear flows as well. Furthermore, such studies might lead to the formulation of new physical hypotheses concerning the actual mechanism of turbulence in shear flows. The fact that experimental methods and theoretical analysis are always complementary to each other in the search for understanding in the physical sciences lends credence to this approach.

Recently many experimental investigations have been made in turbulent shear flows. In the case of turbulent flow in a pipe, Romano

(1954) measured the energy-spectrum function, Brookshire (1961) measured intensity and microscale, and Jordan (1963) studied the distribution of microscale and macroscale. The investigations of Laufer (1951, 1954) on the structure of turbulent shear flows in pipes and two-dimensional channels are the first and the most exhaustive. All of the above studies were made in air flows using hot-wire anemometers as sensors. But no such systematic investigations have been made in the past into the structure of turbulent shear flows either in smooth or rough open channels, presumably because of a lack of a reliable liquid-turbulence measuring probe with the necessary sensitivity, response, and strength. Some partial attempts have been made by Ippen (1957) and Clyde (1961), who used diaphragm types of pressure tranducers whose maximum frequency responses were low.

In order to overcome this deficiency of experimental data on the structure of turbulent shear flows in open channels, this project has been undertaken. For this investigation, a total-head tube with a barium titanate ceramic tranducer, as the sensor, was constructed, similar to the one developed by Eagleson et al. (1959). The device has a sufficiently high, as well as low, frequency response. Such a total-head probe was believed to have clear advantage over other types for measurements in unclear water even though it has the serious disadvantage of measuring only one of the three components of the fluctuating velocity vector.

The objectives of this research are:

1. To study the turbulence-energy distribution as a function of relative position and Reynolds number.
2. To determine the existence of local isotropy in the wave-number space and the applicability of the spectral laws of locally-isotropic turbulence.
3. To determine whether or not the pattern of the distribution of relative intensity of turbulence versus relative depth in the case of a rough boundary differs from the published results for smooth-boundary flows.
4. To determine autocorrelation functions and obtain therefrom the distribution of the mean macroscale of turbulence as a function of relative depth and Reynolds number.
5. To determine the distribution of microscale as a function of relative position and Reynolds number.
6. To make an attempt to obtain some relationships between the statistical quantities describing nonisotropic flows.

Literature pertinent to the structure of turbulence is examined critically as a basis for this experimental investigation. Also theoretical studies concerning the shape of turbulence energy spectrum are reviewed and compared with the shape determined by experiment.

A concluding discussion will point out the contributions of this research as well as the limitations imposed by the instrumentation used. In

the light of the experience gained during this research, some suggestions for further investigations are offered in the closing chapter.

CHAPTER II

EQUATIONS OF MOTION AND ENERGY FOR TURBULENT FLOW IN TWO-DIMENSIONAL OPEN CHANNELS

Osborne Reynolds (1894) was the first to make systematic experimental and theoretical investigations of turbulent flow. He assumed that the Navier-Stokes equations describe the turbulent motion at every instant. He also suggested that the instantaneous velocity and pressure could each be expressed as the sum of their time average and fluctuation, i. e. ;

$$U_i = \overline{U}_i + u_i \qquad i = 1, 2, 3 \tag{1}$$

where

$$\overline{U}_i = \frac{1}{2T} \int_{-T}^{T} U_i(t)\, dt$$

$$\overline{u}_i = \frac{1}{2T} \int_{-T}^{T} u_i(t) dt = 0$$

Similarly

$$P = \overline{P} + p \tag{2}$$

Reynolds substituted equations (1) and (2) into the Navier-Stokes equations for steady incompressible fluid flow and took time averages in the resulting equations term by term and obtained the following equations for the mean flow:

$$\rho \bar{U}_j \frac{\partial \bar{U}_i}{\partial x_j} = - \frac{\partial}{\partial x_i} (\bar{P} + \gamma \bar{h}) + \mu \frac{\partial^2 \bar{U}_i}{\partial x_j \partial x_j} - \rho \frac{\partial \overline{u_i u_j}}{\partial x_j} \qquad (3)$$

These equations differ from the Navier-Stokes equations only in the presence of additional terms involving velocity fluctuations. The term $\rho \overline{u_i u_j}$ is usually referred to as the Reynolds-stress tensor. The Reynolds equations (3) could not be solved, as there are ten unknowns with only four equations including the continuity equation. The Reynolds stresses must be known before there is any hope of solving the equations of motion for turbulent flow.

In steady unidirectional flow in an open channel,

$$\bar{U}_1 = \bar{U}_1(x_2)$$

$$\bar{U}_2 = 0$$

$$\bar{U}_3 = 0$$

In fully-developed uniform turbulent flow the means of the squares of fluctuating velocities and means of the products of fluctuating velocities are functions of x_2 alone.

Therefore, equation (3) becomes

$$\frac{\partial}{\partial x_1} (\bar{P} + \gamma \bar{h}) = \mu \frac{\partial^2 \bar{U}_1}{\partial x_2^2} - \frac{\partial \overline{u_1 u_2}}{\partial x_2} \qquad (4)$$

$$\frac{\partial}{\partial x_2}(\bar{P} + \gamma\bar{h}) = - \rho \frac{\partial \overline{u_2^2}}{\partial x_2} \tag{5}$$

Equation (5) reduces to

$$\bar{P} + \gamma\bar{h} + \rho \overline{u_2^2} = F(x_1) \tag{6}$$

Let $- \frac{\partial}{\partial x_1}(\bar{P} + \gamma\bar{h}) = e$

Equation (4) becomes

$$- e x_2 = \mu \frac{d\bar{U}_1}{dx_2} - \rho \overline{u_1 u_2} + \text{Const}$$

At $x_2 = 0$, $u_1 = u_2 = 0$ and $\tau = \tau_o$

$$\therefore (\tau_o - e x_2) = \mu \frac{d\bar{U}_1}{dx_2} - \rho \overline{u_1 u_2} \tag{7}$$

This is the equation of motion for turbulent flow in an open channel.

Multiplication of the equation (7) by the mean-velocity gradient $\frac{d\bar{U}_1}{dx_2}$ leads to

$$(\tau_o - e x_2) \frac{d\bar{U}_1}{dx_2} = \mu\left(\frac{d\bar{U}_1}{dx_2}\right)^2 - \rho \overline{u_1 u_2} \left(\frac{d\bar{U}_1}{dx_2}\right) \tag{7a}$$

This is the mean-energy balance equation. The term at the left represents the rate per unit volume at which mechanical energy is lost by the mean

flow; the first term at the right is the rate of energy dissipation by the direct action of viscosity, and the second is the rate of turbulence production. Klebanoff (1954) compared the production of turbulent energy and viscous dissipation for the region near the wall $(0 < y^* < 30)$ in his turbulent boundary layer studies and concluded that approximately 40 per cent of the energy extracted from the mean flow is directly dissipated by viscosity and, of the remaining 60 per cent which is converted into turbulent energy, 30 per cent is produced in the same region. From this it is evident that, in order to obtain a complete picture of turbulent-energy balance, conditions near and within the laminar sublayer have to be known. This is a very difficult task from the experimental point of view.

Further insight into the mechanism of turbulent action results from a study of energy equations which describe the energy balance for the turbulence at a given section. These equations can be derived by utilization of the Reynolds technique of substituting mean and fluctuating components for the instantaneous values of velocity and pressure and by following his rules for taking averages. For more details reference may be made to books by Hinze (1959), Rouse (1959), and Townsend (1956).

Multiplying the Navier-Stokes equations by U_i, the following equation is obtained:

$$\rho\, U_i U_j \frac{\partial U_i}{\partial x_j} = - U_i \frac{\partial}{\partial x_i} (P + \gamma \bar{h}) + \mu U_i \frac{\partial^2 U_i}{\partial x_j \partial x_j} \qquad (8)$$

Upon rearrangement,

$$\frac{1}{2}\rho\frac{\partial(U_iU_iU_j)}{\partial x_j} = -U_i\frac{\partial(\gamma\bar{h})}{\partial x_i} - \frac{\partial(PU_i)}{\partial x_i} +$$

$$\frac{1}{2}\mu\frac{\partial^2(U_iU_i)}{\partial x_j\,\partial x_j} - \mu\frac{\partial U_i}{\partial x_j}\frac{\partial U_i}{\partial x_j} \qquad (9)$$

Introduction of the velocity and pressure perturbations

$$U_1 = \bar{U}_1 + u_1$$

$$U_2 = u_2$$

$$U_3 = u_3$$

$$P = \bar{P} + p$$

into equations (9) and utilization of the fact that the mean and fluctuating velocities are functions of x_2 only, the following turbulence energy equation is obtained:

$$\rho\overline{u_1u_2}\frac{d\bar{U}_1}{dx_2} + \rho\bar{U}_1\frac{d\overline{u_1u_2}}{dx_2} + \frac{1}{2}\rho\frac{d}{dx_2}\overline{u_2(u_1^2+u_2^2+u_3^2)}$$

$$= \gamma S_o\bar{U}_1 - \frac{d}{dx_2}(\overline{pu_2}) + \mu\bar{U}_1\frac{d^2\bar{U}_1}{dx_2^2} +$$

$$\frac{1}{2}\mu\frac{d^2}{dx^2}\overline{(u_1^2+u_2^2+u_3^2)} - \overline{\mu\left(\frac{\partial u_i}{\partial x_j}\right)\left(\frac{\partial u_i}{\partial x_j}\right)} \qquad (10)$$

In light of equation (4), equation (10) can be simplified to

$$\tau \frac{d\bar{U}_1}{dx_2} = \frac{d}{dx_2}\left[\rho u_2 \left(\frac{u_1^2 + u_2^2 + u_3^2}{2}\right) + u_2 p\right] + \mu\left(\frac{d\bar{U}_1}{dx_2}\right)^2 - \frac{1}{2}\mu \frac{d^2}{dx_2^2}\left(u_1^2 + u_2^2 + u_3^2\right) + \mu\left(\frac{\partial u_i}{\partial x_j}\right)\left(\frac{\partial u_i}{\partial x_j}\right) \qquad (11)$$

Von Karman (1937) obtained this form for the case of turbulent flow between parallel plates in connection with the discussion of non-isotropic flow in terms of the statistical theory of turbulence. The terms from left to right have the following physical meaning: The first term corresponds to the rate of production of turbulent energy per unit volume by the action of the shearing stresses at a point. The second term represents the rate of convective diffusion by turbulence of the total turbulence energy. The third term stands for the rate of dissipation of energy by the action of the viscous shear stresses. The fourth term is the rate of energy diffusion by viscous forces. The fifth term expresses the rate of turbulent-energy dissipation into heat by the action of viscosity. The diffusion terms vanish upon integration of equation (11) over the space. This means that the diffusion process acts only to transfer energy from one place to another and the energy is neither created nor destroyed, nor is there any net exchange in energy with another direction of diffusion.

In the absence of a statistical theory of shear turbulence, extensive experimental studies were made by Laufer (1951, 1954), Klebanoff and Diehl (1951), Klebanoff (1954), and Schubauer (1954) to sketch out adequately the spatial budget of energy in nonhomogeneous shear flows which occur in turbulent boundary layers in pipes and channel flows. The basis used was that formed by the equations of the type (7a) and (11), incorporating the ideas of the Reynolds number, similarity, and self-preservation. For a high Reynolds number flow it was shown by Laufer (1951) that the second and third terms on the right side of equation (11) may be neglected. Hence, the equation (11) reduces to

$$\tau \frac{d\bar{U}_1}{dx_2} = \frac{d}{dx_2}\left[\overline{\rho u_2 \left(u_1^2 + u_2^2 + u_3^2\right) + u_2 p}\right] + \mu \overline{\left(\frac{\partial u_i}{\partial x_j}\right)\left(\frac{\partial u_i}{\partial x_j}\right)} \qquad (12)$$

The term on the left side of the equation can be obtained directly from the measurements of τ and from the mean-velocity profile. The determination of the dissipative derivatives is the most difficult task because of the importance of the region near the wall. Since only five terms (first four and seventh) in the dissipation function can be measured in the vicinity of the wall, the remaining four were estimated by Laufer (1954) and Klebanoff (1954) using isotropic relationships. From the known distributions of turbulence-energy production and dissipation, the distribution of diffusion of energy can easily be calculated from equation (12). Because of the limitations of the piezoelectric probe, no attempt could be made to

measure the distributions of the various terms in equation (12) in this investigation.

For later use, the salient points in the conclusions of the studies of Laufer and Klebanoff are summarized briefly: The flow section can be divided into three regions; the wall or inner region, intermediate region, and the outer region, or fully turbulent region. In the inner region various energy rates, production, diffusion, and dissipation are of equal importance and show a sharp maximum, within $y^* < 30$. Klebanoff speculated that in a small region near the wall ($y^* < 20$) the rate of dissipation is greater than the rate of production and the deficiency is compensated by an inward flow of energy toward the wall from the outer region, because of the action of the pressure forces. In the outer region the production is negligible, and the gain of energy resulting from the flux of kinetic energy by turbulent diffusion from the wall region compensates for the loss by dissipation. In the intermediate region (the major part of the section), turbulence-energy balance is furnished by production and dissipation only. If these conclusions were correct, 85 per cent of the total dissipation (viscous and turbulent) takes place in $y^* < 30$, signifying the importance of the region near the wall. This qualitative picture of turbulence-energy balance could be vindicated only with detailed measurements in the wall region by improved instrumentation, even though the above conclusions are quite plausible. Some of the terms in the equation (12) will be used later to analyze the statistical characteristics of nonisotropic turbulent flow.

CHAPTER III

STATISTICAL THEORY OF TURBULENCE

The phenomenological theories of turbulence proved to be fruitful to describe momentum, mass, and heat transfer processes, not so much because they describe correctly the mechanism underlying turbulent transport processes, but because they have resulted in useful and practical semi-empirical relationships. Neither Prandtl nor Taylor discusses in detail the mechanism by which the lumps of fluid adapt their transferable property to their new environments. Due to pressure fluctuations, the momentum of each lump of fluid does not remain constant during its travel over a distance equal to the mixing length as Prandtl assumed in his theory. The constancy of vorticity during the travel of the lump over a distance as assumed by Taylor is true only in the two-dimensional case, and the extension of the theory to three-dimensions is too involved to be of much practical use. Even though von Karman was successful in suggesting a similarity theory of turbulence independent of any physical model, his theory is restricted to the low-frequency components of turbulence only because he assumed that the turbulence mechanism is independent of viscosity except in the laminar sublayer.

The statistical theory of turbulence introduced by Taylor (1921, 1935) describes in a statistical way the character and properties of

turbulence such as the intensity of turbulence, the scale of turbulence, and the eddy-diffusion coefficient by means of correlation coefficients and the energy spectrum of turbulence without speculating as to the mechanism of turbulence itself. Before treating these parameters in greater detail, some discussion about how the behavior of a turbulent flow field could be represented mathematically and what kind of simplifying assumptions may be made is desirable.

There are two distinct ways of representing a turbulent flow field, namely Eulerian and Lagrangian. In the Eulerian representation, the variation of statistical parameters at one or two fixed points in the turbulent flow field is considered. In the Lagrangian description, attention is focused on a single fluid particle and the variation of statistical parameters with time as the fluid particle travels through the flow field is considered.

Although the Lagrangian description has certain advantages over the Eulerian description in the development of theory of turbulent diffusion in particular, it has a serious disadvantage in that the experimental determination of Lagrangian statistical quantities can only be obtained through a tedious process of data reduction, whereas Eulerian quantities can be determined directly by the modern electronic instruments.

The statistical theory of real turbulent flows (shear flows) is very complicated and mathematically intractable. Therefore, in the development of the theory, Taylor and subsequent investigators considered for

mathematical simplicity an idealized homogeneous and isotropic turbulent flow in the absence of mean motion. Homogeneous turbulence is characterized by the invariance of the statistical characteristics for any translation of the coordinate system in the space occupied by the fluid. If, in addition to homogeneity, the mean value of any function of the turbulent velocity components and their space derivatives is invariant with respect to rotation and reflection of the coordinate system, the turbulent field is isotropic. Thus, from isotropy it follows that

$$\overline{u_1^2} = \overline{u_2^2} = \overline{u_3^2} = \text{Const}$$

$$\overline{u_1 u_2} = \overline{u_2 u_3} = \overline{u_3 u_1} = 0 \tag{13}$$

Isotropic turbulence is an idealized flow situation that can be realized even approximately only under controlled laboratory conditions. Homogeneity permits the sampling point to be chosen arbitrarily. Most of the real flows are nonisotropic; consequently, it is extremely difficult to realize homogeneity even in one direction, except in axisymmetric flow. For the more general case of nonisotropic turbulence,

$$\overline{u_1^2} \neq \overline{u_2^2} \neq \overline{u_3^2}$$

$$\overline{u_1 u_2} \neq \overline{u_2 u_3} \neq \overline{u_3 u_1} \neq 0 \tag{14}$$

Even though the statistical theory of nonisotropic or turbulent shear

flows has not been developed yet, the various statistical parameters and concepts applicable to isotropic turbulence are equally applicable to turbulent shear flows as well.

In turbulence theory, the fluid motion is assumed to consist of the superposition upon a mean flow of eddies covering a range of sizes with distinguishable upper and lower limits. The upper size limit of the eddies is usually determined by and is of the order of magnitude of the dimension of the containing apparatus. The lower limit is determined by viscosity effects and decreases with increase in average velocity, other conditions remaining the same. As the eddy becomes smaller, the velocity gradient in the eddy becomes larger, and thus the viscous shear becomes larger. This increase in viscous shear counteracts the eddying motion, thus further limiting the size of the smaller eddies. Even in the limit for moderate flow velocities, for example, air flows at speeds below about 200 ft/sec and water flows up to still higher speeds if there is no cavitation (Corrison, 1961), the size of the smallest eddies is much greater than the mean free path of molecules so that fluid flow could still be treated as a continuum flow.

Statistical Specification of Turbulent Fields

The velocity vector $u(x, t)$ in a turbulent flow field is a random function of position and time whose values conform to probability distributions which are determined for any particular problem by the boundary

conditions and initial conditions. The values of 'u' at various positions and instants of time are connected by means of joint-probability distribution functions as a consequence of the equations of motion and continuity. As pointed out by Townsend (1956) and Batchelor (1953), for the detailed statistical description of a turbulent field, a knowledge of the complete system of joint-probability distributions of the values of the velocity 'u' at 'n' points of the space at the appropriate value of 't' is required, since it is supposed that the statistical properties of the turbulence field at different values of 't' are uniquely related by the equations of momentum and continuity. From the viewpoint of the experimenter, the above statement is an admission that it will never be possible to describe completely the statistical properties of even the simplest turbulent flow. Nevertheless, some progress has been made in the development of the theory of turbulence using correlation and spectrum functions even though these functions give an incomplete description of turbulent motion. As Townsend points out,

> The central role that the correlation and spectrum functions play in current theory and experiment is due to their comparative simplicity and convenience of measurement. The correlation function is one of the infinite set of integral moments of the basic joint-probability distribution function, and attempts to use the correlation function as a complete description amount, mathematically, to making a hypothesis concerning the nature of the complete probability distribution function and, physically, to making statements about the eddy structures that exist in fully developed turbulence. (Townsend, 1956, p. 12)

Intensity of Turbulence

Since the fluctuating component of velocity is a property of vital interest in the statistical treatment of turbulence, an average value of this fluctuating velocity which is non-zero must be defined. An average value of 'u' that has received wide use is the root-mean-square. The reason for this popularity is that the root-mean-square (a measure of the spread of the probability-density curve of the random variable) of 'u' is easy to measure with existing experimental equipment and the mean square of 'u' occurs quite naturally in many of the equations governing the turbulent flow. The root-mean-square of the fluctuating velocity is also known as the intensity of turbulence and may be defined mathematically,

$$u_i' = \left(u_i^2\right)^{1/2} = \left[\int_{-\infty}^{\infty} u_i^2 f(u_i)\, du_i\right]^{1/2} \quad i = 1, 2, 3 \tag{15}$$

This definition of turbulence intensity was first introduced by Dryden and Kuethe (1930).

It should be noted that the average defined above is a statistical or ensemble average. From the viewpoint of the statistical theory of turbulence, it is the ensemble average that should be used; but it is usually not possible to measure the ensemble average experimentally. For example, if the ensemble average value of the fluctuating velocity in a channel at a given time is to be measured, it would require that the

averaging process be made in an infinite number of identical channels in which the physical conditions are the same with the component of fluctuating velocity being measured at the same time in all channels. This is, of course, experimentally impossible. The impossibility of measuring ensemble averages has led to the extensive use of time average that could easily be measured by conventional measuring instruments. Therefore, it is necessary to prove that a time average is identical with a statistical average for the experimental field (ergodic theorem). Unfortunately, no ergodic theorem has yet been proved in fluid dynamics, as pointed out by Pai (1957). Since the experimental field of turbulence is such that the velocity at a fixed point is a stationary random function of time, applicability of ergodicity could be assumed reasonably; and thereby time average and statistical average are considered identical here as is customary in the turbulence literature. So time average of square root of variance may be written as:

$$u_i' = \left(\overline{u_i^2}\right)^{1/2} = \left[\frac{1}{\Delta t}\int_0^{\Delta t} u_i^2\, dt\right]^{1/2} \qquad (16)$$

The relative intensity of turbulence is defined as

$$\frac{\sqrt{\overline{u_i^2}}}{\overline{U}_i} \quad \text{i. e.} \quad \frac{u_i'}{\overline{U}_i} \qquad i = 1, 2, 3 \qquad (17)$$

It should be noted that the turbulence intensity characterizes only the magnitude, but not the frequency, of the turbulence fluctuations.

Double-Velocity Correlation Function

The statistical theory of turbulence is not concerned with the joint-probability distribution functions themselves, but rather with the correlations between various velocity components. A large part of the theory is concerned with the properties of the covariance of the velocities at the two points or the double-velocity correlation. Von Karman and Howarth (1938) introduced the correlation-tensor function as a generalization of the particular correlation coefficients discussed by Taylor (1935).

The velocity-correlation tensor for two points separated by space vector $\vec{r}$ is

$$R_{ij}(\vec{r}) = \overline{u_i(\vec{x})\, u_j(\vec{x} + \vec{r})} \tag{18}$$

It should be noted that since physical quantities under a mean-value sign are taken at the same instant, explicit reference to time is omitted. Von Karman first pointed out that $R_{ij}(\vec{r})$ forms a tensor of the second order. Under the assumption of isotropic turbulence in the absence of mean flow, von Karman and Howarth considered the special case where the line connecting the two points is parallel to one of the cartesian coordinate axes and showed that all the components but two of the

correlation tensor vanish. The two nonvanishing components are the longitudinal- and lateral-velocity correlations which depend only on the distance 'r' between the two points. The longitudinal-velocity correlation function and lateral-velocity correlation function first introduced by von Karman and Howarth (1938) are given by

$$\overline{u^2}\, f(r) = R_{11}(\vec{r}) \tag{19}$$

$$\vec{r} = (r, 0, 0)$$

$$\overline{u^2}\, g(r) = R_{22}(\vec{r}) \tag{20}$$

These investigators also showed that $f(r)$ and $g(r)$ are not independent, but are related by the equation

$$g(r) = f(r) + \frac{r}{2}\frac{df(r)}{dr} \tag{21}$$

which follows from the continuity condition. The correlation tensor $R_{ij}(\vec{r})$ can thus be expressed in terms of a single scalar function, either $f(r)$ or $g(r)$. The simpler two-point triple-velocity correlation is given by

$$T_{ij,k}(\vec{r}) = \overline{u_i(\vec{x})\, u_j(\vec{x})\, u_k(\vec{x} + \vec{r})} \tag{22}$$

Von Karman and Howarth (1938) showed that this forms a tensor of the third order, and under conditions of isotropy all but three of the components of the triple-correlation tensor vanish. The nonvanishing components

$h(r)$, $k(r)$, and $q(r)$ are given by

$$\left(\overline{u^2}\right)^{3/2} h(r) = T_{22,1}(\vec{r}) \tag{23}$$

$$\left(\overline{u^2}\right)^{3/2} k(r) = T_{11,1}(\vec{r}) \qquad \vec{r} = (r, 0, 0) \tag{24}$$

$$\left(\overline{u^2}\right)^{3/2} q(r) = T_{21,1}(\vec{r}) \tag{25}$$

For incompressible flow, from the continuity condition it follows that $h(r)$, $k(r)$, and $q(r)$ are related by the relations

$$k(r) = -2h(r) \tag{26}$$

$$q(r) = -h(r) - \frac{r}{2}\frac{\partial h(r)}{\partial r} \tag{27}$$

Thus it follows from the above relations that $T_{ij,k}(\vec{r})$ can be expressed in terms of a single scalar function. Using the above relations and the Navier-Stokes equations of motion, von Karman and Howarth (1938) obtained the following dynamical equation for the propagation of the correlation function $\overline{u^2} f(r)$:

$$\frac{\partial}{\partial t}\left(\overline{u^2} f\right) + 2\left(\overline{u^2}\right)^{3/2}\left[\frac{\partial h}{\partial r} + \frac{4h}{r}\right] = 2\nu\overline{u^2}\left[\frac{\partial^2 f}{\partial r^2} + \frac{4}{r}\frac{\partial f}{\partial r}\right] \tag{28}$$

This equation is the fundamental equation for studying the dynamical behavior of a homogeneous and isotropic turbulence. The only case for

which the equation (28) can be said to have been completely solved is for turbulence in the final period of decay where the inertial term $h(r)$ (the triple correlation) can be neglected. A satisfactory solution applicable to the major portion of the time history of turbulence has not been obtained.

The chief difficulty lies in obtaining a determinate set of dynamical equations. From the momentum and continuity equations and from equations involving moments (correlation functions) of the fluctuating velocity, components of any order can be constructed. Each n-order equation so obtained involves the moments of order $n + 1$ as a direct consequence of the nonlinearity of the Navier-Stokes equations. The various methods of approximation proposed to make the infinite set of dynamical equations finite can be divided into two broad classes. In the first class, models of dynamical processes are postulated on physical grounds. The examples are the theories of Kolmogoroff (1941) and Heisenberg (1948), etc., which are treated later. The second class consists of schemes for systematic analytical approximations.

So far, two different approaches have been taken in the second class. One of them consists of ignoring moments of 'n + 1' order in equations for 'n' order moments. This method was used by Deissler (1958, 1960) for the study of the decay of homogeneous turbulence at earlier times or at higher Reynolds numbers. It is not known whether this approximation yields satisfactory results for interesting cases of the very large Reynolds number.

Another approach is to introduce the hypothesis that the fourth-order moments of the distribution of simultaneous velocity components are related to second-order moments as they would be for a normal probability distribution. Fourth-order moments can then be expressed in terms of second-order moments, and the set of moment equations is closed. Proudman and Reid (1954) and Tatsumi (1957) have extensively discussed the decay process of isotropic three-dimensional turbulence on the basis of this hypothesis. The dynamical equations for two-dimensional isotropic turbulence that follow from this hypothesis were derived by Ogura (1962a). Ogura (1962a, b) solved numerically the dynamical equations for two- and three-dimensional turbulence for the whole time history of turbulence. The most distinct feature revealed by his calculation is that the energy spectrum becomes negative for medium-sized eddies. He tentatively concluded that the generation of unphysical negative energy is most likely the consequence of the quasi-normality hypothesis.

Loitsianskii (1945) took from each term of equation (28) the fourth moment and showed that

$$\overline{u^2} \int r^4 f(r)\, dr = L \tag{29}$$

is an invariant under the assumptions that

$$\lim_{r \to \infty} \left(r^4 \frac{\partial f}{\partial r} \right) = 0$$

and

$$\lim_{r \to \infty} \left(r^4 k(r) \right) = 0$$

The integral (29) is usually referred to as Loitsianskii's invariant. The interpretation given by Loitsianskii is that the integral gives the total amount of disturbance introduced by the turbulence generating system.

Besides the correlation coefficients $f(r)$ and $g(r)$, the auto-correlation coefficient $R_{E_1}(\tau)$ between the values of u_1 at the same point but different times t and $t + \tau$ is important and is given by

$$R_{E_1}(\tau) = \frac{\overline{u_1(t)\, u_1(t+\tau)}}{\overline{u_1^2}} \tag{30}$$

The correlation coefficient is a measure of the relatedness of the variable u_1 at the two times t and $t + \tau$. As τ tends to be zero, $R_{E_1}(\tau)$ tends to be equal to one. As τ becomes larger, R_{E_1} approaches zero. This means that $u_1(t)$ and $u_1(t + \tau)$ are no longer correlated but they may not be independent. From a plot of $R_{E_1}(\tau)$ vs τ, two inferences could be drawn. First the rapidity with which the relatedness is lost with time delay is shown and, second, detection of a periodic signal hidden in the random velocity fluctuation is indicated by peaks in the plot at intervals of 'τ' equal to the period of the periodic signal.

Scales of Turbulence

The concept of a scale representative of a particular turbulence under consideration was used by Prandtl (1926) and Taylor (1915) in the mixing-length theories. However, their definition of the scale was based on the assumption that the fluid elements act like the molecules in a gas. Hence the scales so defined are fictitious and lack in physical reality. This fact led Taylor (1935) to introduce a number of scales which characterize various statistical aspects of turbulence. The macroscale and microscale gained widest acceptance. Taylor set forth the following definition for the scale of turbulence in the Eulerian system:

> It is clear that whatever we may mean by the diameter of an eddy a high degree of correlation must exist between the velocities at two points which are close together when compared with this diameter. On the other hand, the correlation is likely to be small between the velocity at two points situated many eddy diameters apart. If, therefore, we imagine that the correlation R_{x_2} between the values of u_1 at two points distant x_2 apart in the direction of the x_2 coordinate axis has been determined for various values of x_2 we may plot a curve of R_{x_2} against x_2 and this curve will represent, from the statistical point of view, the distribution of u_1 along the x_2 axis. (Taylor, 1935, p. 426.)

With these words he defined

$$L_{x_2} = \int_0^\infty R_{x_2} \, dx_2 \tag{31}$$

The length L_{x_2} is considered as a possible definition of the average size of the eddies and is termed the integral scale or macroscale of

turbulence. Correspondingly, a length L_{x_1} may be defined by the relation:

$$L_{x_1} = \int_0^\infty R_{x_1} \, dx_1 \tag{32}$$

where R_{x_1} is the correlation coefficient between the values of the component u_1 at two points separated by distance x_1 in the direction of x_1—coordinate axis. Another macroscale using the autocorrelation coefficient may be defined as

$$L_{x_1} = \bar{U}_1 \int_0^\infty R_{E_1}(\tau) \, d\tau \tag{33}$$

Taylor (1935) showed that R_{x_2} can be expanded in a series such that

$$R_{x_2} = 1 - \frac{1}{2!} \frac{x_2^2}{\overline{u_1^2}} \overline{\left(\frac{\partial u_1}{\partial x_2}\right)} + \frac{1}{4!} \frac{x_2^4}{\overline{u_1^2}} \overline{\left(\frac{\partial^2 u_1}{\partial x_2^2}\right)^2} - \cdots \tag{34}$$

If the above series is truncated at the second term then

$$R_{x_2} = 1 - \frac{1}{2!} \frac{x_2^2}{\overline{u_1^2}} \overline{\left(\frac{\partial u_1}{\partial x_2}\right)^2} \tag{35}$$

Hence, the curvature of the R_{x_2} versus x_2 curve at $x_2 = 0$ is a measure of

$$\overline{\left(\frac{\partial u_1}{\partial x_2}\right)^2}.$$

This relationship can be expressed as

$$\left(\overline{\frac{\partial u_1}{\partial x_2}}\right)^2 = 2\,\overline{u_1^2} \quad \underset{x_2 \to 0}{\text{Lim}} \left(\frac{1 - R_{x_2}}{x_2^2}\right) \tag{36}$$

Taylor intorduced the Eulerian microscale of turbulence, λ defined as

$$\frac{1}{\lambda^2} = \underset{x_2 \to 0}{\text{Lim}} \left(\frac{1 - R_{x_2}}{x_2^2}\right) \tag{37}$$

Thus, λ^2 is a measure of the radius of curvature of the R_{x_2} curve at $x_2 = 0$.

The general expression for the mean rate of turbulent-energy dissipation per unit mass (Goldstein, 1938, p. 222) is:

$$\epsilon = \nu \left[2\overline{\left(\frac{\partial u_1}{\partial x_1}\right)^2} + 2\overline{\left(\frac{\partial u_2}{\partial x_2}\right)^2} + 2\overline{\left(\frac{\partial u_3}{\partial x_3}\right)^2} + \overline{\left(\frac{\partial u_2}{\partial x_1} + \frac{\partial u_1}{\partial x_2}\right)^2} + \overline{\left(\frac{\partial u_3}{\partial x_2} + \frac{\partial u_2}{\partial x_3}\right)^2} + \overline{\left(\frac{\partial u_1}{\partial x_3} + \frac{\partial u_3}{\partial x_1}\right)^2} \right] \tag{38}$$

which reduces to

$$\epsilon = 7.5\ \nu \overline{\left(\frac{\partial u_1}{\partial x_2}\right)^2} \tag{39}$$

in case of incompressible isotropic turbulence, as first proved by Taylor (1935). Combination of equations (36), (37), and (39) gives

$$\epsilon = 15 \frac{\nu \overline{u_1^2}}{\lambda^2} \tag{40}$$

The 'λ' value may now be regarded as a measure of the diameters of the smallest eddies which are responsible for the dissipation of energy. For this reason, λ is sometimes called dissipation scale or length.

The theory proposed by Taylor does not predict the distribution of the scale of turbulence or the distribution of the intensity of turbulence for any type of flow. In fact there are no theories that will predict the distribution of the scale of turbulence. Therefore, experimental data must be relied upon to determine how the scale of turbulence is distributed across a channel. Laufer (1951) has determined the distribution of the scale of turbulence in a two-dimensional channel flow of air, but there is no data available to show the distribution of the scale of turbulence in an open channel (either smooth or rough).

Turbulence Energy Spectral Density Function

A more detailed character of turbulence can be obtained by considering the distribution of the total kinetic energy of turbulence among eddies of different sizes, i.e., turbulence spectrum. It is convenient to consider the energy variation with either frequency or wave number.

Taylor (1938) introduced the concept of spectrum into turbulence. Taylor's one-dimensional energy spectrum $E_1(n)$ may be defined as

$$\int_0^\infty E_1(n)\,dn = \overline{u_1^2} \quad \text{or} \quad \int_0^\infty E_1(k_1)dk_1 = \overline{u_1^2} \tag{41}$$

$E_1(n)dn$ is the contribution to $\overline{u_1^2}$ over the frequencies between n and $n + dn$. The normalized one-dimensional energy spectrum $F_1(n)$ or $F_1(k_1)$ may be defined as

$$\int_0^\infty F_1(n)dn = 1 \quad \text{or} \quad \int_0^\infty F_1(k_1)dk_1 = 1 \tag{42}$$

Taylor (1938) showed that $F_1(n)$ and the normalized longitudinal correlation function $f(x_1)$ are Fourier cosine transforms of each other, i. e. ,

$$f(x_1) = \int_0^\infty F_1(n)\ \mathrm{Cos}\left(\frac{2\pi n x_1}{\overline{U}_1}\right)dn \tag{43}$$

and

$$F_1(n) = \frac{4}{\overline{U}_1}\int_0^\infty f(x_1)\ \mathrm{Cos}\left(\frac{2\pi n x_1}{\overline{U}_1}\right)d x_1 \tag{44}$$

From Equations (32) and (44), when $n = 0$

$$L_{x_1} = \frac{\overline{U}_1 F_1(n)_{n=0}}{4} \tag{45}$$

Therefore, the value of L_{x_1} can be obtained from the intercept of the $F_1(n)$ curve at $n = 0$.

It could also be shown that the normalized autocorrelation function $R_{E_1}(\tau)$ and $F_1(n)$ are Fourier cosine transforms of each other, i. e.

$$R_{E_1}(\tau) = \int_0^\infty F_1(n) \operatorname{Cos}(2\pi n\tau)\,dn \tag{46}$$

$$F_1(n) = 4\int_0^\infty R_{E_1}(\tau) \operatorname{Cos}(2\pi n\tau)\,d\tau \tag{47}$$

Spectrum function is more intuitive than that of correlation function, and one of the advantages of working with the spectrum function is that various relations can be deduced without the restrictive assumptions of isotropy; the field need only be homogeneous.

In view of the three-dimensional character of turbulence, it is obvious that the energy-spectrum function must also have a three-dimensional character. Therefore, it should be noted that Taylor's spectrum function is a one-dimensional section of what is in fact the three-dimensional spectrum function. It should also be pointed out that even though the one-dimensional spectrum function is very convenient for experimental measurements, it is not too convenient for theoretical study. Heisenberg (1948), therefore, introduced a three-dimensional-space spectrum function E(k); while Batchelor (1953) and Kampé de Fériet (1940) introduced a spectrum tensor $E_{ij}(\vec{k})$. For this purpose the relation between correlation tensor $R_{ij}(\vec{r})$ and energy-spectrum tensor $E_{ij}(\vec{k})$ is to be studied. They are related by the following three-dimensional Fourier transform pair:

$$R_{ij}(\vec{r}) = \int E_{ij}(\vec{k}) \, e^{i\vec{k}\cdot\vec{r}} \, d\vec{k} \tag{48}$$

$$E_{ij}(\vec{k}) = 1/_{8\pi^3} \int R_{ij}(\vec{r}) \, e^{i\vec{k}\cdot\vec{r}} \, d\vec{r} \tag{49}$$

where $\vec{k}$ is a wave-number vector and $d\vec{r} = dr_1 \cdot dr_2 \cdot dr_3$ and $d\vec{k} = dk_1 \cdot dk_2 \cdot dk_3$. Physical significance can be attached to the quantity $E_{ij}(\vec{k})$ by substituting $\vec{r} = 0$ in equation (48).

$$R_{ij}(0) = \overline{u_i(\vec{x}) \, u_j(\vec{x})} = \int E_{ij}(\vec{k}) \, d\vec{k} \tag{50}$$

Therefore, $E_{ij}(\vec{k})$ represents a density in wave-number space of contributions to $\overline{u_i(\vec{x}) \, u_j(\vec{x})}$. Thus it describes how the energy associated with each velocity component is distributed over the various wave-numbers in a harmonic resolution of the velocity field. It is this physical significance that makes $E_{ij}(\vec{k})$ the most important single quantity describing the field of turbulence.

Correlation and spectrum functions of a single scalar variable can be obtained by averaging $R_{ij}(\vec{r})$ and $E_{ij}(\vec{k})$ over all directions of the vector arguments $\vec{r}$ and $\vec{k}$:

$$T_{ij}(r) = \frac{1}{4\pi r^2} \int R_{ij}(\vec{r}) \, dA(r) \tag{51}$$

and

$$\Psi_{ij}(k) = \int E_{ij}(\vec{k})\, dA(\vec{k}) \tag{52}$$

where dA is an element of area on a sphere with a radius equal to the magnitude of the vector. These scalars are related by Fourier Sine transforms from equations (50) and (52)

$$1/2\ R_{ii}(0) = 1/2\ \overline{u_i(\vec{x})\ u_i(\vec{x})} = \int_0^\infty 1/2\ \Psi_{ii}(k)\, dk \tag{53}$$

The quantity $1/2\ \Psi_{ii}(k)$ is the contribution to the turbulent kinetic energy in the wave-number range k to $k + dk$ and will be called $E(k)$, the three-dimensional energy spectral-density function of Heisenberg and hence

$$E(k) = 1/2\ \Psi_{ii}(k) \tag{54}$$

$$\int_0^\infty E(k)\, dk = 1/2\ \overline{u_i(\vec{x})\ u_i(\vec{x})} \tag{55}$$

Batchelor (1953) has shown that for the case of isotropic turbulence $E_1(k_1)$ is related to $E(k)$ by

$$E_1(k_1) = 1/2 \int_{k_1}^\infty \left(1 - \frac{k_1^2}{k^2}\right) \frac{E(k)}{k}\, dk \tag{56}$$

or

$$E(k) = k^3 \frac{d}{dk}\left[\frac{1}{k_1} \frac{dE_1(k_1)}{dk_1}\right] \tag{57}$$

Equation (56) can be used to transform the quantity $E(k)$ established from theory to a quantity $E_1(k_1)$ that can be measured in the laboratory, if the turbulent field established in the laboratory is isotropic. Conversely, equation (57) can be used to transform laboratory data into a form that can shed light on the mechanism of energy transfer.

The dynamic equation of energy spectrum can be obtained by taking a Fourier transform of the von Karman-Howarth equation (28) as shown by Lin (1947).

$$\frac{\partial}{\partial t} E(k) = W(k) - 2 \nu k^2 E(k) \tag{58}$$

or

$$\frac{\partial}{\partial t} \int_0^k E(k)\, dk = \int_0^k W(k)\, dk - 2 \nu \int_0^k E(k)\, k^2\, dk \tag{59}$$

The left-hand side of this equation represents the change of total kinetic energy of turbulence. The first term on the right represents the interaction of eddies of different wave-numbers, thereby transferring energy by inertial effects to or from the eddies in the wave number region 0 to k and, therefore, $W(k)$ is referred to as the transfer-spectrum function. The second term on the right can be shown to represent the dissipation of turbulence energy into heat. The weighting factor k^2 in the integral in equation (59) clearly shows that the dissipation of energy is practically all associated with high wave-number components which contain a negligible amount of energy. This deduction has a very important bearing on later developments of the theory of energy spectrum.

Knowledge of the spectrum function $E(k)$ is sufficient to describe the turbulent field completely; and, therefore, determination of $E(k)$ is one of the basic problems in the study of turbulence. To determine $E(k)$ either equation (58) or (59) may be used. The complete solution of equation (58) could not be obtained as the form of the transfer-spectrum function $W(k)$ is unknown. There have been two approaches to overcome this difficulty. In the first approach-similarity-equation (58) is discarded and some conclusions about the functional form of $E(k)$ are drawn from more basic physical principles, namely dimensional considerations. The contributions of Kolmogoroff (1941), OnSager (1945), von Karman and Lin (1949) belong to this approach.

In the second approach, (physical transfer theories) an explicit functional form for $W(k)$ is assumed which makes possible the solution of the dynamical equation (58). This second approach was used by Obukoff (1941), Kovasznay (1948), Heisenberg (1948), Chandrasekhar (1949), Tachen (1953), and von Karman (1948). Among the two approaches, only those studies concerning the determination of the energy-spectrum function in the equilibrium range will be briefly considered in a later section.

Kolmogoroff's Theory of Local Isotropy

The following model for turbulent-energy production and dissipation at high Reynolds numbers was suggested by Kolmogoroff (1941): The mechanism of turbulence production from the instability of the mean flow is

determined by the boundary conditions. Pulsations of small wave number produced from the instability of the mean flow give rise to pulsations of higher wave number because of the inertial forces, and these in turn break down into pulsations of much higher wave number. Turbulence energy cascades from the region of low wave numbers to a region of high wave numbers. This cascading of turbulent energy continues until wave numbers of pulsations are so high that not all the energy is transferred to the next higher order, but part is dissipated into heat by viscous forces. Kolmogoroff reasoned that, at high Reynolds numbers, the range between wave numbers of pulsations characteristic of mean flow and those dissipating all their energy by viscosity is large. In this case, the region of pulsations of high wave numbers should be far enough removed in the cascading process from the production region to be independent of the production mechanism. Therefore, in any turbulent field at high Reynolds number, a domain Q can be defined which is small enough that it will possess local isotropy. The domain Q will contain pulsations of high wave number describing a motion that is isotropic and steady-state.

The fundamental quantities upon which the structure of the motion in the domain Q may depend are the mean dissipation of energy per unit time per unit mass of the fluid ϵ (which determines the intensity of the energy flow in the cascading phenomenon) and the kinematic viscosity 'ν' . These considerations led Kolmogoroff to make his first hypothesis: "At sufficiently high Reynolds number there is a range of high wave

numbers where the turbulence is statistically in equilibrium and the probability distributions defining the turbulence are uniquely determined by the quantities, ϵ and ν." (Hinze, 1959, p. 184.)

When this equilibrium range is sufficiently wide, it is further argued that the lower wave-number components in the equilibrium range will contribute so little to the total viscous dissipation that a subrange will exist in which the properties will be determined solely by ϵ. This concept provides Kolmogoroff's second hypothesis: "At the lower wave number end of the equilibrium range there is an inertial subrange in which the probability distribution defining turbulence is uniquely determined by ϵ." (Hinze, 1959, P. 186.)

The concept of local isotropy has exerted profound influence and served as the starting point for many later investigations. One of the most important problems of turbulent shear flows is the estimation of the rate of turbulence-energy dissipation.

The theoretical equation for the rate of turbulence-energy dissipation (second term on the right side of the equations (12)) per unit volume of fluid could not be availed of for practical computations as all the nine terms contained in it cannot be measured. But for isotropic turbulence, the expression for the rate of turbulence-energy dissipation per unit mass given by equation (40) is very simple to make use of as it is fairly easy to measure velocity fluctuation and the associated micro-scale. Hence if the existence of local isotropy in the domain of turbulent

shear flows is proved, usage of the expression for 'ϵ' in isotropic turbulence for estimation of the rate of energy dissipation in nonisotropic turbulence would be justified. Besides, the concept of local isotropy facilitates the application of the results of studies in isotropic turbulence to the phenomena in actual turbulence (nonisotropic turbulence) that are determined mainly by the fine scale structure where local isotropy prevails.

Spectral Laws of Locally Isotropic Turbulence

Similarity hypothesis

The concept of Kolmogoroff and his two hypotheses can be used to determine the energy-distribution function $E(k)$ in locally-isotropic turbulence. According to Kilmogoroff's first hypothesis, the structure of the equilibrium range at the end of high wave numbers is determined by ϵ and ν. If the structure is expressed in terms of the energy-spectrum function $E(k)$, similarity considerations lead to a spectrum function of the form

$$E(k) = \epsilon^{1/4} \nu^{5/4} \phi(\eta k) \tag{60}$$

where $\eta = (\nu^3/\epsilon)^{1/4}$ and ϕ is a universal dimensionless function of ηk.

From Kolmogoroff's second hypothesis at the high Reynolds number equation (60) must reduce to a form independent of viscosity. From similarity conditions it follows that

$$E(k) = \alpha \epsilon^{2/3} k^{-5/3} \tag{61}$$

where α is an absolute constant. This is called Kolmogoroff's spectrum law. From equations (56) and (61), the longitudinal one-dimensional spectrum function takes the form

$$E_1(k_1) = \frac{18}{55} \alpha \epsilon^{2/3} k_1^{-5/3} = \alpha' \epsilon^{2/3} k_1^{-5/3} \tag{62}$$

where $\alpha' = \frac{18}{55} \alpha$.

Laboratory data obtained at high Reynolds numbers should, therefore, give a straight line with slope $-5/3$ when plotted on logarithmic paper if Kolmogoroff's hypotheses are correct.

Physical transfer theories

The basic assumption made in the development of physical-transfer theories is that $W(k)$ is determined by $E(k)$ only. The specific form of relationship between $W(k)$ and $E(k)$ depends on the particular mechanism of energy transfer considered. Among the physical-transfer theories the most successful one is the eddy-viscosity transfer theory due to Heisenberg (1948).

While considering the rate of dissipation of energy by eddies with wave numbers less than a particular k, Heisenberg distinguished between the energy directly dissipated in the form of molecular motion and thermal energy and the energy transferred in the form of kinetic energy to all eddies with wave numbers exceeding the specified k. He argued that

the mechanism governing the transfer of energy is similar to the one governing the viscous dissipation provided the molecular viscosity is replaced by a suitable eddy viscosity. Therefore, the expression for the energy transfer is

$$\int_0^k W(k)\,dk = -2\,\nu_t(k) \int_0^k k^2 E(k)\,dk \tag{63}$$

Heisenberg further assumed that $\nu_t(k)$ can be expressed as an integral over the spectrum in the form

$$\nu_t(k) = k_H \int_k^\infty \sqrt{\frac{E(k)}{k^3}}\,dk \tag{64}$$

where k_H is a numerical constant of order unity. Substitution of equation (63) in equation (59) leads to

$$\frac{\partial}{\partial t}\int_0^k E(k)\,dk = -2\left[\nu + k_H \int_k^\infty \sqrt{\frac{E(k)}{k^3}}\,dk\right]\int_0^k k^2 E(k)\,dk \tag{65}$$

For the equilibrium range,

$$\frac{\partial}{\partial t}\int_0^k E(k)\,dk \simeq \frac{\partial}{\partial t}\int_0^\infty E(k)\,dk = -\epsilon = -2\nu\int_0^k k^2 E(k)\,dk \tag{66}$$

Combination of equations (65) and (66) results in

$$\epsilon = 2\left[\nu + k_H \int_k^\infty \sqrt{\frac{E(k)}{k^3}}\,dk\right]\int_0^k k^2 E(k)\,dk \tag{67}$$

Bass (1949) and, independently, Chandrasekhar (1949) obtained an exact solution of (67) in the form

$$E(k) = \left(\frac{8\epsilon}{9k_H}\right)^{2/3} k^{-5/3} \left[1 + \frac{8}{3}\frac{\nu^3}{k_H^2 \epsilon} k^4\right]^{-4/3} \tag{68}$$

In the region where the effect of viscosity is negligible, equation (68) reduces to

$$E(k) = \left(\frac{8\epsilon}{9k_H}\right)^{2/3} k^{-5/3} \tag{69}$$

which is identical with Kolmogoroff's spectrum law in the inertial subrange. For large values of 'k' where viscosity plays an important part equation (68) reduces to

$$E(k) = \left(\frac{\epsilon k_H}{2\nu^2}\right)^2 k^{-7} \tag{70}$$

Equations (69) and (70) can be transformed to equations for the longitudinal one-dimensional spectrum function by substituting in equation (56) to give for the low wavenumber region and the high wave-number region, respectively,

$$E_1(k_1) = \frac{9}{55}\left(\frac{8\epsilon}{9k_H}\right)^{2/3} k_1^{-5/3} \tag{71}$$

and

$$E_1(k_1) = \frac{1}{63}\left(\frac{\epsilon k_H}{2\nu^2}\right)^2 k_1^{-7} \tag{72}$$

By substitution of equation (68) into equation (56) the longitudinal one-dimensional spectrum function for the entire region is obtained.

$$E_1(k_1) = 1/2 \int_{k_1}^{\infty} Mk^{-8/3} \left[1 + Pk^4 \right]^{-4/3} dk - 1/2\, k_1^2 \int_{k_1}^{\infty} Mk^{-14/3} \left[1 + Pk^4 \right]^{-4/3} dk \tag{73}$$

where

$$P = \frac{8\nu}{3k_H^2 \epsilon} \text{ and } M = \left(\frac{8\epsilon}{9k_H} \right)^{2/3} \tag{74}$$

Equation (73) can only be solved over the entire range by graphical integration once P and M have been determined.

Kovasznay (1948) postulated that the contribution to W(k) comes from a narrow wavenumber band in the immediate vicinity of k. Since, under these circumstances, W(k) can only be a function of E(k) and k, it follows from dimensional arguments that

$$\int_0^k W(k)\, dk = - \alpha \left[E(k) \right]^{3/2} k^{5/2} \tag{75}$$

where α is an absolute constant.

Substituting (75) in (59) he solved for E(k) and obtained

$$E(k) = \left(\frac{\epsilon}{\alpha^{10}} \right)^{1/3} k^{-5/3} \left[1 - \frac{\alpha^{2/3}}{2} \left(\frac{k}{kd} \right)^{4/3} \right]^2 \tag{76}$$

where $k_d = \left[\epsilon/\nu^3\right]^{1/4}$.

Obukhoff (1941) assumed that the energy transfer across the wave numer 'k' is analogous to the energy transfer from the main motion to the turbulent motion through the turbulent shear stresses; and it follows, therefore,

$$\int_0^k W(k)\,dk = -\alpha\left[2\int_0^k k^2 E(k)\,dk\right]^{1/2}\int_k^\infty E(k)\,dk \qquad (77)$$

where α is an absolute constant.

Substituting (77) in equation (59) he obtained a solution for $E(k)$ which reduces to const. $\times k^{-5/3}$ in the inertial subrange.

Von Karman (1948) visualized that the transfer function $W(k)$ may be interpreted as the difference between the energy supplied by the eddies with wave numbers less than 'k' and the energy transferred to the smaller eddies with wave numbers greater than 'k'. On this basis he defined

$$W(k) = 2\alpha\left[E^\beta k^\gamma \int_0^k E^{\beta'} k^{\gamma'}\,dk - E^{\beta'} k^{\gamma'}\int_k^\infty E^\beta k^\gamma\,dk\right] \qquad (78)$$

which includes, as special cases, the assumptions made by Obukoff, Kovasznay, and Heisenberg and obtained

$$E(k) = E(k_e)2^{17/6}\,\frac{(k/k_e)^4}{\left[1+(k/k_e)^2\right]^{17/6}} \qquad (79)$$

where k_e is a function of time.

Homogeneous Shear Turbulence

Most of the research in turbulence so far has dealt with the case of infinite homogeneous isotropic turbulence fields. Extensions to specific isotropic turbulence fields were made by Batchelor (1946) and Chandrasekhar (1950 a, b). They studied axisymmetric turbulence, a field of turbulence with constant mean velocity where the average value of any function of the velocities and of their derivatives is invariant with respect to rotations and reflections about a fixed axis. However, in many practical problems in fluid mechanics such as in turbulent boundary layers, pipe flow, and channel flows, the fields of turbulence are nonhomogeneous with mean velocity gradients. No theoretical studies of nonhomogeneous turbulent shear flows have been made to date. But in the recent years some theoretical studies of homogeneous turbulence with a uniform transverse velocity gradient have been made by Tachen (1953), Burgers and Mitchner (1953), Reis (1952), Deissler (1961, 1962), Fox (1964), and Lumley (1964). Even though the homogeneous turbulent shear flow is a hypothetical one, it will be a better representation of the actual turbulence than the one considered before.

The development of the theory of homogeneous shear turbulence has often followed the ideas developed in the theory of homogeneous isotropic turbulence. Analogous to Heisenberg's theory, there exist the nearly identical theories of Tachen (1953), Reis (1952), and Burgers and Mitchner (1953). Analogous to the work of Proudman and Reid (1954),

there is the work of Craya (1957). Deissler's (1961) work in shear turbulence follows similar lines to his work in homogeneous decaying turbulence. The following treatment briefly outlines the significant results of these studies of homogeneous shear turbulence.

Most of the investigators of homogeneous shear turbulence obtained general two-point correlation equations by use of the Navier-Stokes equations. After taking the Fourier transform of each term in the correlation equations and introducing suitable substitutions, the investigators obtained the following dynamic equation for the energy spectrum:

$$\frac{\partial}{\partial t}\int_0^k E(k,t)\,dk + \frac{d\bar{U}_1}{dx_2}\int_0^k \epsilon(k,t) = \int_0^k F(k,t)\,dk - 2\nu\int_0^k E(k,t)k^2 dk \tag{80}$$

In the case of stationary shear flow, the equation for the energy spectrum is

$$\epsilon = 2\nu\int_0^k E(k)k^2 dk - \frac{d\bar{U}_1}{dx_2}\int_k^\infty \epsilon(k)\,dk - \int_0^k F(k)\,dk \tag{81}$$

On the basis of this equation, a few solutions for $E(k)$ were obtained that are valid in the range of large wave numbers.

In obtaining a solution of the equation (81), Tachen (1953) considered two cases: 1. The vorticity $\frac{d\bar{U}_1}{dx_2}$ of the main motion is small compared with the vorticity of the turbulence in the wave-number range under consideration. 2. The vorticity of the main motion is comparable

to the vorticity of the turbulence in the wave-number range under consideration. Utilizing the concepts of Boussinesq and Heisenberg, he expressed the second term (representing the interaction between the mean flow and its fluctuating part) and the third term (representing turbulent transfer) on the right hand side of the equation (81) in terms of the energy-spectrum function E(k). Then he solved the equation (81)for not too large "k" and for very large "k" and obtained for case one

$$E(k) \propto k^{-5/3} \tag{82}$$

and

$$E(k) \propto k^{-7} \tag{83}$$

These spectral laws were obtained by Heisenberg for the nonviscous subrange and viscous subrange in isotropic turbulence respectively. Burgers and Mitchner (1953) obtained the same solution as (82) assuming that the second term on the right side of equation (81) can be neglected.

In case two, Tachen argued that there will be violent interactions between the vorticities of the two motions and violent resonance may occur. It is reasonable to expect that it will occur in the non-viscous subrange where "k" is not large. As the result of resonance, the production function predominates the viscous dissipation function and eddy transfer function; hence the first and third terms on the right side of the equation (81) were neglected by him to obtain a solution for E(k) as

$$E(k) \propto k^{-1} \tag{84}$$

The corresponding longitudinal one-dimensional spectrum function takes the form

$$E_1(k_1) \propto k^{-1} \tag{85}$$

Tachen further showed that strong interaction between the main motion and the turbulence can occur only in the $\overline{u_1^2}$ component of turbulence as the turbulence production by the main motion occurs only in that component in homogeneous parallel shear flow. Hence "k^{-1}" spectral law can be expected only for the energy spectrum of the longitudinal component of turbulence.

Reis (1952) obtained a solution of equation (81) assuming Heisenberg's expression for the turbulent-transfer term, and making a hypothesis on the form of the term for the interaction between main flow and turbulence. For large wave numbers, his solution is similar to the one obtained by Bass and Chandrasekhar (refer to equation 68) for the case of isotropic turbulence. Thus $k^{-5/3}$ and k^{-7} spectral laws are again obtained by him. However, from his analysis he found a fundamental difference between isotropic and shear turbulence in the equilibrium range: The greater the mean velocity gradient, the larger will be the amount of energy in the equilibrium range, whereas in isotropic turbulence the amount of energy in this range is negligible and the range of validity of the $k^{-5/3}$ law will extend further to higher wave-numbers. These results may be attributed to this: As the mean-velocity gradient increases, the characteristic time of the mean flow

decreases; and it will approach the reaction times of the small eddies, resulting in a greater interaction between the mean flow and the small eddies in the equilibrium range.

Deissler's (1961) analysis is based on the general two-point equations for the velocity correlations and for the pressure-velocity correlations. He assumed the turbulence to be weak enough for triple correlations to be negligible compared to double ones. He derived the corresponding equation for the rate of change of the spectral tensor E_{ij}. For the case of initially isotropic turbulence, solutions for E_{22}, E_{12}, E_{ii} components of E_{ij} were obtained by Deissler and solutions for the remaining components were obtained by Fox (1964). They utilized these solutions to obtain a complete description of the redistribution of turbulent energy $\overline{u_i u_i}$ among its directional components $\overline{u_1^2}$, $\overline{u_2^2}$, $\overline{u_3^2}$ by the effects of mean transverse velocity gradient as the turbulence decays. Their study leads to the following description of the sequence of turbulent-energy processes. The turbulent-energy production by the mean-velocity gradient occurs only in the $\overline{u_1^2}$ component of the energy and predominantly in the low wave-number or large-eddy region. The pressure forces which depend on the velocity gradient transfer the energy into other components. In doing this, the pressure forces increase the anisotropy of the turbulence; and, in particular, they oppose local isotropy in the high wave-number region. But the triple correlations which are neglected by them can also affect the pressure forces at high Reynolds numbers and may tend to

increase isotropy. Hence, their results cannot be taken as definitive, but they may serve as a warning to use caution in assuming local isotropy in boundary-layer flows especially very near to boundaries.

The two approaches above do not provide the detailed mechanism of the transfer of energy from one wave number to another. Improvement in the study can be made by considering not only the equations for the two-point double correlations, but also the equations for three-point triple correlations. Closure of this system of equations can be made by the application of the quasi-gaussian hypothesis. Craya (1957) adopted this procedure and derived the dynamical equations for the energy-spectral tensors. These equations are too complicated to obtain any solution.

Lumley (1964) derived spectral-energy equations for wall turbulence, that is, turbulence which obeys similarity relations and in which the only characteristic length is the distance to the wall. He made use of those equations for qualitative study of the spectral budget of energy. The picture of spectral-energy budget obtained as a result of his study was summarized by Lumley and Panofsky in lucid terms and is quoted here:

> Energy removed from the mean motion by working of the Reynolds stresses against gradients of the mean velocity is fed in at lower wave numbers. The spectrum is anisotropic here. Distortion of the eddies by the mean strain rate serves to transfer energy from the lower to the higher end of the anisotropic part; inertia forces or vortex stretching, due to the fluctuating velocity gradients serve to transfer energy from the low wave-number anisotropic range to higher wave numbers. As the wave number increases, under the influence of pressure forces, the spectrum becomes

more isotropic and feeding falls off. For sufficiently large Reynolds number, there is a range of wave numbers in which no significant feeding or dissipation is taking place, only inertial transfer; finally, at sufficiently high wave numbers, dissipation takes place. The spectrum in the ranges in which only inertial transfer and dissipation take place may be regarded as isotropic. (Lumley and Panofsky, 1964, p. 82.)

Relationships Between Statistical Quantities of Turbulent Shear Flows

In the previous sections, several statistical quantities which constitute the structure of turbulent shear flows have been considered. Not only do they depend on the position of the sampling point and the Reynolds number of flow, but they must be related to the representative mean values of flow as well. If they could be related to easily measurable mean quantities such as the relative depth of flow, the resulting relationships could form a basis for the application of the statistical theory of turbulence to practical problems.

The rate of energy dissipation per unit volume in turbulent shear flows may be expressed on the basis of the analogy with the case of isotropic turbulent flow, as

$$\epsilon_o = \text{const.} \quad \rho \nu \frac{\overline{u_1^2}}{\lambda_{x_1}^2} \tag{86}$$

Provided that u_2' and u_3' are proportional to u_1' the expression for turbulence energy per unit volume is given by

$$E = 1/2\ \rho\left(\overline{u_1^2} + \overline{u_2^2} + \overline{u_3^2}\right) = \text{Const.}\ \rho\,\overline{u_1^2} \tag{87}$$

This turbulent energy is dissipated by the action of viscosity in the time of decay defined by $\int_0^\infty R_{L_{V_1}}(\tau)\,d\tau$, where $R_{L_{V_1}}(\tau)$ is the Lagrangian correlation coefficient of a turbulent fluid particle velocities at an interval of time τ. The time of decay is related to the Eulerian system such that

$$\int_0^\infty R_{L_{V_1}}(\tau)\,d\tau \;\alpha\; \frac{L_{x_1}}{u_1'} \tag{88}$$

The rate of turbulent-energy dissipation is given by

$$\epsilon' = \text{Const.}\ \rho\ \frac{(u_1')^3}{L_{x_1}} \tag{89}$$

A combination of equations (86) and (89) leads to the following relation:

$$\frac{\lambda_{x_1}^2\, u_1'}{\nu\, L_{x_1}} = \text{Const} \tag{90}$$

The experiments of Laufer (1951, 1954) proved that the dissipation of turbulence is nearly balanced with the production rate of turbulence in the range of approximately $(0 < \frac{x_2}{\bar{h}} \leq 1/2)$ and with the diffusion rate in the outer region $(0.8 < y/\bar{h} \leq 1)$. In addition, the turbulence intensities referred to the friction-velocity u_* are functions of $x/\bar{h}$. On the basis of this conclusion, the macroscale of turbulence relative to the flow depth

can be expressed as a function of relative depth as indicated by Hino (1960).

The rate of production of energy in steady unidirectional flow is given by

$$\tau \frac{d\overline{U_1}}{dx_2} = \frac{\rho}{\kappa x_2}\left(1 - \frac{x_2}{\bar{h}}\right) u_*^3 \tag{91}$$

The rate of dissipation of turbulent energy can be expressed as

$$\epsilon' = C_1 \rho \left(\frac{u_1'}{u_*}\right)^3 \frac{u_*^3}{L_{x_1}} \tag{92}$$

Reference to equation (11) reveals that the rate of diffusion of turbulent energy is given by (the first term on right-hand side).

$$= \frac{d}{dx_2}\left[\rho \overline{u_2 \frac{\left(u_1^2 + u_2^2 + u_3^2\right)}{2}}\right]$$

$$= C_2 \frac{\rho u_*^3}{\bar{h}} \frac{d}{d\left(x_2/\bar{h}\right)} \frac{u_1'^2 u_2}{u_*^3} \tag{93}$$

In light of the isotropic character in the outer region, the diffusion rate as well as the dissipation rate should nearly be constant in this range; and, therefore, equation (93) can be rewritten as

$$\text{Diffusion rate} = C_2 \frac{\rho u_*^3}{\bar{h}} \tag{94}$$

If equation (92) is equated to equations (91) and (94)

$$\frac{L_{x_1}}{\bar{h}} = \begin{cases} B_1 \dfrac{x_{2/\bar{h}}}{1 - x_{2/\bar{h}}} \left(\dfrac{u'_1}{u_*}\right)^3 \phi\left(x_{2/\bar{h}}\right) & 0 < x_{2/\bar{h}} < 0.5 \\ B_2 \left(\dfrac{u'_1}{u_*}\right)^3 = \phi'\left(\dfrac{x_2}{\bar{h}}\right) & 0.8 < x_{2/\bar{h}} < 1 \end{cases} \tag{95}$$

This relation is analogous to the experimental result, obtained by Nikuradse (Schlichting, 1960, p. 511) from his measurements on artificially roughened pipes in that the variation of the mixing length with the wall distance (ℓ/R) is independent of Reynolds number and wall roughness and is a function of $\frac{x_2}{R}$ only, provided the flow is fully-developed turbulent flow. The validity of the above approximate relationship will be tested in Chapter VI, making use of the experimental data obtained.

CHAPTER IV

EXPERIMENTAL APPARATUS AND PROCEDURE

Description of Apparatus

Flow system

The flow system used in this study was a flume which is 3 feet wide, 2 feet deep, and 24 feet in length (see Figure 1). The slope of the flume is adjustable from 0 to 4 per cent. At the head end of the flume a head tank equipped with a diffusion partition receives the discharge from the reservoir directly through a 1.0 foot-diameter pipe which is provided with a regulating valve near the head tank. Discharges up to 5 c.f.s. were possible and were measured by an electromagnetic flow-meter.

The entrance to the experimental flume was provided with a rounded inlet which was designed to provide a smooth transition from the relatively quiet conditions in the head tank to the flow of the main channel. At the entrance to the flume, a sluice gate was provided for regulating the flow in the flume in addition to the valve on the supply pipeline. In the entrance to the flume, a series of screens were placed across the head tank for suppressing surface waves and eliminating secondary currents. At high flows, secondary rollers appeared in the entrance section. These were suppressed by manipulating the sluice gate. During the investigation, there was no evidence of the persistence of such disturbances if ever

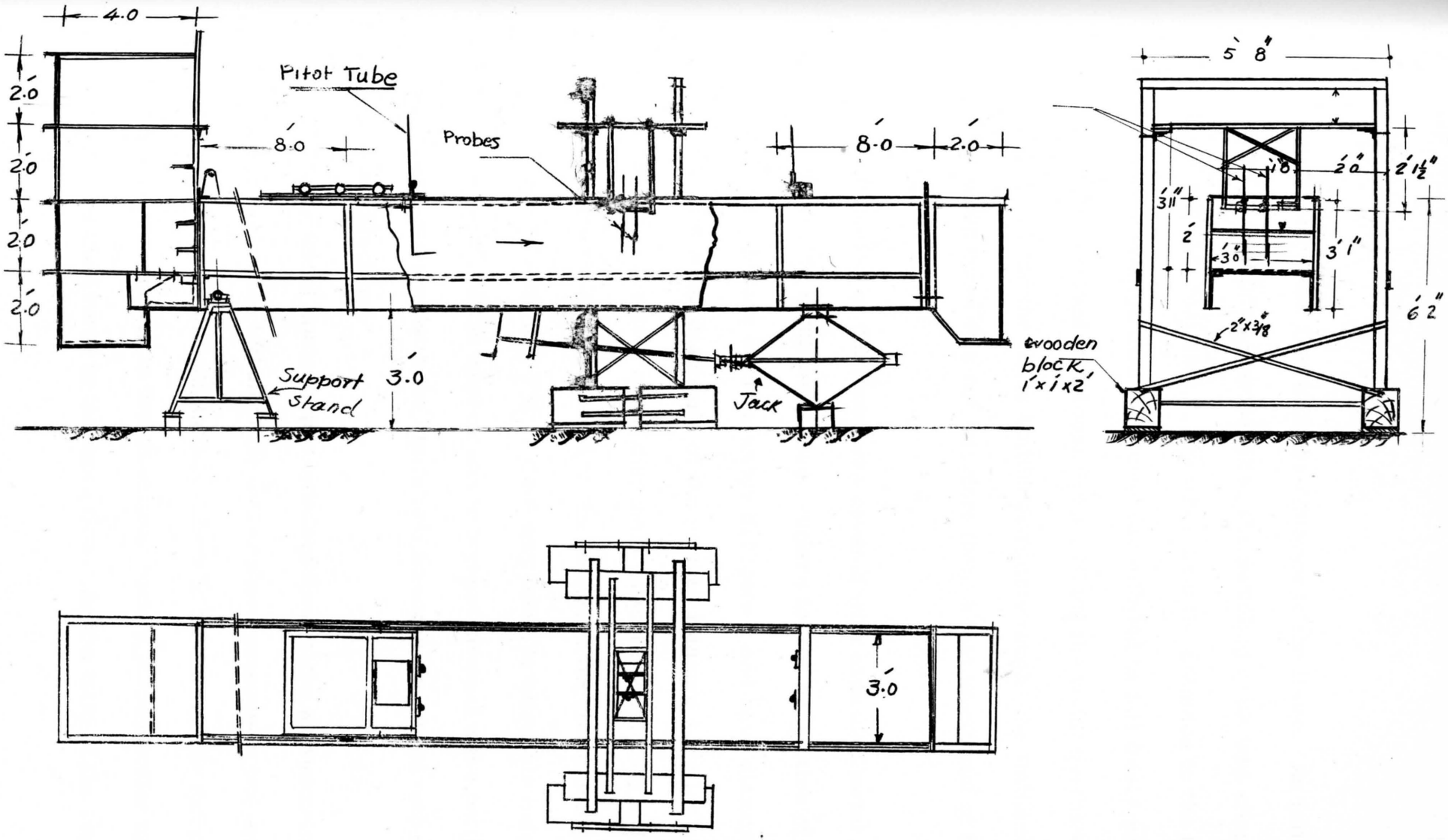

Figure 1. Experimental flume -- plan and sectional elevation

present beyond a few feet from the entrance to the flume. As further insurance to guarantee homogeneity, the sampling point was chosen at a distance of 15 feet and 7.25 inches from the entrance to the flume.

The discharge from the flume was allowed to fall freely into a channel which drained into Logan River. Since the water depths were normally small and the flume bottom extremely rough, the influence of the draw-down curve was not felt more than 6 feet up-stream of the end of the flume.

The bottom of the flume was covered with expanded metal screens in order to provide a uniformly rough surface for the generation of turbulence. These screens are illustrated in Figure 2 and have diamond shaped openings. The minor diagonals of the meshes measure 13/8 inch and 5/16 inch while the respective major diagonals measure 27/8 inch and 5/8 inch. The screens were attached to the bottom of the flume using marsh adhesive and Silastic RTV-731. Care was taken to eliminate bulges or dips in the height of the meshes and to prevent unusual wave patterns which might interfere with the statistical homogeneity in the turbulence in the axial direction.

The simplest nonisotropic turbulent flow is the axisymmetric flow in a pipe in which the turbulent field is nonhomogeneous in one direction only. In the case of uniform turbulent flow in the flume, the turbulent field is nonhomogeneous in two directions, namely, perpendicular to the mean flow and transverse to the mean flow. As the ratio of the breadth

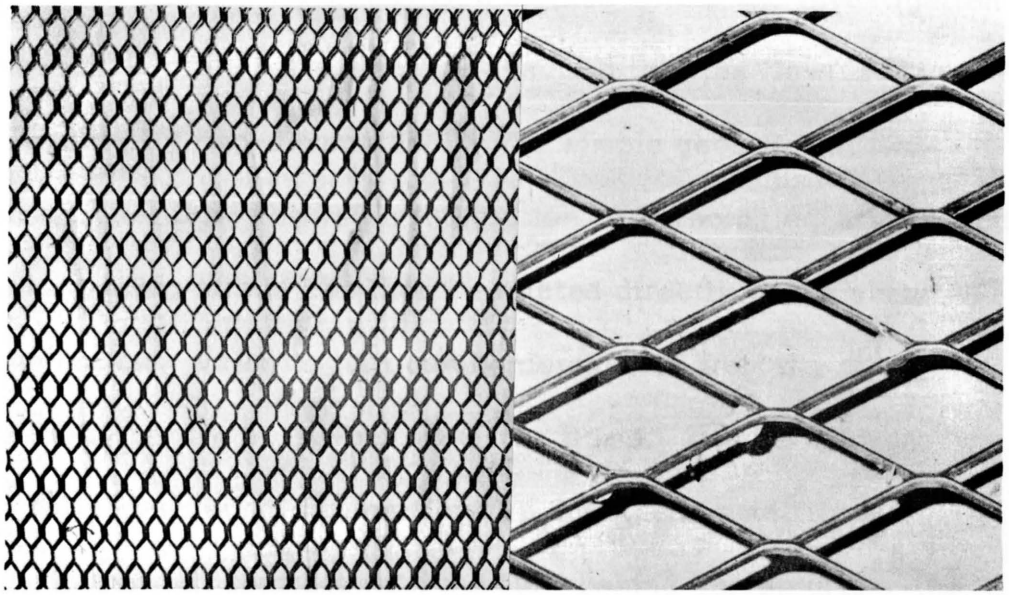

Series A Series C

Figure 2. Flume bed roughness meshes.

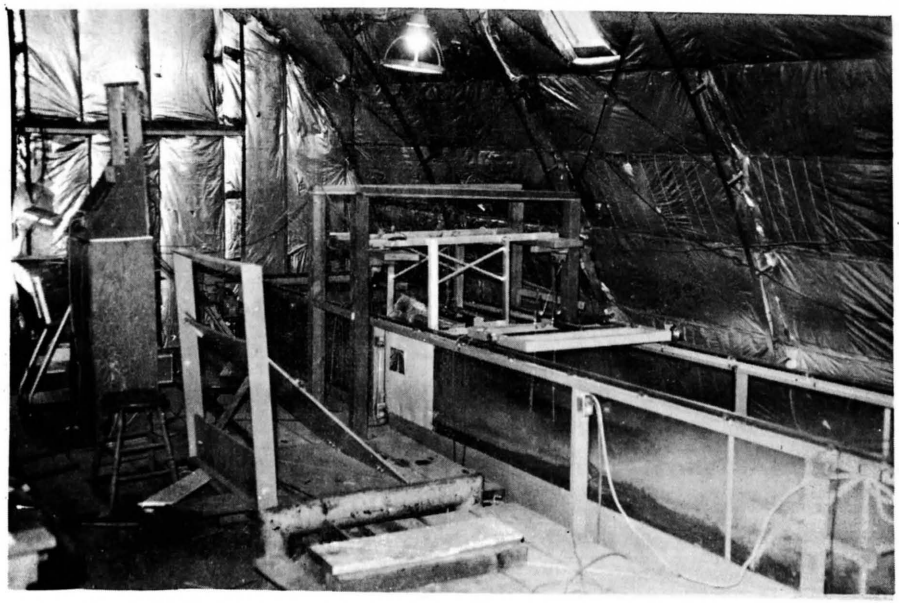

Figure 3. Experimental flume and staging--General view.

of the flume to the maximum depth of flow worked within the investigation is more than 12, it could be reasonably assumed that the flow used in the flume was essentially two-dimensional. The simple geometry of two-dimensional channel flow allows an integration of Reynolds equations; and the turbulent shearing stress can then be related directly to the shearing stress on the bottom, which in turn can be determined from the slope of the mean-velocity profile at the bottom of the flume. Another advantage of choosing fully-developed channel flow as an experimental flow system in this study is that, in contrast with the flow behind screen grids, the mean-flow conditions are steady. Furthermore, no decay of mean or fluctuating quantities exists in the direction of the flow because the turbulence generated by the bottom roughness of the flume was in equilibrium with turbulence decay. The position of the sampling point in the transverse direction was chosen in the center of the flume.

The Reynolds number of the flow was calculated using depth of flow as the characteristic length. The depth of flow was measured from the effective bed which was arbitrarily chosen at a height equal to half of the thickness of the mesh measured from the bed of the flume.

The location of the test section ranged from 12 feet 0 inches to 19 feet 0 inches downstream from the entrance of the flume. The variation of depth of flow in that reach was not more than 5 per cent.

In order to isolate the tranducer from the oscillations of the flume, a separate staging across the flume was erected; and the tranducer probe

was mounted on the frame, which was resting on the staging, which rested on the floor. The details are shown in Figure 3.

Tranducer probe

A radially-polarized hollow cylindrical barium titanate ceramic, 1/16 inch in outside diameter and 0.033 inch in inside diameter and 1/2 inch in length purchased from Gulton Industries, Inc., Metuchen, New Jersey, was used as the pick-up. It was supplied with a very thin waterproof coating of silicone varnish. It was provided with electrical leads already soldered to the inner and outer faces. The inside lead is 32 gauge stranded, insulated copper wire with outside diameter not greater than 0.030 inch and length 18 inches. The lead on the outer face is a gold foil tab 1/16 inch wide, 1 inch long, and 0.0015 inch thick.

The details of the various parts of the probe are shown in Figure 4. The following steps were followed in its construction: The rear portion of the tip connector was tinned with silver solder, and while it was still hot the connector was screwed tightly into a 1/8-inch stainless-steel tube. This provided a good physical and electrical connection between the two parts. The tranducer was then glued to the exposed end of the tip connector with a very thin layer of hard drying "Epoxy glue." The inner lead of the tranducer was carried back through the tube to a "Glenite C5-R1" miniature cable connector. The gold foil tab was fastened to the flat on the tip connector with a small amount of silver

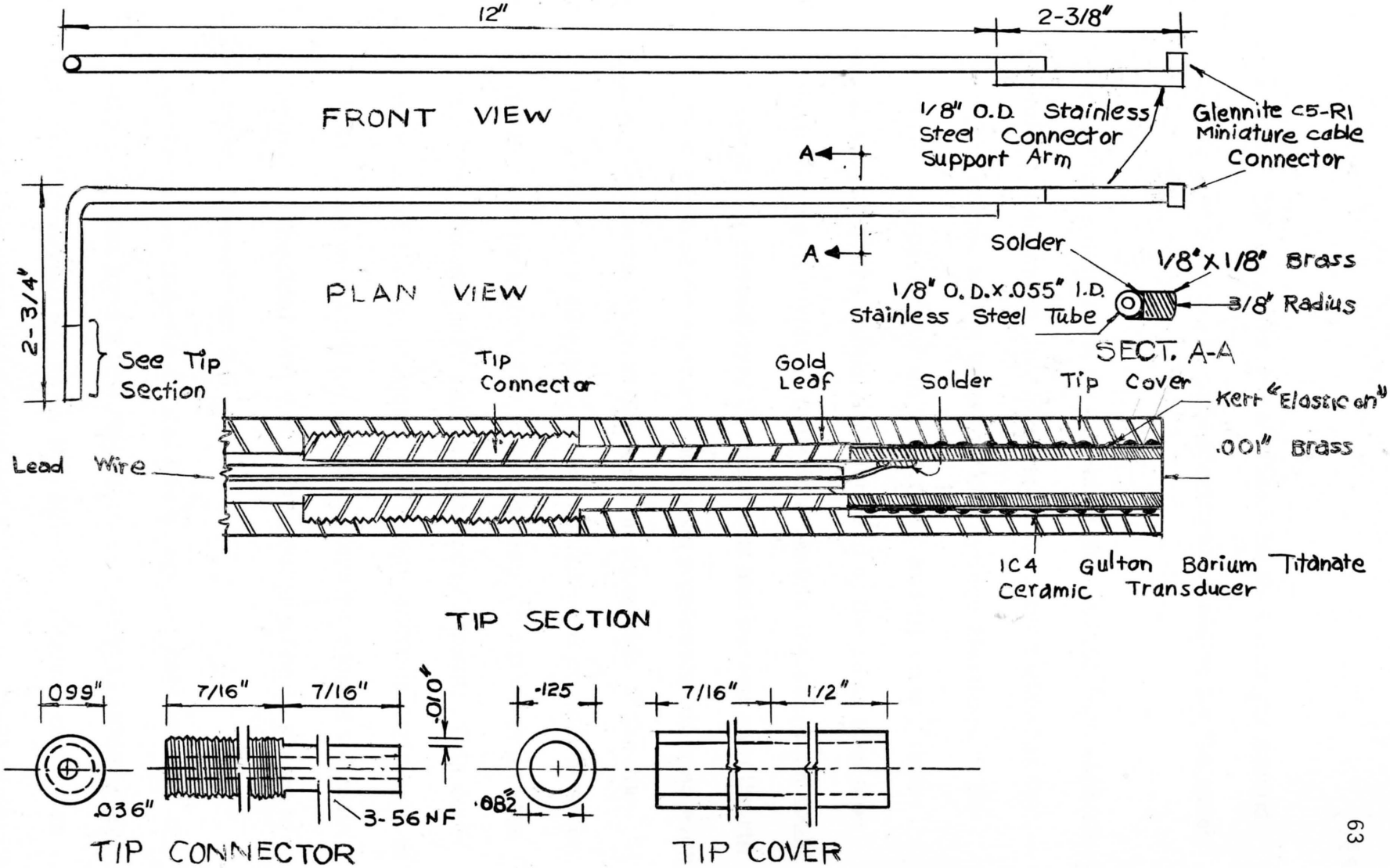

Figure 4. Design details of the tranducer probe.

conducting paint. The tip connector and the tube thus form the ground lead from the ceramic and also provide electrical shielding for the inner lead.

Then the brass diaphragm was punched from 0.001 inch shim stock and very carefully soldered to the tip cover. The outer surface of the ceramic was then coated with a layer of "Kerr Syringe Elasticon." Its purpose is to fill the space between the ceramic and tip cover, thus giving lateral support to the ceramic element and at the same time providing a certain degree of vibration isolation. Before the elasticon could set, the tip cover was slipped over the tranducer and pushed onto the tip connector. The length of the tip cover had been previously adjusted such that when pushed on as far as possible a slight deflection of the diaphragm by the ceramic was effected. This ensured good contact between the diaphragm and the ceramic. The joint between the tip cover and the main portion of the tube was then sealed with epoxy cement. This completed the assembly of the tip section. To provide additional strength to the tube, a brass strip was soldered along the forward edge of the main portion of the tube. The final shape of the tranducer probe is shown in Figure 5 along with ceramic crystal.

Since the barium titanate crystal has a very low capacitance, the external cable must also have a low capacitance in order to achieve high sensitivity. For this reason Amphenol No. 621-685 shielded cable was used to connect the tranducer electrodes and the "Glenite C5-R1 miniature

cable connector" at the other end. In order to increase the low-frequency response of the tranducer probe, a Glenite cathode follower Model F-407 with an input impedance of at least 100 megohms was connected to the miniature cable connector. A Glenite C22-5 low noise cable was used to connect the cathode follower and the input provided on the power panel of the power supply to the cathode follower.

Electronic instrumentation

DISA random signal indicator and correlator. Figures 6 and 7 show the electronic system used to measure the response of the tranducer probe to the turbulent fluctuations. The particulars of each one of the units are furnished below.

The DISA random-signal indicator and correlator type 55A06 shown in Figure 6 could be used to measure the two root-mean-square voltages of the two input signals, "A" and "B", the time derivative of signal "A" as well as the root-mean-square value of the sum and difference of the signals "A" and "B" irrespective of their wave form. The principle of its operation would be clear by looking at the block diagram of the internal circuit shown in Appendix D. The input signals A and B are applied to identical preamplifiers via separate calibrated attenuators. The amplified signals are applied to the output terminals A and B and to a summing amplifier whose output provides the amplified A + B signal. Preamplifiers A and B consist of the amplifier proper followed by an isolating amplifier. The isolating amplifier in amplifier B is also

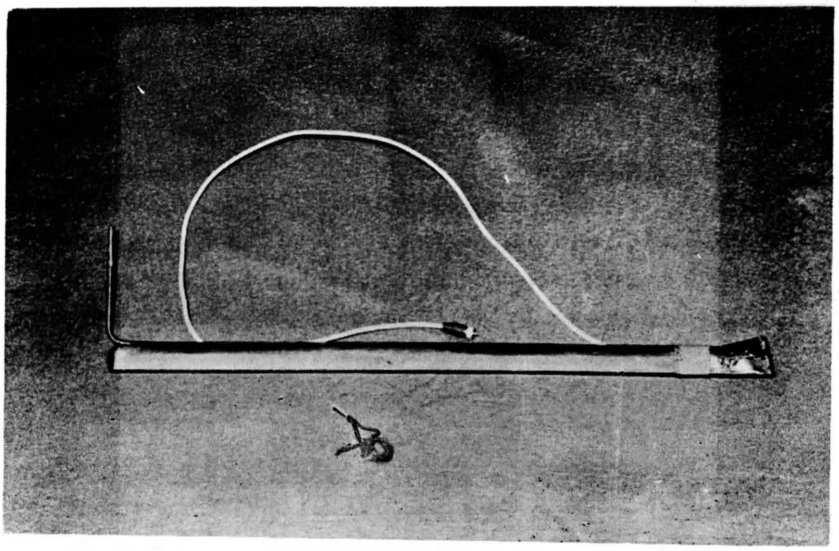

Figure 5. Photograph of the final shape of the tranducer probe.

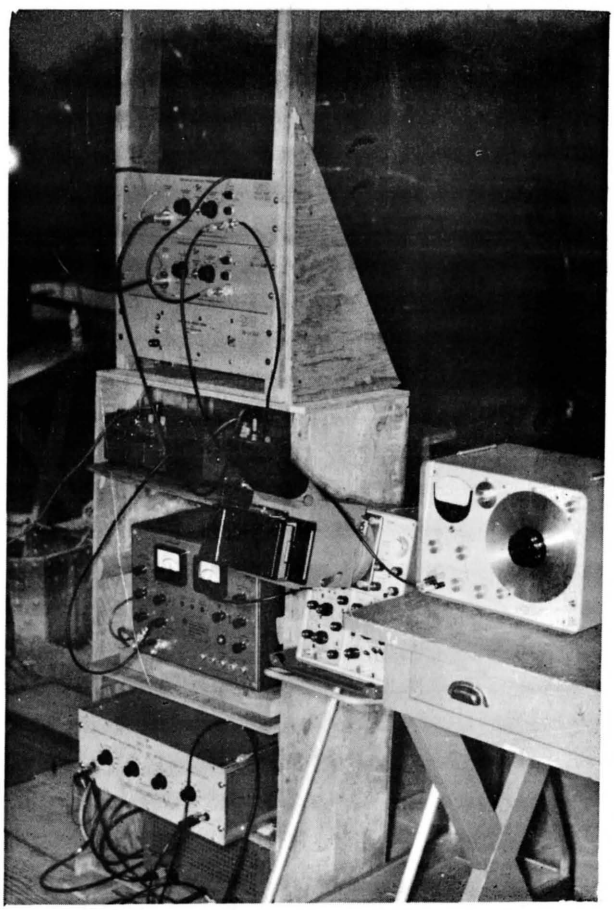

Figure 6. A general view of the instrumentation set-up.

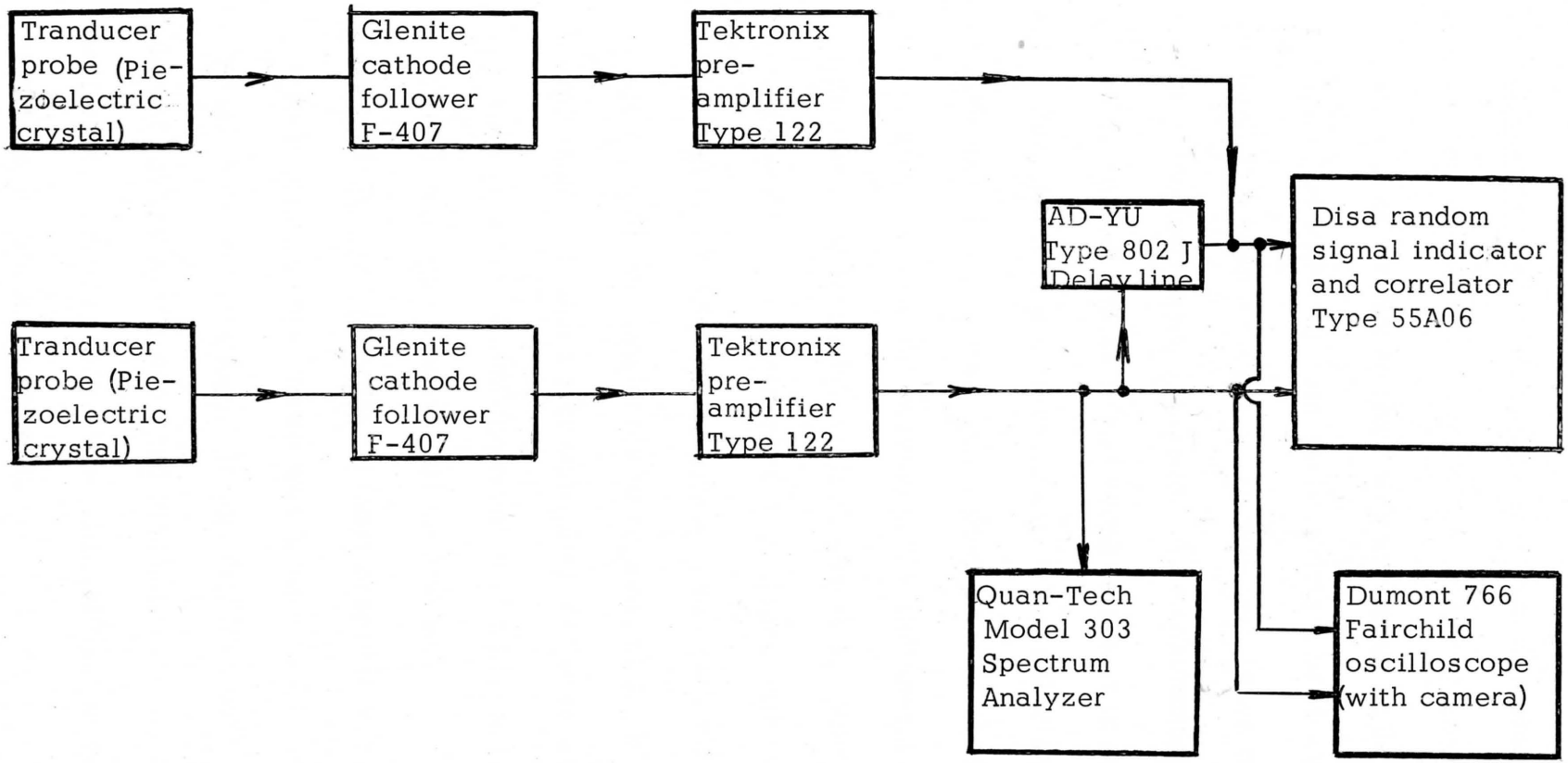

Figure 7. Block diagram of the tranducer probe and associated electronic instrumentation.

Spectrum analyzer. The energy spectrum was obtained with the aid of wave and noise spectrum analyzer Model 303 of Quan-Tech which analyzes an input signal present in the frequency range of 30 cycles to 100 K. C. It is provided with four selectable constant band widths of 10, 30, 100 and 1000 C. P. S. Band-widths of 10 and 30 cycles enable accurate measurement in the low frequency range. All measurements were made with 30 C. P. S. band-width as it was found to result in easier reading of the analyzer output. It is also provided with two selectable time constants .01 sec (fast) and 1 sec (slow). Slow position was used throughout the measurements since it made the reading of the instrument easier. The R. M. S. voltmeter is calibrated in various scales as selected by the millivolt full scale switch. The instrument is equipped with two input terminals X1 and X10, and it is also provided with a meter multiplier which is to be set to a range higher than the signals to be measured. In the measurements reported here, input X1 and meter multiplier 10 were used. To obtain an absolute voltage measurement the reading in milli-volts should be multiplied by 10 with gain control full clockwise.

Data indicator and recorder. Visual observation of the signal and noise at various points in the circuit was made with Dumont Type 766 transistorized dual trace oscilloscope. It was provided with a Dumont Type 450A polaroid camera which was used for photographing the signal traces on the oscilloscope screen. Some typical oscilloscope pictures of total-head fluctuations are shown in Figure 8.

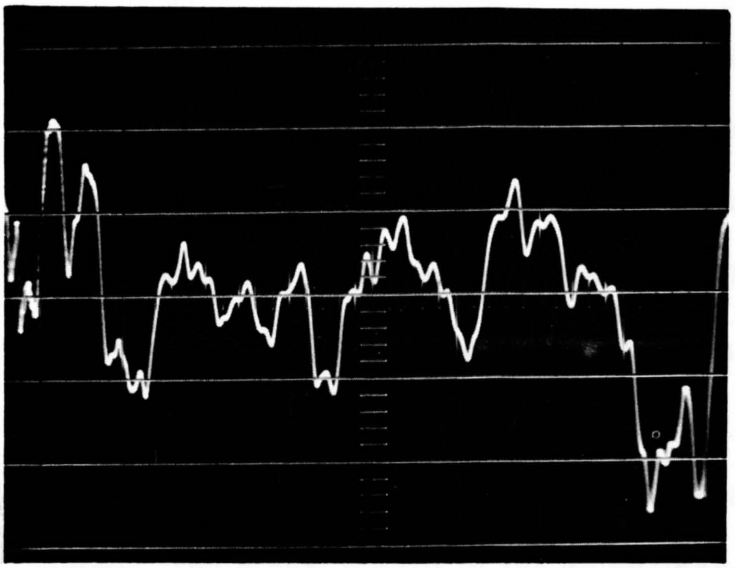

At $x_2/\bar{h} = 0.56$

Scale:
1 volt per centimeter
10 milliseconds per centimeter

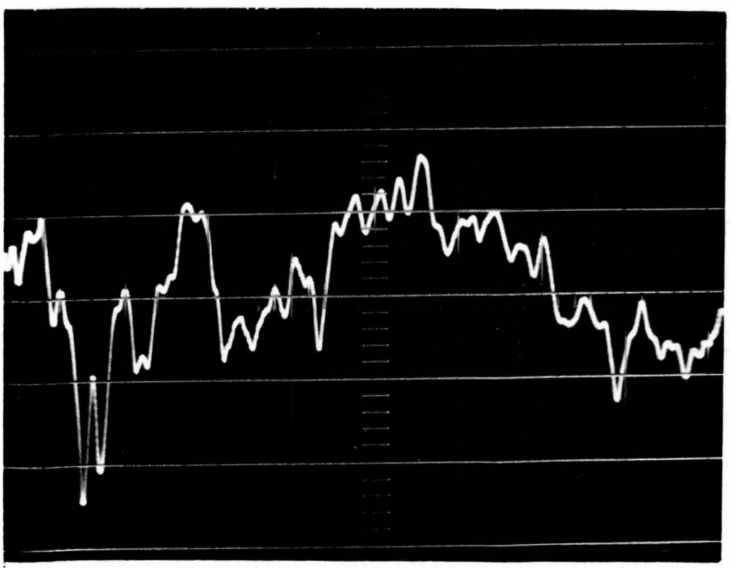

At $x_2/\bar{h} = 0.31$

Figure 8. Typical oscilloscope pictures of turbulent total head fluctuations at $R_N = 7.25 \times 10^4$ -- Series A.

Variable time-delay network. Type 802 J Decade variable delay-line supplied by AD-YU Electronics, Inc., was used in conjunction with the correlator to obtain autocorrelations. It is capable of delaying the signal from 2μS to 200,000 μS. It is provided with four switches; and when all of them are set at maximum, total delay is obtained. The cutoff frequency at 3 db varies with the amount of delay corresponding to the maximum setting of each one of the switches.

Care was taken to have impedance matching at the input and output terminals of the delay line. The signal source of the delay line was input "A" of correlator. As the source impedance was higher than the input impedance of delay line, a variable resistor was connected parallel to the input terminal of the delay unit. The output terminal of the delay line was connected to input "B" of correlator with a resistor of 2200Ω connected parallel. As the input voltage requirement of the correlator is low, it was not found necessary to amplify the output of the delay line before the signal was fed to input "B" of the correlator.

Auxiliary instruments. The Glenite cathode follower Model F-407 was used for coupling the tranducer probe with the input of the Tektronix preamplifier Type 122 in order to achieve maximum power transfer by matching the high output impedance of the probe with the high input impedance of the cathode follower probe which was kept very near the tranducer probe to minimize the shunt capacitance for maximum sensitivity. The output of the cathode-follower probe was connected to the input on the power panel

with a low-noise Glenite C22-5 cable. Single-ended output on the power panel was connected to the input of the preamplifier. Most of the time the preamplifier gain was set at 1000. The low-frequency and high-frequency response selectors on the preamplifiers were set at 8 c. p. s. and 10 K. C., respectively, as it was found expedient from the considerations of the range of frequencies of fluctuations present in the flow system and the noise contributed by selected band width of frequency components.

All the connections between the units were made with Belden type 8254 RG-62/U and Amphenol No. 621-685 shielded cables with SO-235 or BNC connectors in order to minimize noise. Preamplifiers were provided with a separate power supply. All the units had power supplied from a regulated power source. Extreme precautions were taken to ground the measuring system properly to eliminate, as much as possible, the 60-cycle noise and to reduce the noise as much as possible from various other sources.

Details of procedure

Measurement of average velocity. In order to determine the rates of energy dissipation and mean-friction velocity in the experimental channel, it was essential to determine the slope of the total-energy line (S_e) within the test section. To obtain 'S_e', mean-velocity distributions at the two ends of the test section were to be measured. Besides, at all locations where measurements were made with the tranducer probe for

intensity of turbulence, energy-spectrum, microscale, and autocorrelations, local mean velocities were also to be determined.

Dwyer pitot tubes or total-head tubes were used to measure mean velocities. These tubes have an outside diameter of 1/8 inch and an inside diameter of 0.047 inch. Literature concerning the effect of turbulence on total-head tube readings was reviewed by Hinze (1959); but in the absence of an accurate procedure to account for the effect, it was neglected in this study. In order to compute the local mean velocity at a point, it is essential to know the difference between the total and static heads. The inner and outer tubings of the total-head tube were connected to an inclined manometer board. Water was used as the manometer fluid. For every position of total-head tube at least five to ten minutes were allowed for manometer liquid levels to reach steadiness before readings were taken. For calculating mean-velocity distributions, at least 15 to 20 measurements were taken at each section.

Measurement of autocorrelation coefficient.

The signal "A" from the Tektronix amplifier output terminal was connected to the input "A" of the correlator. The input terminal of the external variable time-delay network was connected to the input "A" of the correlator. The signal from the output terminal of the time-delay network, designated signal "B" was connected to input "B" of the correlator. Input "A" and input "B" of the correlator were connected to the oscilloscope. With zero time delay, both signals "A" and "B" on the

oscilloscope trace were identically the same. To measure the correlation coefficient, the instantaneous sum and difference of the two time-dependent signals "A" and "B" were first derived. The ratio of the root-mean-square of the sum and difference signals was then measured by means of an r. m. s. ratio-meter. It could be shown that the measured ratio is an unique function of the correlation coefficient if the r. m. s. value of the signals "A" and "B" had been made equal. This equalization was performed in the variable-gain pre-amplifiers. Then from the precalibrated scale for the correlation coefficient, the value of the correlation coefficient was obtained. At zero time delay, the value of the correlation coefficient was found to be nearly one, as it should be. The same procedure was repeated for increasing time delays until the delayed signal "B" was attenuated to such an extent that the signal trace was distorted considerably.

Measurement of spatial correlation coefficients

Besides the autocorrelation coefficient, attempts were made to measure $R_{x_1 u_1}$, $R_{x_2 u_1}$ and $R_{x_3 u_1}$ by simultaneous measurement of the turbulent fluctuations af two different points located along x_1, x_2, and x_3 axes using two tranducer probes No. 3 and No. 2. The signals from the two probes were amplified by two Tektronix preamplifiers, and the output terminals of the preamplifiers were connected to the two inputs "A" and "B" of the correlator.

To measure $R_{x_1 u_1}$, one probe was placed very closely behind the other; and it was found that the probe located downstream was affected by

the wake of the other. To overcome this difficulty the downstream probe was placed slightly to one side of the other with a longitudinal spacing of 1/8 inch. The correlation coefficient obtained was 0.5. At a distance of 1/4 inch the correlation became negative; and at distances more than that, correlation remained negative.

Similarly, to measure $R_{x_3 u_1}$, the two probes were placed adjacent to each other with zero spacing; and the correlation coefficient found was 0.6. When the spacing was increased to 3/8 inch, the correlation became negative; and at increased spacings the correlation coefficient remained negative. Similar readings occurred with the measurement of $R_{x_2 u_1}$. As sufficient data could not be obtained for plotting correlation curves for each one of these spatial correlation coefficients, no further measurements were made. It was concluded that much finer tranducer probes, such as a hot-film anemmometer, were needed to measure, successfully, spatial correlations.

Measurement of longitudinal microscale of turbulence

A method suggested by Townsend (1947) was used to measure λ_{x_1}. It has been found experimentally by Townsend that the mean square of the time derivative agrees closely with the mean square of the space derivative in the direction of the mean motion; that is

$$\overline{\left(\frac{\partial u_1}{\partial t}\right)^2} \approx \overline{U}_1^2 \overline{\left(\frac{\partial u_1}{\partial x_1}\right)^2} \qquad (96)$$

The microscale λ_{x_1} is defined by equations (36) and (37), namely,

$$\frac{1}{\lambda_{x_1}^2} = \frac{1}{2\overline{u_1^2}} \overline{\left(\frac{\partial u_1}{\partial x_2}\right)^2} \tag{97}$$

There is a definite relationship between $\overline{\left(\frac{\partial u_1}{\partial x_2}\right)^2}$ and $\overline{\left(\frac{\partial u_1}{\partial x_1}\right)^2}$ as shown by Taylor (1935), such that

$$\overline{\left(\frac{\partial u_1}{\partial x_2}\right)^2} = 2 \overline{\left(\frac{\partial u_1}{\partial x_1}\right)^2} \tag{98}$$

Combining equations (96), (97), and (98)

$$\frac{1}{\lambda_{x_1}^2} \approx \frac{1}{\overline{u_1^2}} \frac{1}{\overline{U_1^2}} \overline{\left(\frac{\partial u_1}{\partial t}\right)^2} \tag{99}$$

or

$$\lambda_{x_1} = \overline{U}_1 \frac{\sqrt{\overline{u_1^2}}}{\sqrt{\overline{\left(\frac{\partial u_1}{\partial t}\right)^2}}} \tag{100}$$

The differentiater, incorporated in the random-signal indicator and correlator (See Figure 6), provides the product of the time derivative of the amplifier output signal and a selective time constant "τ." The RMS ratiometer of the correlator now measures the root-mean-square value of the ratio "r" of the input signal from the amplifier output terminal to its time derivative multiplied by τ. Then the numerical value of the microscale is computed from the following relation:

$$\lambda_{x_1} = \overline{U}_1 \cdot \tau \cdot r \qquad (101)$$

Measurement of turbulence-energy spectrum and intensity of turbulence

Every time the spectrum analyzer was used for making energy-spectrum measurements, nulling was done and the calibration of the r. m. s. voltmeter of the analyzer was checked. The details of the calibration of the analyzer are outlined in Appendix C.

Measurements of energy spectrum and turbulence intensity were made in the following four steps: (1) measurement of the Fourier component of turbulence intensity, (2) measurement of corresponding noise output, (3) measurement of total output for turbulence intensity, (4) measurement of corresponding noise output. In steps 2 and 4, the probe was sealed from contact with pressure fluctuations in the flow. In step 1, the signal from the amplifier output terminal was fed into the input terminal of the analyzer. The frequency dial was tuned to 20 c. p. s. and the reading was taken from the r. m. s. voltmeter of the analyzer when the output stayed steady at least for 5 minutes. This procedure was repeated at different tunings of the frequency dial until the output of the analyzer was negligibly small. Exactly the same data-taking procedure was used in step 2.

In steps 3 and 4, the spectrum analyzer was by-passed, and total outputs for turbulence intensity and noise were measured with the r. m. s. voltmeter of the random-signal indicator and correlator.

The entire above procedure was repeated for every position of the probe for a particular flow condition.

CHAPTER V

DATA PROCESSING

Sample calculations are presented to illustrate the procedure used in processing of the experimental data to evaluate the relative intensity of turbulence, one-dimensional energy spectral-density function, longitudinal average macroscale of turbulence, and longitudinal microscale of turbulence.

Relative Intensity of Turbulence

The total signal V_T obtained with the uncovered tranducer probe consists of real turbulence signal V_R and noise V_N arising from the structural vibration of the probe, accoustical noise in the surroundings, thermal noise, microphonics, etc.

$$V_T = V_R + V_N \tag{102}$$

Squaring both sides of the equation (102) and taking time averages,

$$\overline{V_T^2} = \overline{V_R^2} + 2\,\overline{V_R\,V_N} + \overline{V_N^2} \tag{103}$$

Since the turbulence signal and the noise signal are two independent random signals, they are not correlated and hence

$$\overline{V_R\,V_N} = 0 \tag{104}$$

Therefore, equation (103) reduces to

$$\overline{V_R^2} = \overline{V_T^2} - \overline{V_N^2} \tag{105}$$

Equation (105) provides a convenient method of resolving the true signal from the noise.

The following example for the calculation of the intensity of turbulence is based on the readings of the tranducer probe at a relative height of $x_{2/\bar{h}} = 0.065$ in the run of Series B at $R_N = 8.3 \times 10^4$.

$V'_T = 1.40$ volt at a gain of 1000

$V'_N = 0.52$ volt at a gain of 1000

As shown in Appendix B, the sensitivity of tranducer probe No. 3 is 14.0 millivolts per p. s. i. of pressure change. This is equal to 6.066 millivolts per foot of head change. Including 1000 times amplification, it becomes 6.066 volts per foot of head change. Designating the r. m. s. voltmeter reading due to true turbulence signal as V'_R, the above sensitivity combined with equation (2) in Appendix A gives

$$6.066 \frac{\bar{U}_1}{g} u'_1 = V'_R \tag{106}$$

Using equation (105) and the above values of V'_T and V'_N, the corresponding value of V'_R is given by

$V'_R = 1.30$ volt

and

$$\overline{U}_1 = 9.75 \text{ ft/sec}$$

Substituting the above values in equation (106),

$$\frac{6.066}{32.2} \times 9.75\, u_1' = 1.30$$

$$u_1' = \frac{1.30}{1.838} = \underline{0.707} \text{ ft/sec}$$

One-Dimensional Energy Spectral Density Function

From equation (3) in Appendix A,

$$\Delta \overline{V_R^2} = \Delta \overline{u_1^2} \quad \frac{C^2 \overline{U}_1^2}{g^2} \tag{107}$$

or

$$\Delta \overline{u_1^2} = \frac{g^2}{C^2 \overline{U}_1^2} \quad \Delta \overline{V_R^2} \tag{108}$$

Similarly,

$$\Delta \overline{u_1^2}\,(n) = \frac{g^2}{C^2 \overline{U}_1^2} \Delta \overline{V_R^2}\,(n) \tag{109}$$

The wave number is related to the frequency by the expression,

$$K_1 = \frac{2\pi n}{\overline{U}_1} \tag{110}$$

$$\Delta K_1 = \frac{2\pi}{\overline{U}_1} \Delta n \tag{111}$$

Equation (109) may also be written in the form,

$$\Delta \overline{u_1^2}\ (k_1) = \frac{g^2}{C^2 \overline{U}_1^2} \Delta \overline{V_R^2}\ (k_1) \tag{112}$$

where

$\Delta \overline{V_R^2}\ (k_1)$ = mean square of the output of the wave analyzer in volts resulting from turbulence fluctuations contained within the band width provided by the analyzer at wave number k_1 corresponding to the frequency set on the wave analyzer

$\Delta \overline{u_1^2}\ (k_1)$ = turbulence energy of fluctuations contained in the band width at k_1 corresponding to frequency set on the wave analyzer.

Dividing equation (112) by equation (111),

$$\frac{\Delta \overline{u_1^2}\ (k_1)}{\Delta k_1} = E_1(k_1) = \frac{g^2 \Delta \overline{V_R^2}\ (k_1)\ \overline{U}_1}{C^2 \overline{U}_1^2 \times 2\pi \Delta n}$$

$$\therefore \quad E_1(k_1) = \frac{g^2 \Delta \overline{V_R^2}\ (k_1)}{C^2 \overline{U}_1\ 2\pi \Delta n} \tag{113}$$

The selected nominal band width = 30 c. p. s.

Actual band width established by the analyzer (see Appendix C) = 59.0 c. p. s. The common factor in equation (113)

$$= \frac{g^2}{C^2\, 2\pi \Delta n} = \frac{32.2^2}{6.066^2 \times 2\pi \times 59.0} = \underline{0.076}$$

The following example for the calculation of $E_1(k_1)$ is based upon the spectrum measurements at $x_{2/\bar{h}} = 0.065$ in the run of Series B at $R_N = 8.3 \times 10^4$ at nominal frequency 160 c. p. s. set on the wave analyzer.

The actual frequency is identically the same as the nominal frequency (See Appendix C). The local mean velocity $\bar{U}_1 = 7.53$ ft/sec. The corresponding wave number from equation (110) is

$$k_1 = \frac{2\pi \times 160}{7.53} = 133.5 \text{ ft}^{-1}$$

From measurements, $\Delta \overline{V_R^2}(k_1) = \underline{0.0507}$ volts^2. Substituting the above values in equation (113) one obtains

$$E_1(k_1) = 0.076 \times \frac{0.0507}{7.53} = \frac{7.6 \times 5.07}{7.53} \times 10^{-4}$$

$$= \underline{5.10 \times 10^{-4}} \text{ ft}^3/\text{sec}^2 \qquad k_1 = 133.5 \text{ ft}^{-1}$$

Longitudinal Average Macroscale of Turbulence

The average macroscale of turbulence is given by the equation (33)

$$L_{x_1} = \bar{U}_1 \int_0^\infty R_{E_1}(\tau)\, d\tau$$

Frenkiel (1958) suggested that when the correlation curve is such that the negative correlation coefficients exist, it will then be necessary to measure the coefficients $R_{E_1}(\tau)$ up to values of τ sufficiently large to allow determination of L_{x_1} with sufficient accuracy. Therefore, equation (33) may be rewritten

$$L_{x_1} \approx \overline{U}_1 \int_0^{\tau_c} R_{E_1}(\tau)\, d\tau \tag{114}$$

where τ_c represents the smallest value of τ at which the autocorrelation curve intersects the axis of τ.

The area under the autocorrelation curve up to the intersection point was obtained with a planimeter.

At $x_{2/\overline{h}} = 0.179$ for run of Series B at $R_N = 8.3 \times 10^4$

$$\int_0^{\tau_c} R_{E_1}(\tau)\, d\tau = 4.32 \text{ milliseconds}$$

$$\overline{U}_1 = 9.05 \text{ ft/sec.}$$

$$L_{x_1} \approx 9.05 \times 30.5 \times 4.32 = 1.19 \text{ cm.}$$

Longitudinal Microscale of Turbulence

From equation (101)

$$\lambda_{x_1} = \overline{U}_1 \cdot \tau \cdot r$$

At $x_{2/\bar{h}} = 0.179$ in run of Series B at $R_N = 8.3 \times 10^4$

$\bar{U}_1 = 9.05$ ft/sec

$\tau = 0.5$ milliseconds

$r = 2.00$

$\lambda_{x_1} = 9.05 \times 30.5 \times 0.5 \times 2.0 = \underline{0.276}$ cm .

CHAPTER VI

RESULTS AND DISCUSSION

Distribution of Relative Intensity of Turbulence

For all the series of tests, the boundary-layer growth in the flume has been calculated using the empirical equation of Halbronn (1954), and it is found that at the sampling section the boundary-layer thickness already reached the depth of flow. It is also found that the flow in the channel corresponded to fully rough-wall condition ($u_* k_s/\nu > 70$) for all the runs with the artificial roughness on the bed. The most serious difficulty encountered in performing tests in open-channel flow is to keep the relative roughness constant. It should be noted that the relative roughness in an open-channel, unlike the case of pipe flow, varies with the depth of flow. Hence, variation in the Reynolds number of flow keeping the relative roughness constant has to be attained by varying the slope to increase the velocity. But with the expanded metal mesh glued to the bed of the flume, this could not be achieved while keeping the flow uniform. Thus, attempts to keep the depth of flow constant for all the runs in a series were dropped as it was considered that attainment of uniform-flow conditions was a more important objective. Therefore, even though the relative roughness would be a more pertinent parameter, the absolute roughness size 'k_s' (Nikuradse's equivalent

sand-grain roughness), which remains constant for the runs in a particular series, is chosen in place of relative roughness.

The distribution of relative intensities of turbulence in the open-channel is shown in Figures 9 to 11 for three different series (i. e., for three different bed-roughness conditions) at three Reynolds numbers. Figures 9 and 11 refer to fully-developed turbulent-flow conditions while Figure 10 corresponds to transition regime of flow. Not more than one measurement could be taken in the region of the law of the wall or the constant-stress layer whose thickness varies from 1/5 to 1/7 of the thickness of the boundary layer or the depth of flow in this case. All three figures show that the relative intensity of turbulence decreases over the entire depth of flow as the Reynolds number increases. This result is in agreement with Laufer's (1951) measurements in air flow in a two-dimensional, smooth-surfaced channel. It could also be seen from these figures that the relative intensity of turbulence increases from the outer region of flow towards the bed of the channel. This increase is much more pronounced near the bed in the two cases with artificial roughness on the bed of the channel (Figures 9 and 11) indicating that the effect of roughness is more prominent near the bed than in the region far from the bed. In all cases, there is a tendency for the relative intensity of turbulence to approach a constant value towards the surface indicating that the influence of the variation of the Reynolds number is negligible near the surface. From Laufer's (1951) measurements,

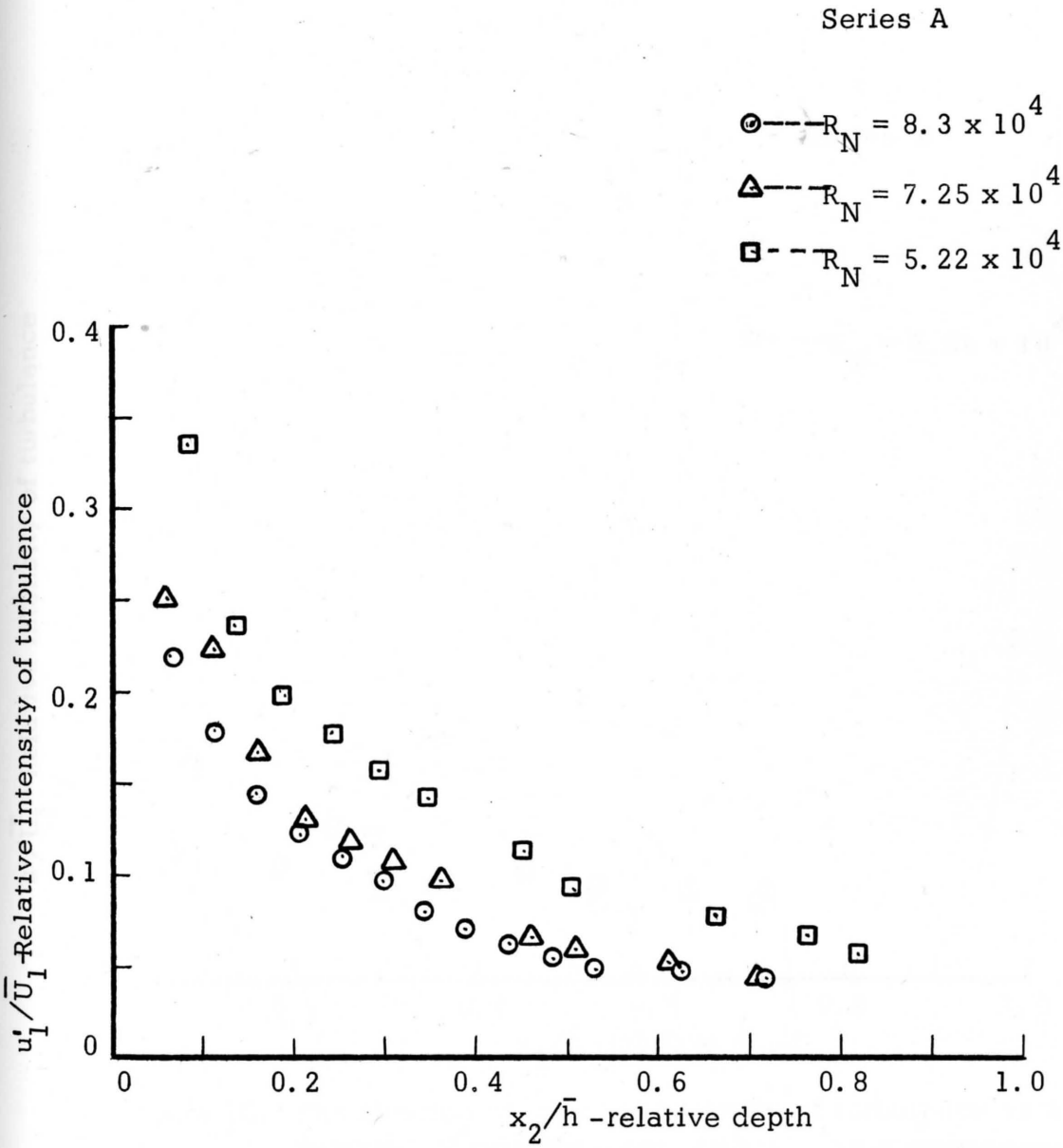

Figure 9. Distribution of relative intensity of turbulence as a function of relative depth with R_N as a parameter -- Series A.

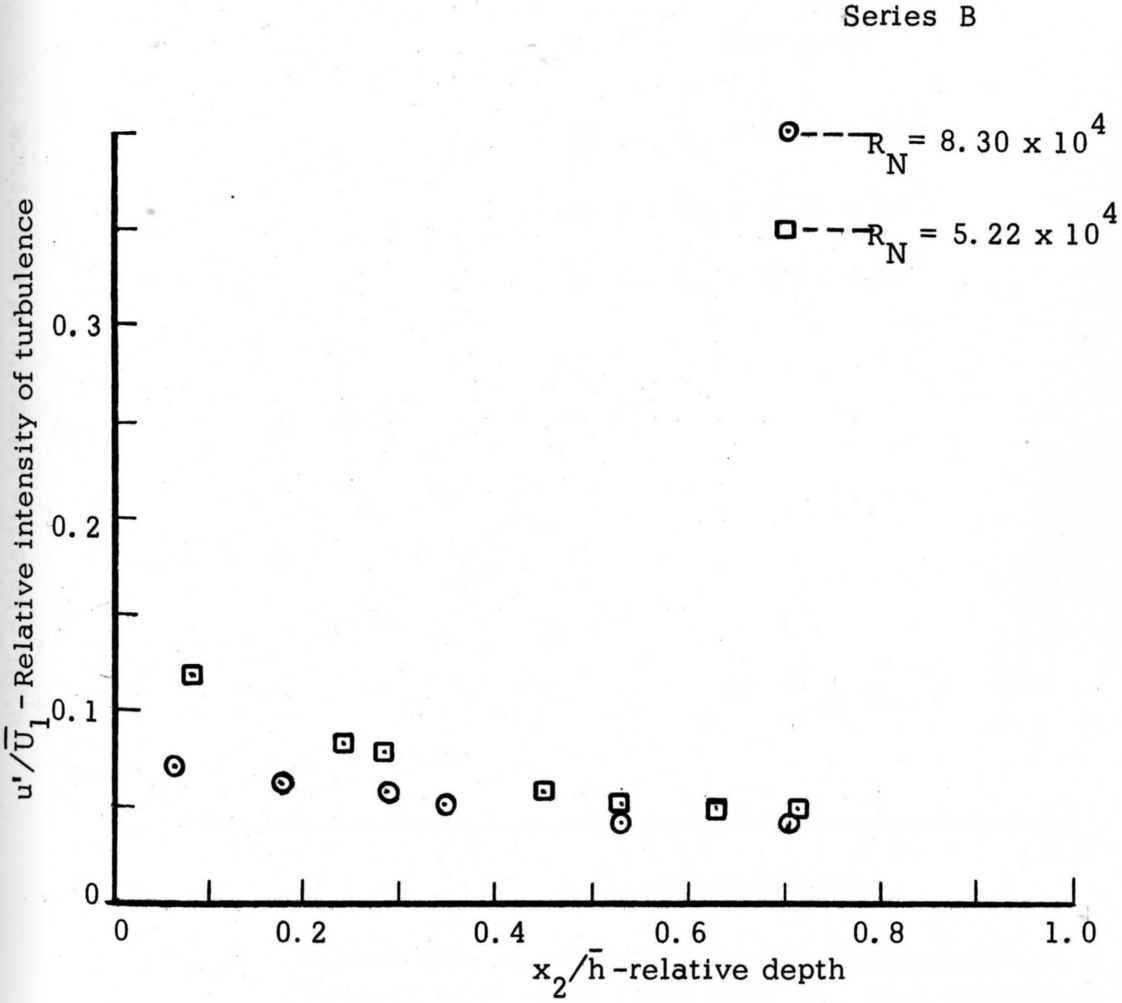

Figure 10. Distribution of relative intensity of turbulence as a function of relative depth with R_N as a parameter--Series B.

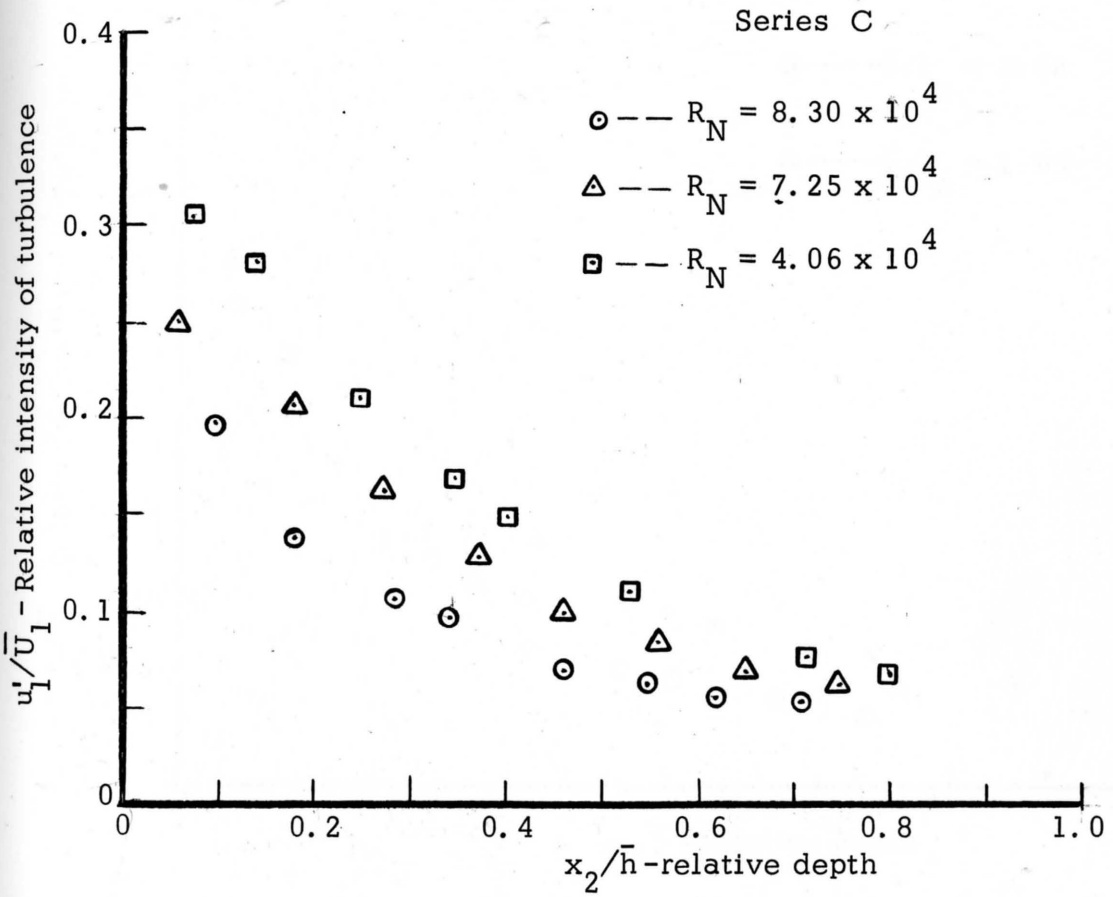

Figure 11. Distribution of relative intensity of turbulence as a function of relative depth with R_N as a parameter--Series C.

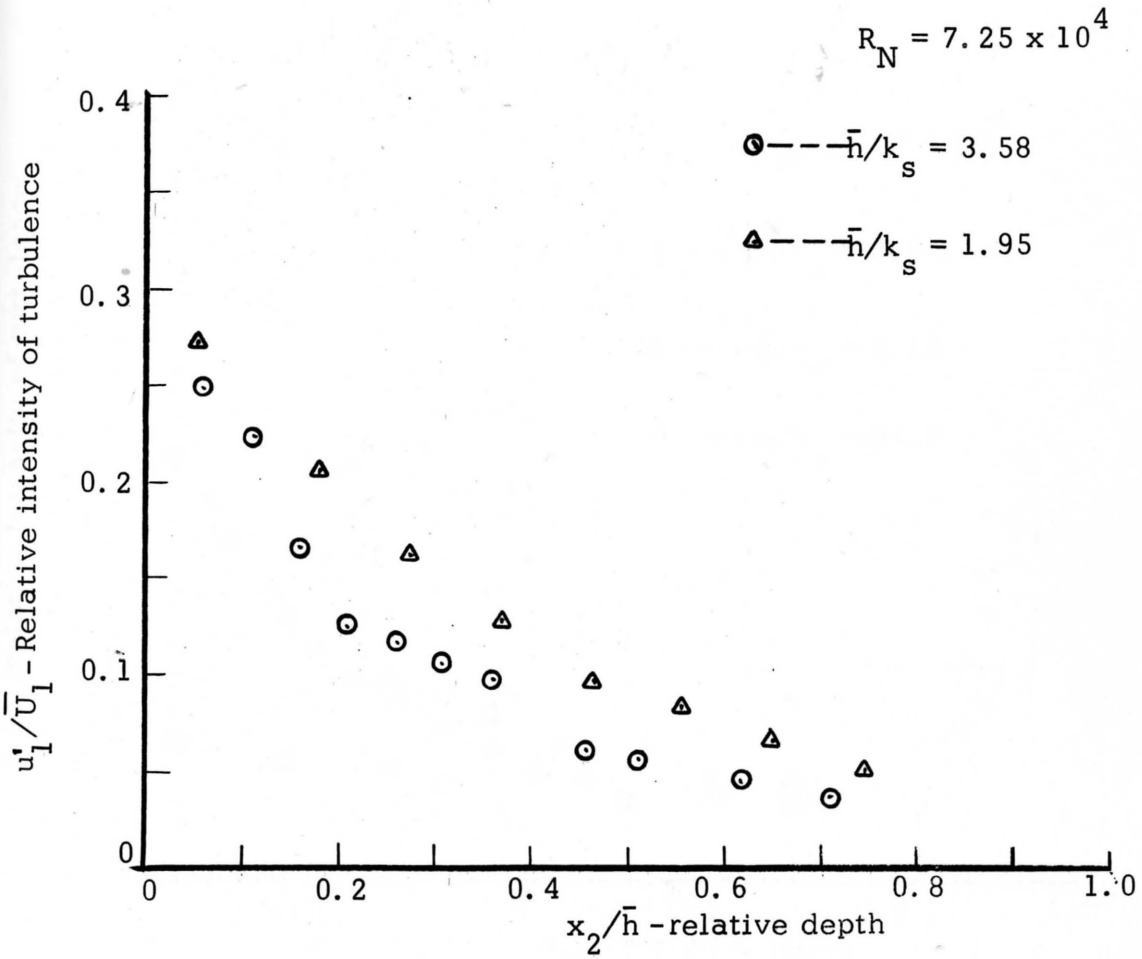

Figure 12: Distribution of relative intensity of turbulence as a function of relative depth with relative roughness as a parameter at $R_N = 7.25 \times 10^4$.

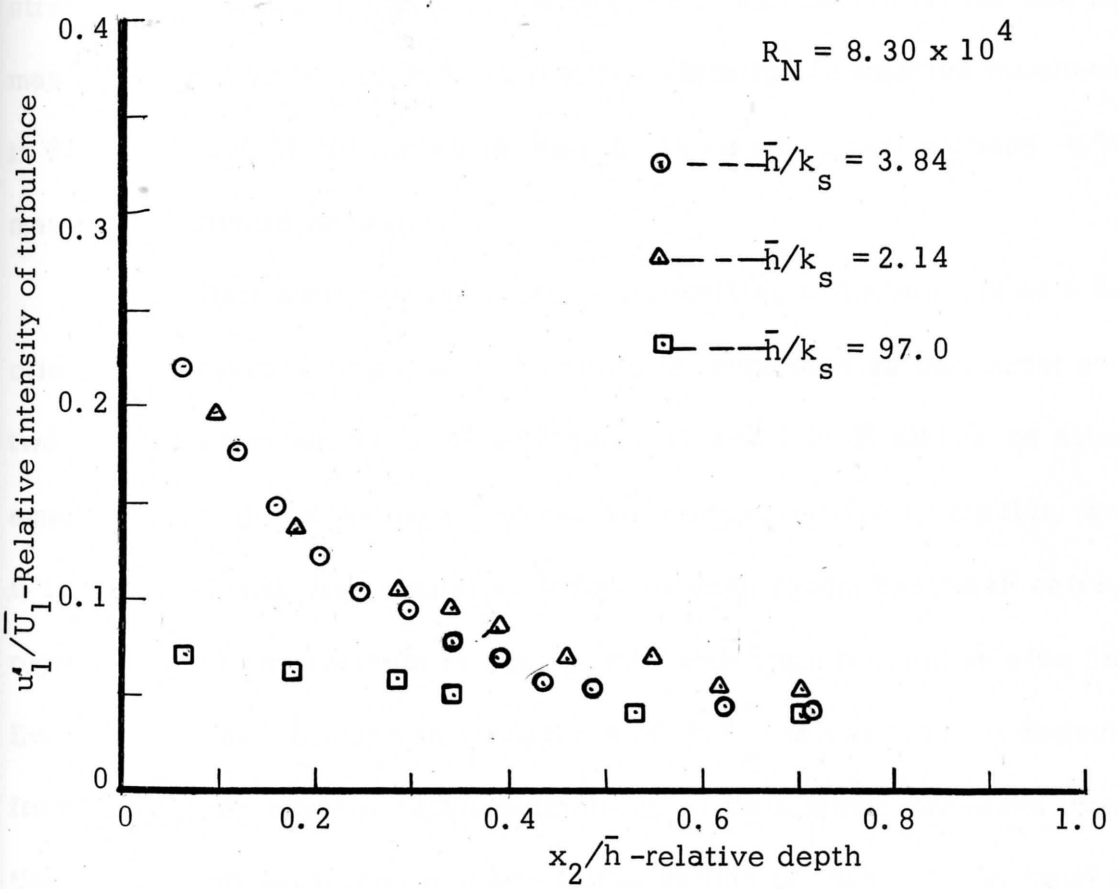

Figure 13. Distribution of relative intensity of turbulence as a function of relative depth with relative roughness as a parameter at $R_N = 8.30 \times 10^4$.

it is known that the relative intensity of turbulence reaches a maximum value at the edge of the laminar sublayer in two-dimensional channel flow over a smooth surface. From the results presented in Figures 9 to 11, it appears that in the case of rough open-channel flow in which the viscous sublayer is completely disrupted at $u_* k_s/\nu > 55$, the maximum value of relative intensity of turbulence is reached somewhere in the constant stress layer, i.e., in the region where the production of turbulence is maximum. It may be pointed out that the variation in relative roughness in Figures 9 and 11 for series A and C is so small that perhaps $\bar{h}/ks$ may be considered constant.

The distribution of the relative intensities of turbulence as a function of the relative depth with the relative roughness as parameter at two Reynolds numbers is shown in Figures 12 and 13. It should be strongly emphasized that the two roughnesses are not geometrically similar, and it is assumed that the cumulative effect of each roughness mesh can be represented by the calculated equivalent sand-grain roughness size "k_s'". Even though the variation in the values of $\bar{h}/k_s$ is not high, it appears from the figures that the relative intensity of turbulence increases over the entire depth with the decrease in the values of $\bar{h}/k_s$. The trend of the variation in the relative intensity of turbulence as a function of the depth of flow is not affected by the roughness at all even though its influence on the rate of variation of $u_1'/\bar{U}_1$ near the bed is quite appreciable.

One-Dimensional Energy-Spectrum Function

Energy spectra in the outer region of flow

The one-dimensional energy spectra of the longitudinal turbulence-velocity component in the turbulent shear flow in an open channel in the outer region and near the bed are presented in Figures 14 through 22. The spectra are all reasonably well fitted by a - 5/3 power law in k_1 over a considerable range as predicted by Kolmogoroff's theory (See Chapter III and equation (62)). This implies that the existence of the region of locally-isotropic turbulence independent of viscosity (inertial subrange) therefore is plausible. It should be strongly emphasized that the straight line fitting of the energy-spectra data having a slope of - 5/3 is not by itself an irrefutable evidence of the existence of the inertial subrange. There are a few other tests which the energy-spectra data should satisfy besides, before one could conclude the presence of local isotropy in wave-number space.

The shear spectrum is a direct test of local isotropy (See Hinze, 1959, p. 502). Corrison (1949) used the technique of measuring the variation of shear correlation coefficient with frequency to verify local isotropy in free-turbulent shear flow in a round jet. In this case the monotonic decrease of the shear correlation coefficient with frequency is a clear indication of the presence of local isotropy. Another method of checking local isotropy is to derive the spectrum function $E_1(k_1)$ from the measured $E_2(k_1)$ using the relation for isotropic turbulence given by Hinze (1959)

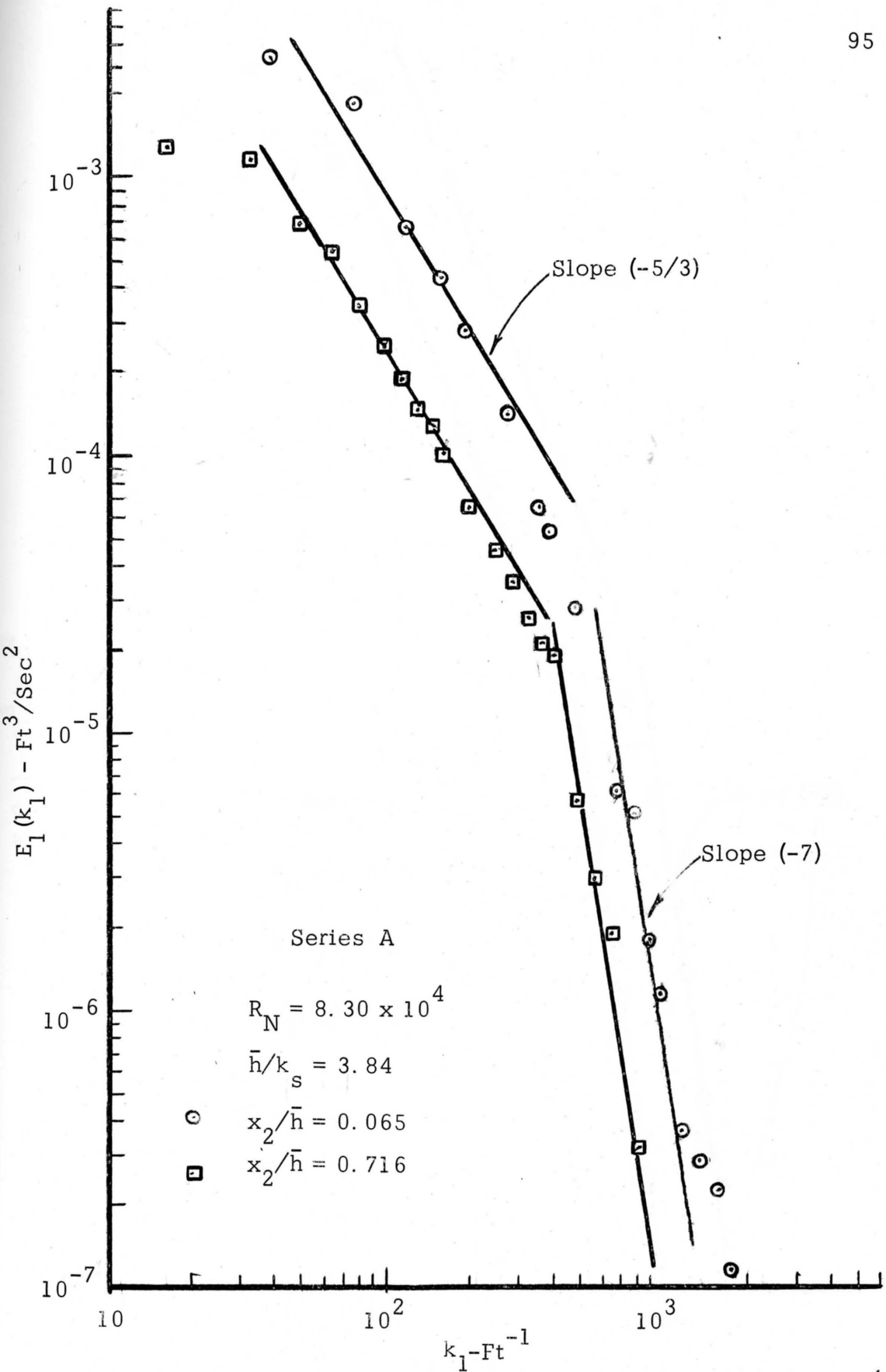

Figure 14. One-dimensional energy spectra at $R_N = 8.30 \times 10^4$--Series A

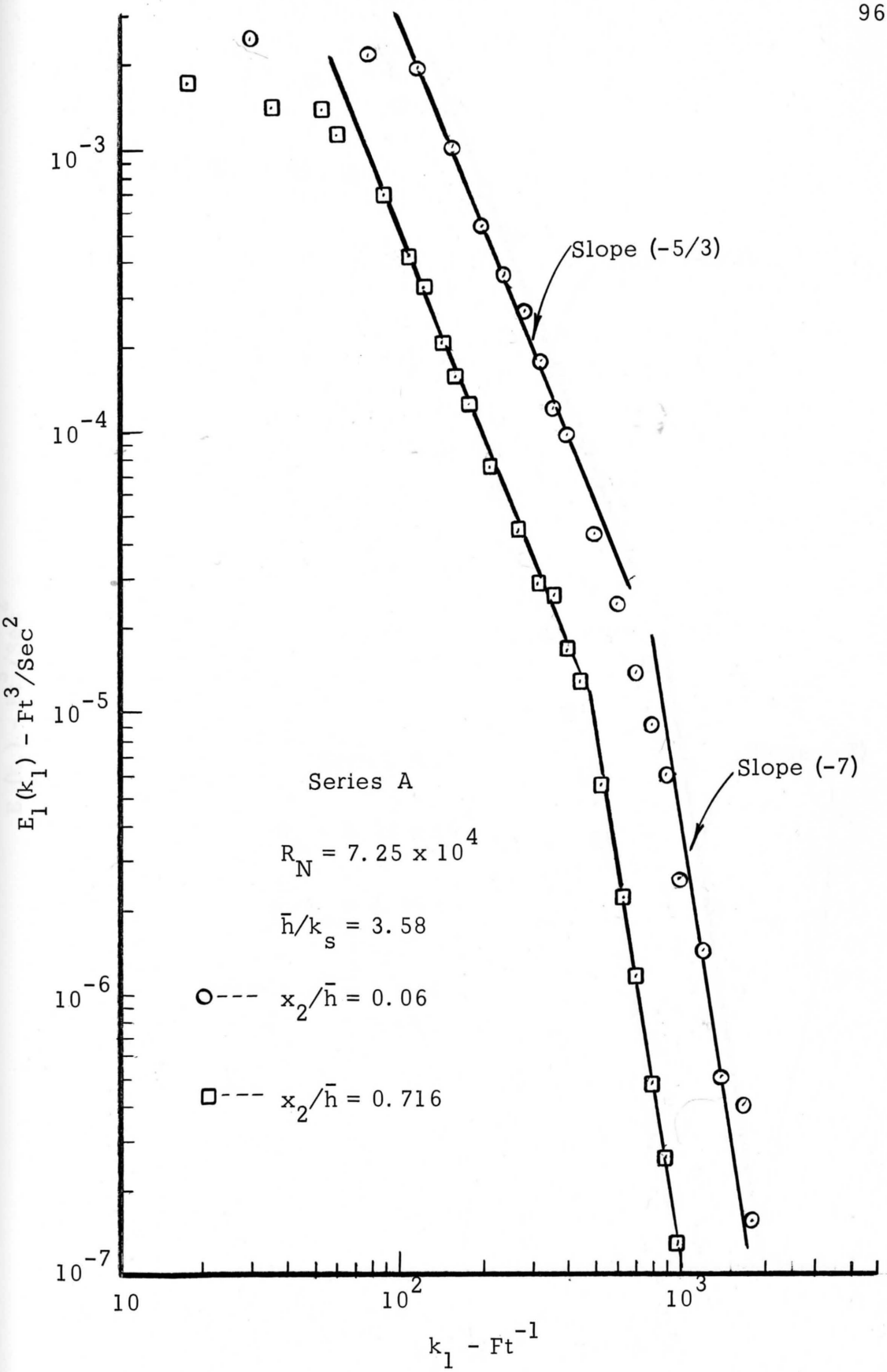

Figure 15. One-dimensional energy spectra at $R_N = 7.25 \times 10^4$-- Series A.

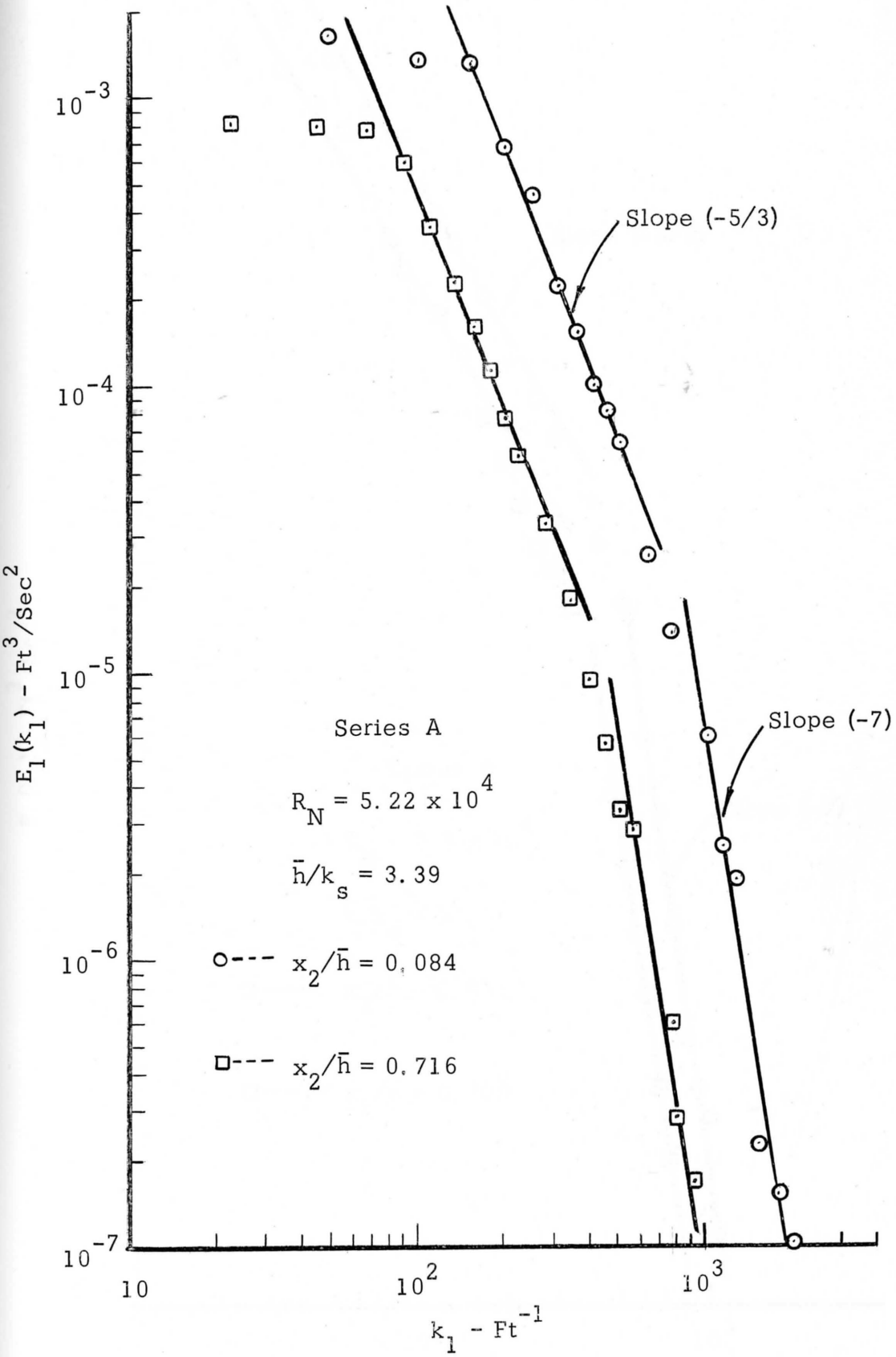

Figure 16. One-dimensional energy spectra at $R_N = 5.22 \times 10^4$-- Series A.

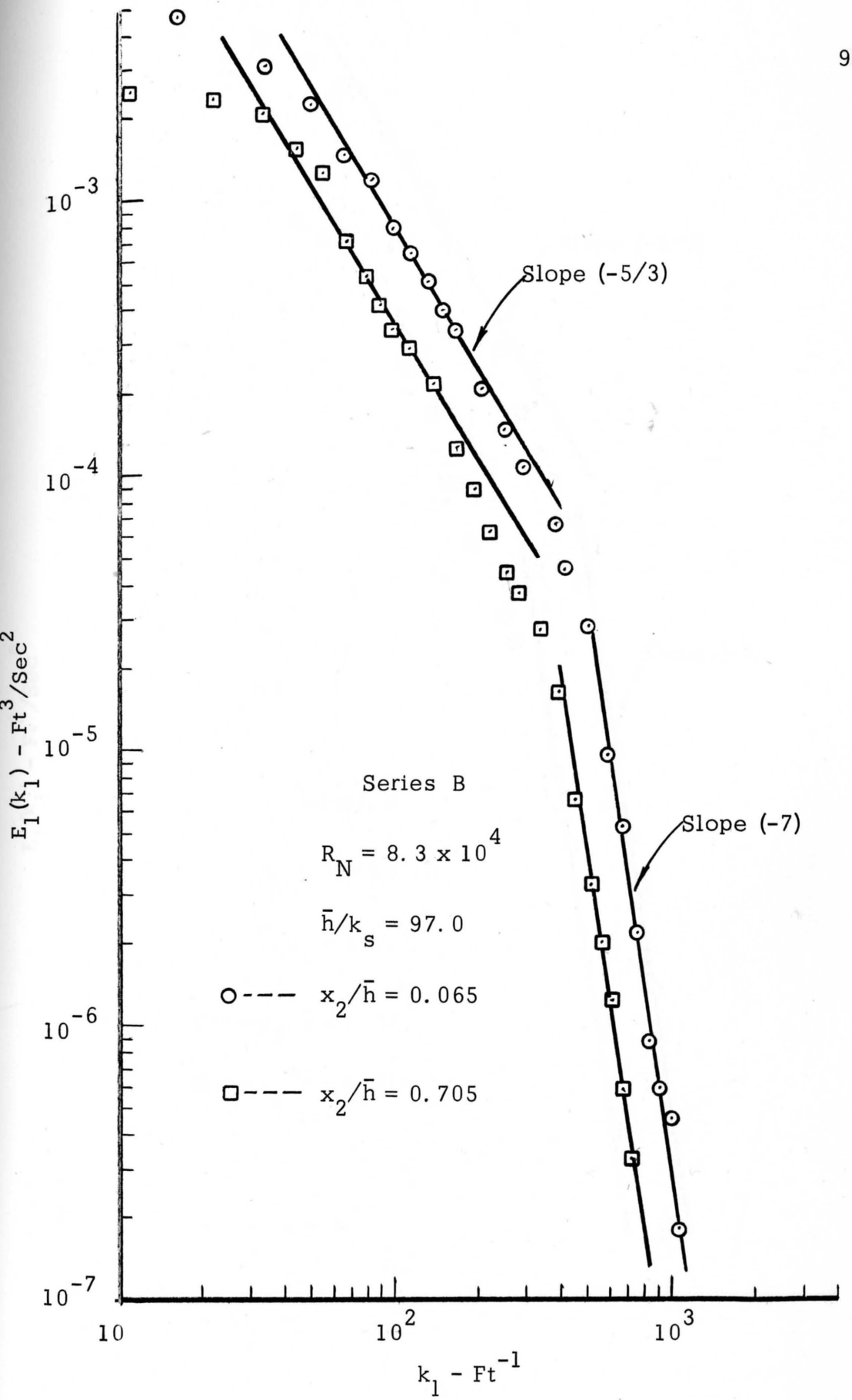

Figure 17. One-dimensional energy spectra at $R_N = 8.3 \times 10^4$ -- Series B

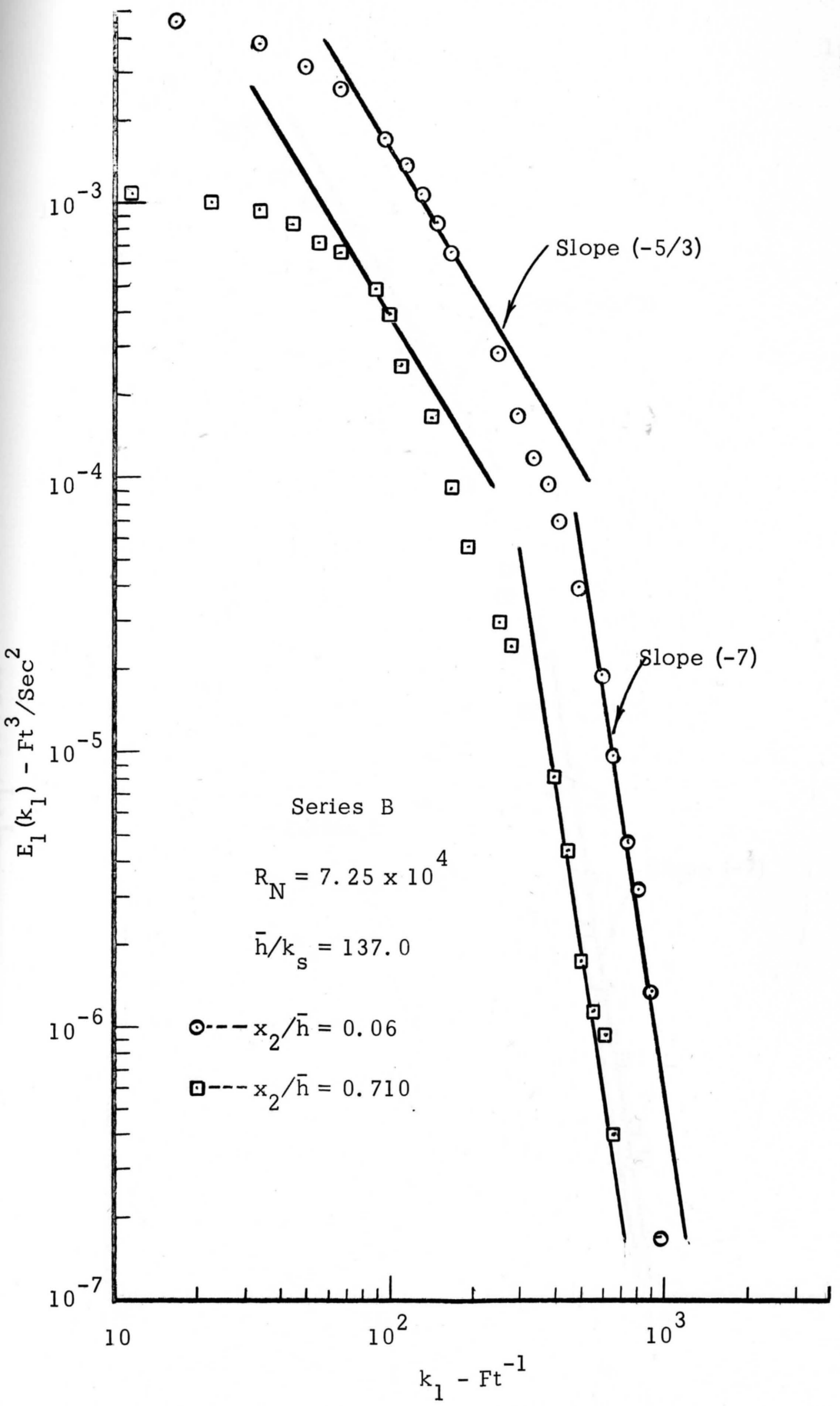

Figure 18. One-dimensional energy spectra at $R_N = 7.25 \times 10^4$--Series B.

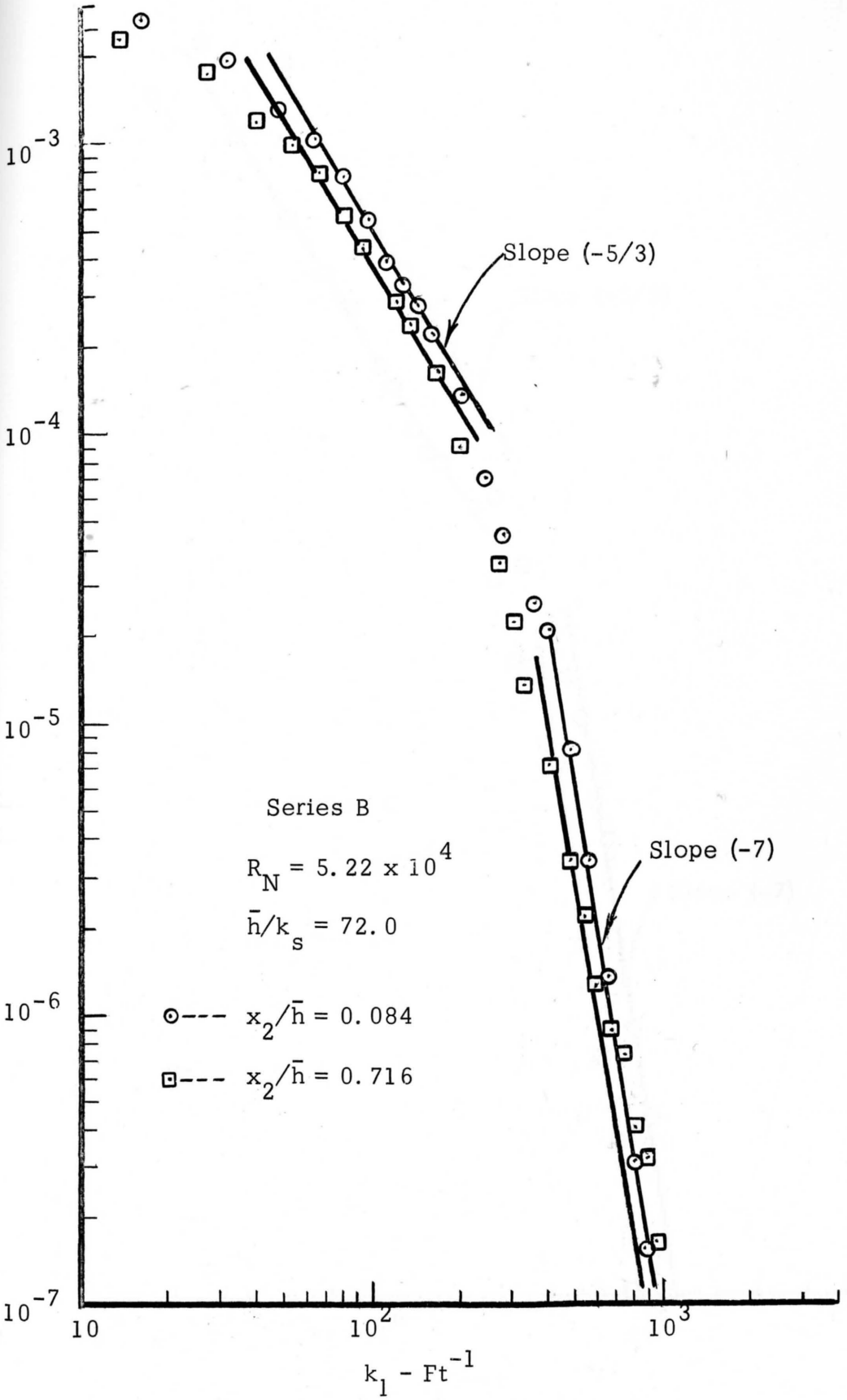

Figure 19. One-dimensional energy spectra at $R_N = 5.22 \times 10^4$ Series B.

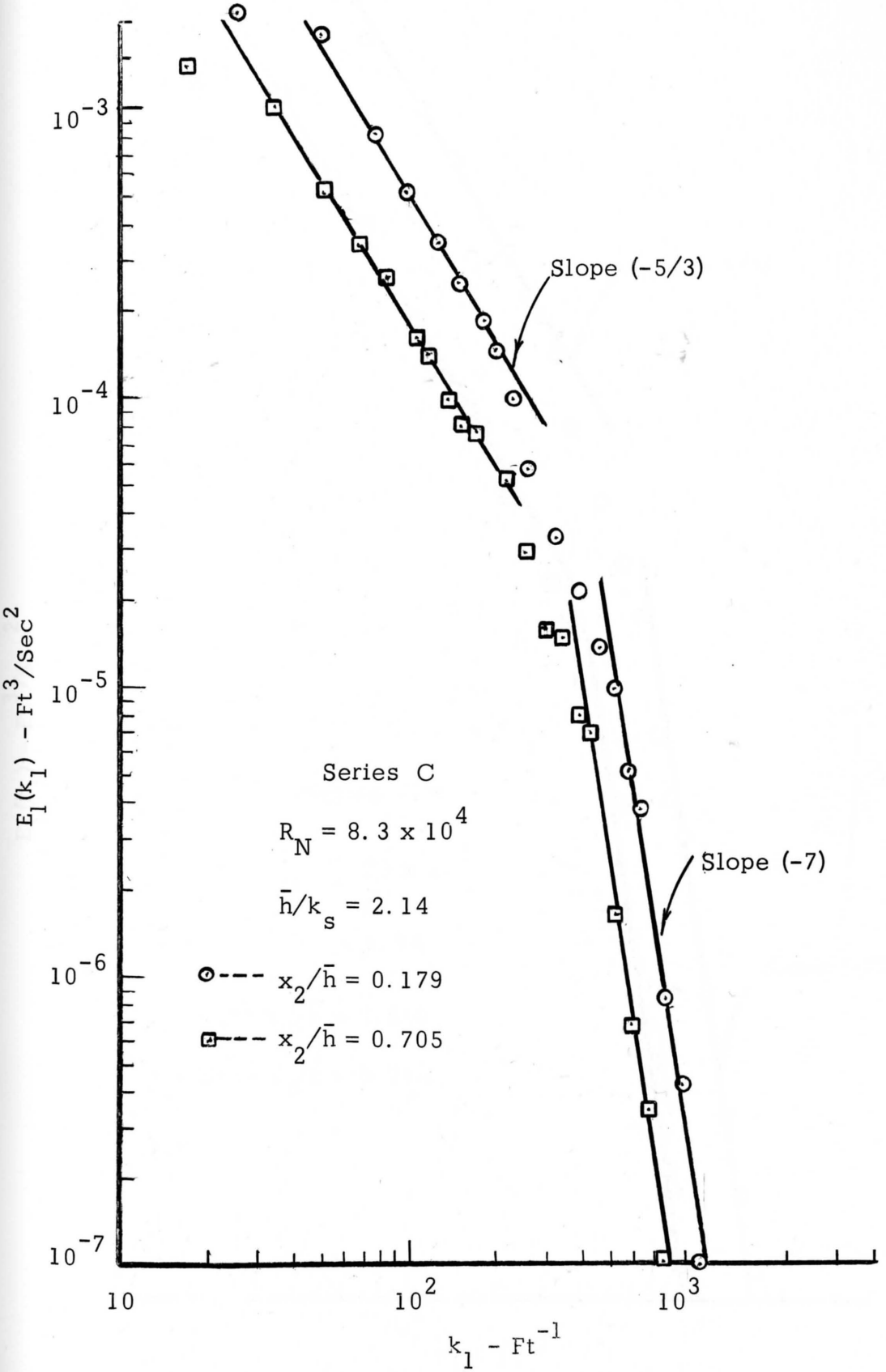

Figure 20. One-dimensional energy spectra at $R_N = 8.3 \times 10^4$-- Series C

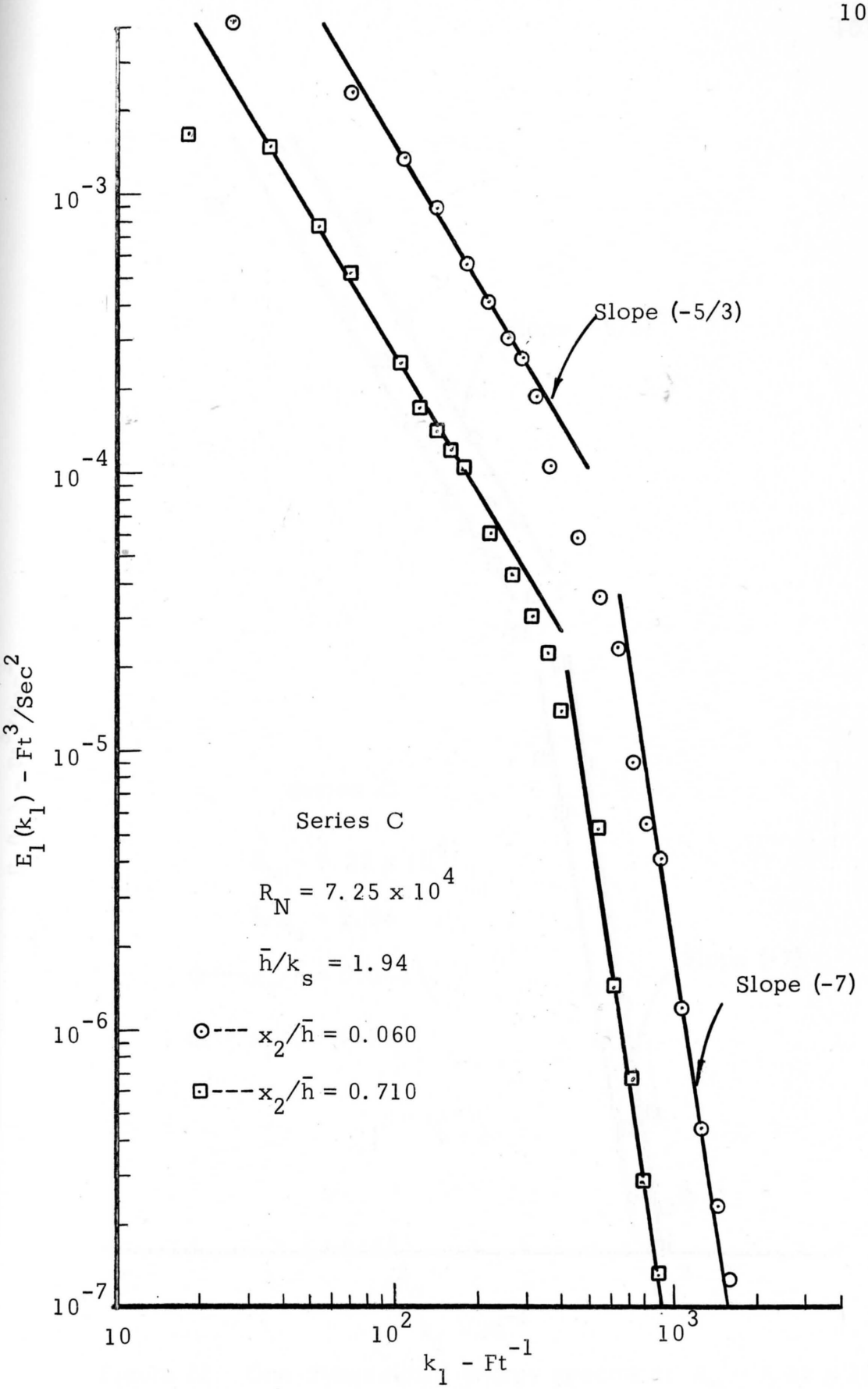

Figure 21. One-dimensional energy spectra at $R_N = 7.25 \times 10^4$-- Series C

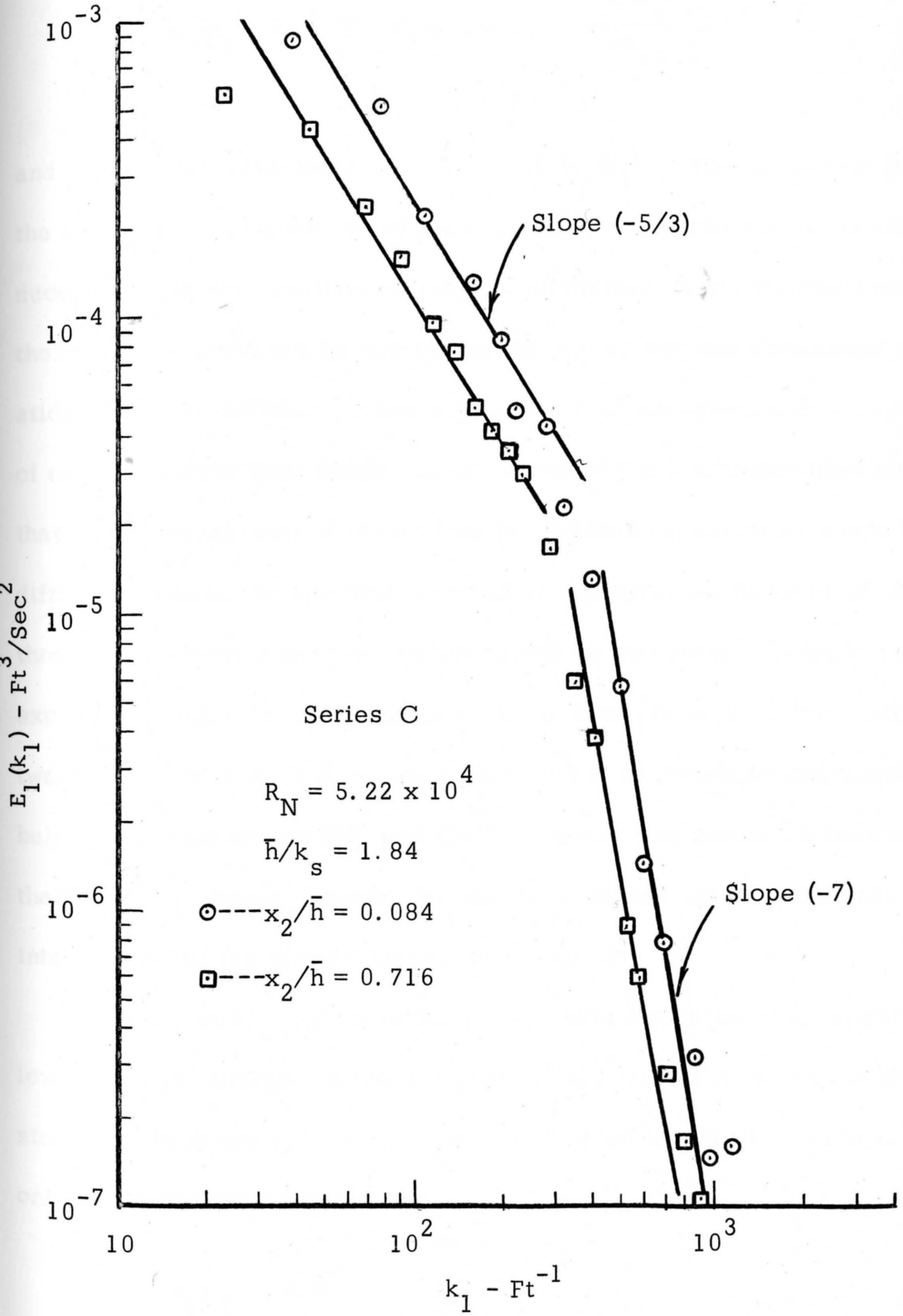

Figure 22. One-dimensional energy spectra at $R_N = 5.22 \times 10^4$--Series C.

$$E_2(k_1) = 1/2 \left(E_1(k_1) - k_1 \cdot \frac{\partial E_1(k_1)}{\partial k_1} \right) \qquad (115)$$

and compare with the measured values of $E_1(k_1)$. The agreement between the two is a good indication of local isotropy. Unfortunately, as the transducer probe is not sensitive to lateral turbulent-velocity fluctuations, these checks could not be applied to the energy spectra data under consideration. Another difficulty common to studies of energy-spectrum in all kinds of turbulent shear flow fields, irrespective of the instrumentation used, is that experimental tests of theoretical predictions on spectrum shape is made difficult because the spectral theories are constructed in terms of the three-dimensional spectrum, which cannot be measured. Comparison with experimental data is not possible in shear flow since the relationship between $E(k)$ and $E_1(k_1)$ is not known, but it is known for isotropic turbulence (See equations (56) and (57)). Hence one has to be content that in some unknown manner the one-dimensional spectrum is still an integral part of the three-dimensional spectrum.

Pond, et al. (1963) deduced a formula for estimating roughly the lower limit of isotropy on the basis of the argument that when the rate of strain to which any volume of fluid is subjected is chiefly due to turbulence only, isotropy can be expected:

$$k_1 x_2 >> 4.5 \qquad (116)$$

The transition wave numbers obtained from energy spectra in the outer region of flow satisfy well the above relation. A convenient criterion for the probable existence of inertial subrange according to Laufer (1954) is that the turbulence should be fully developed and the turbulence Reynolds number $\left(\frac{u_1' \lambda_{x_1}}{\nu} = R_{\lambda_{x_1}} \right)$ should be greater than 200, and according to Corrison (1958) and Hinze (1959) $R_{\lambda_{x_2}}$ should be greater than 500 and 200 respectively. The values of $R_{\lambda_{x_1}}$ calculated are within a range of 196 to 374 . The best confirmation of the - 5/3 law of the inertial subrange comes from Grant et al. (1962) who measured the energy spectra in a tidal channel at a Reynolds number of 10^8, (based on depth of flow) a value which is inconceivable to obtain in laboratory experiments. The value of the Kolmogoroff's universal constant α in equation (61) is found to be between 1.375 and 1.530 on the basis of their spectral measurements. It should be noted that the constant α should be independent of the field of turbulence or the nature of flow involved. Hence this fact could be taken advantage of to verify the existence of local isotropy by estimating the value of α from the energy-spectra data furnished in Figures 14 through 22 and comparing the calculated values with the values quoted above. This will be done in a later section, and up to then the conclusion about the verification of the existence of local isotropy will be deferred.

The wave number at which the transition between local isotropy and anisotropy occurs for each depth of flow at a given position is independent of the Reynolds number according to the mechanism of generation, transfer, and dissipation of turbulent energy in wave number space as suggested by Kolmogoroff. As explained in the section on "Kolmogoroff's theory of local isotropy" (See Chapter III), the pulsations produced from the mean flow are of the order of the size of the characteristic dimension of the boundaries of flow, in this case, the depth of flow. The size of these pulsations characteristic of the production mechanism will not change, therefore, with the Reynolds number. Local isotropy occurs in that region of pulsations that is far enough removed in the cascading process so as to be independent of the production mechanism. Since, for a given depth, the region characteristic of production mechanism is independent of the Reynolds number, the point of transition to the region independent of the production mechanism (region of local isotropy in wave-number space) should also be independent of the Reynolds number. From the above analysis, the size of the pulsations characteristic of the production mechanism varies directly with the depth of flow. The wave number of these pulsations varies inversely as the depth of flow. The wave number at which the transition between locally-isotropic turbulence and anisotropic turbulence occurs should also vary inversely as the depth of flow. The transition wave numbers obtained from Figures 14, 15, and 16 for spectra at $x_{2/\bar{h}} = 0.716$ are plotted against the inverse of the

corresponding depths in Figure 23, which shows agreement between theory and experimental results.

Energy spectra near the bed

The plots of the longitudinal one-dimensional spectra near the bed of the channel are also presented in Figures 14 through 22. Over a wide range in k_1 the data fits well the $-5/3$ power spectral law. But as discussed before in Chapter III, Tachen (1953) showed that near the wall, due to the presence of considerable mean-velocity gradient, the interactions between the vorticities of the main motion and turbulence cause violent resonance. This results in the predominance of the production of turbulence energy over the dissipation and transfer of energy and leads to a spectral law $E_1(k_1) \propto k^{-1}$ in the wave number region where $E_1(k_1) \propto k_1^{-5/3}$ law normally exists when the vorticity of the main motion is small compared to the vorticity of the turbulence. Energy spectral data of Laufer (1954) obtained in pipe flow at $R_N = 5 \times 10^5$ and of Klebanoff and Diel (1952) obtained in boundary-layer flow at $R_N = U_o' \delta/\nu = 7.5 \times 10^4$ demonstrate the k^{-1} law. Since measurements could not be made in this work as close to the wall (or bed) as in the case of their measurements to attain the required conditions, it is suspected that the evidence of k^{-1} law of Tachen is absent in this data. Besides, it should be pointed out that the transition wave numbers obtained from the plots of energy spectral data near the bed of the channel do not satisfy the criterion for the lower limit of local isotropy furnished by the equation (116). In

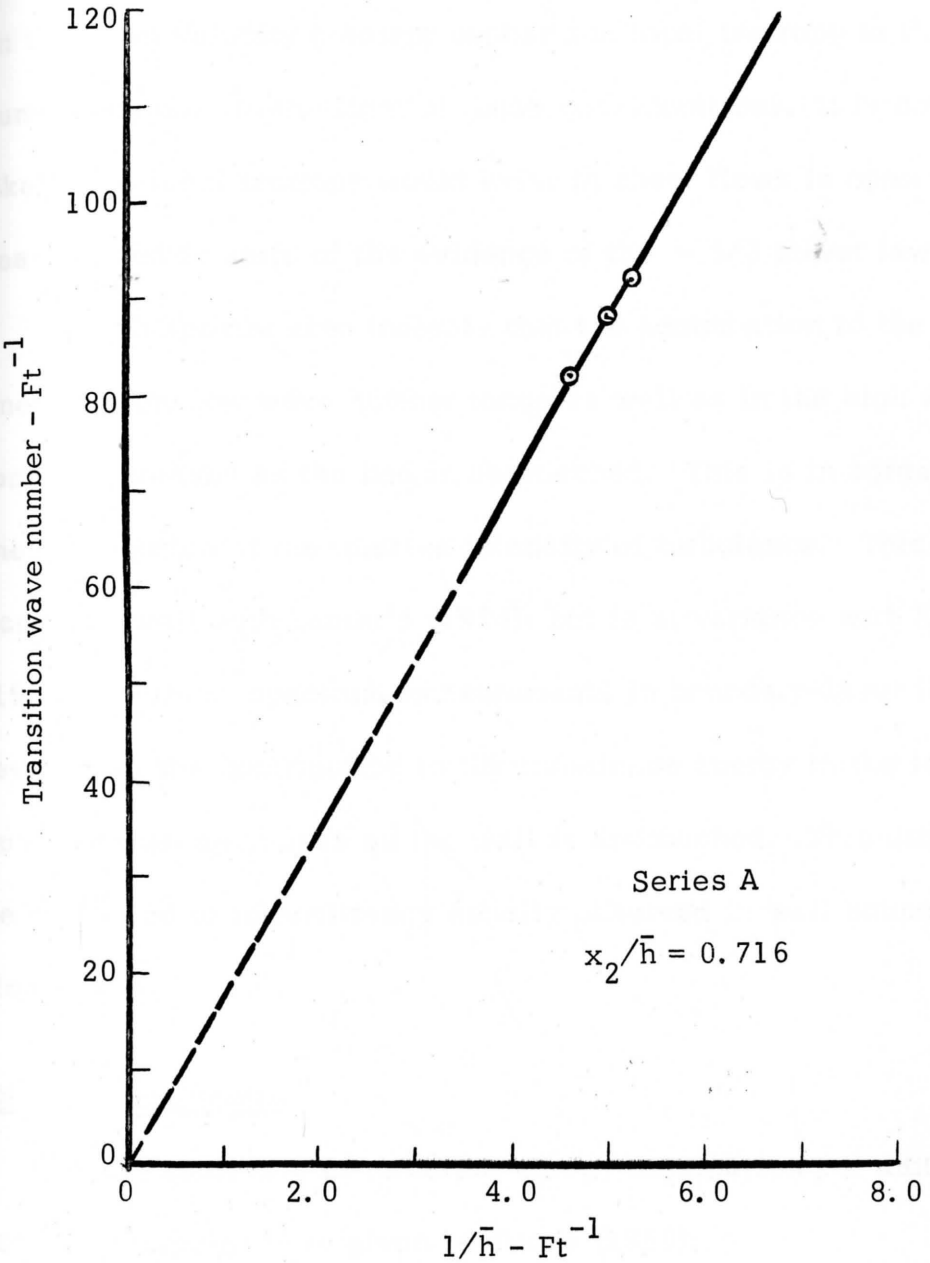

Figure 23. Effect of depth of flow on transition wave number.

addition the approximate analytical studies of Deissler (1961) and Fox (1964) (See Chapter III) indicate that the pressure forces which depend on the mean velocity gradient oppose the local isotropy in the high wave number region. In the light of these considerations, it is considered unlikely that local isotropy would exist in shear flows in open channels near the bed in spite of the evidence of the - 5/3 power law.

The spectra also indicate that the contribution to the turbulence energy in the low wave number range as well as in the high wave number range, increases as the bed is approached. This is in agreement with the distribution of the relative intensity of turbulence. This result also compares well with Laufer's (1954); but is at variance with Klebanoff's (1954) results of spectrum measurements in boundary-layer flow, which reveal that the contribution to the turbulence energy in the low wave number range decreases as the wall is approached. This difference may be attributed to intermittency usually observed in wall boundary-layer flows.

Dissipation spectra

The total rate of turbulent energy dissipation per unit mass in isotropic turbulence is given by Hinze (1959):

$$\epsilon = 2\nu \int_0^\infty k^2 E(k)\, dk = 15\nu \int_0^\infty k_1^2 E_1(k_1)\, dk_1 \qquad (117)$$

The functions of $k^2E(k)$ and $k_1^2E_1(k_1)$ are referred to as dissipation spectra and describe the distribution in wave number of the rate of decay

of turbulent energy to heat. Typical linear plots of one-dimensional dissipation spectra are shown in Figures 24 to 27. Some scatter in the plotted data between wave numbers 200 and 500 may be due to experimental errors. In drawing Figure 24, the general trend observed in Figures 25 to 27 has been followed as a guide. These curves do not differ much in form from those measured by Grant et al. (1959, 1962) in Discovery Passage and tidal channle, Gibson (1962, 1963) in a round jet, and Pond et al. (1963) in atmospheric boundary-layer in spite of the difference in the Reynolds number of flow and of turbulence. These linear plots of dissipation spectra are used to determine the total rate of dissipation assuming that the turbulence is isotropic over the range of wave numbers contributing to the integral in the equation (117). Since the contribution to the integral of the wave numbers below the transition wave number (wave number corresponding to lower-limit of local isotropy) is small compared to the total value of the integral, this assumption is justified. The range of values of ϵ obtained is 1.22×10^{2} to 4.65×10^{2} ergs cm^{-3} sec^{-1}.

The universal constant α' in Kilmogoroff's spectral law (See equation (62)) for inertial subrange is calculated for each run from the known values of ϵ determined as explained above and from the corresponding values of $E_1(k_1)$ equivalent to the intercepts at $k_1 = 10$ of the best fitting line of slope - 5/3 on the logarithmic plots of energy spectral data in Figures 14 to 22. The average value obtained in this work for α' is compared in the table below with those found by the other authors:

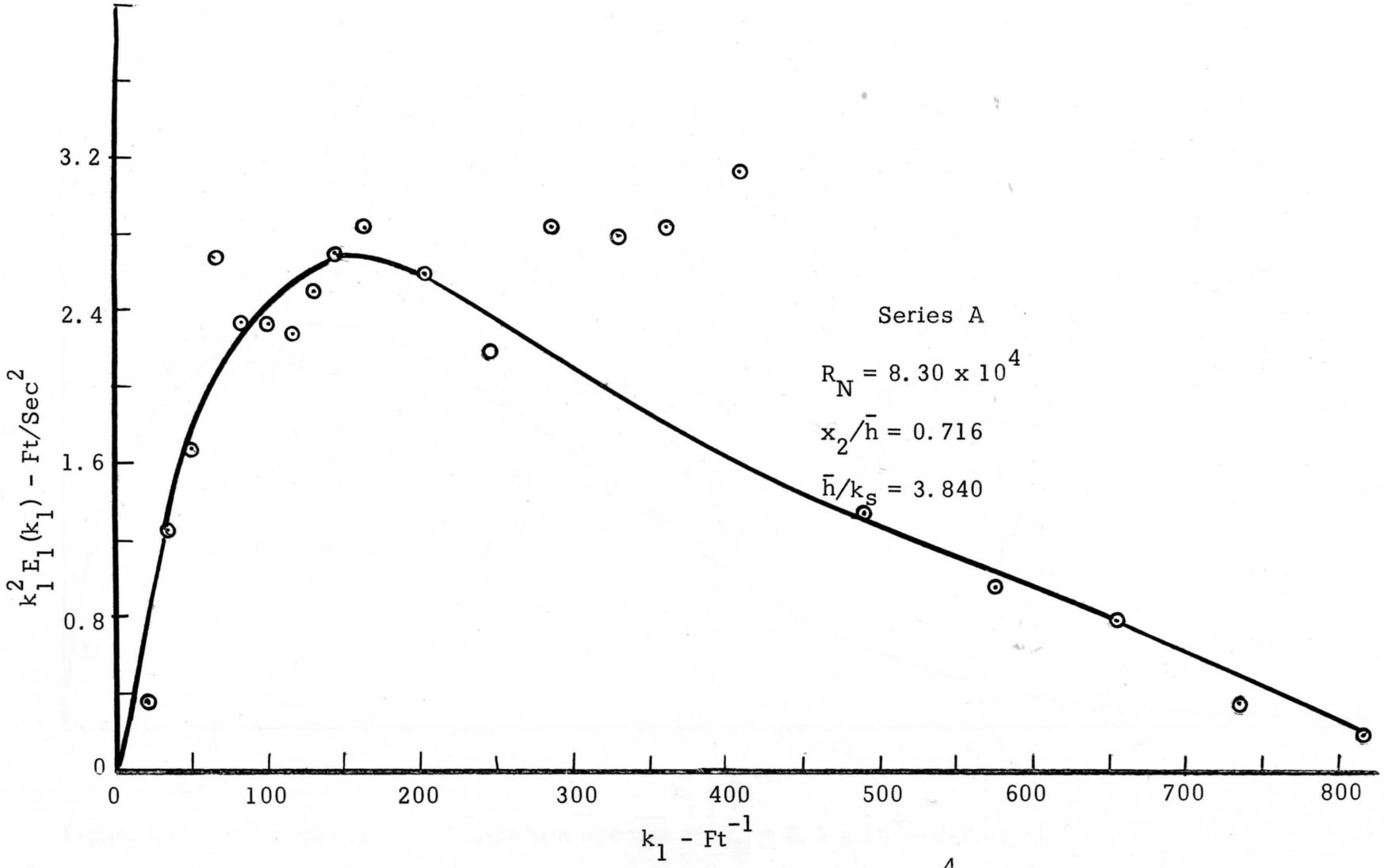

Figure 24. One dimensional dissipation spectra at $R_N = 8.3 \times 10^4$ -- Series A.

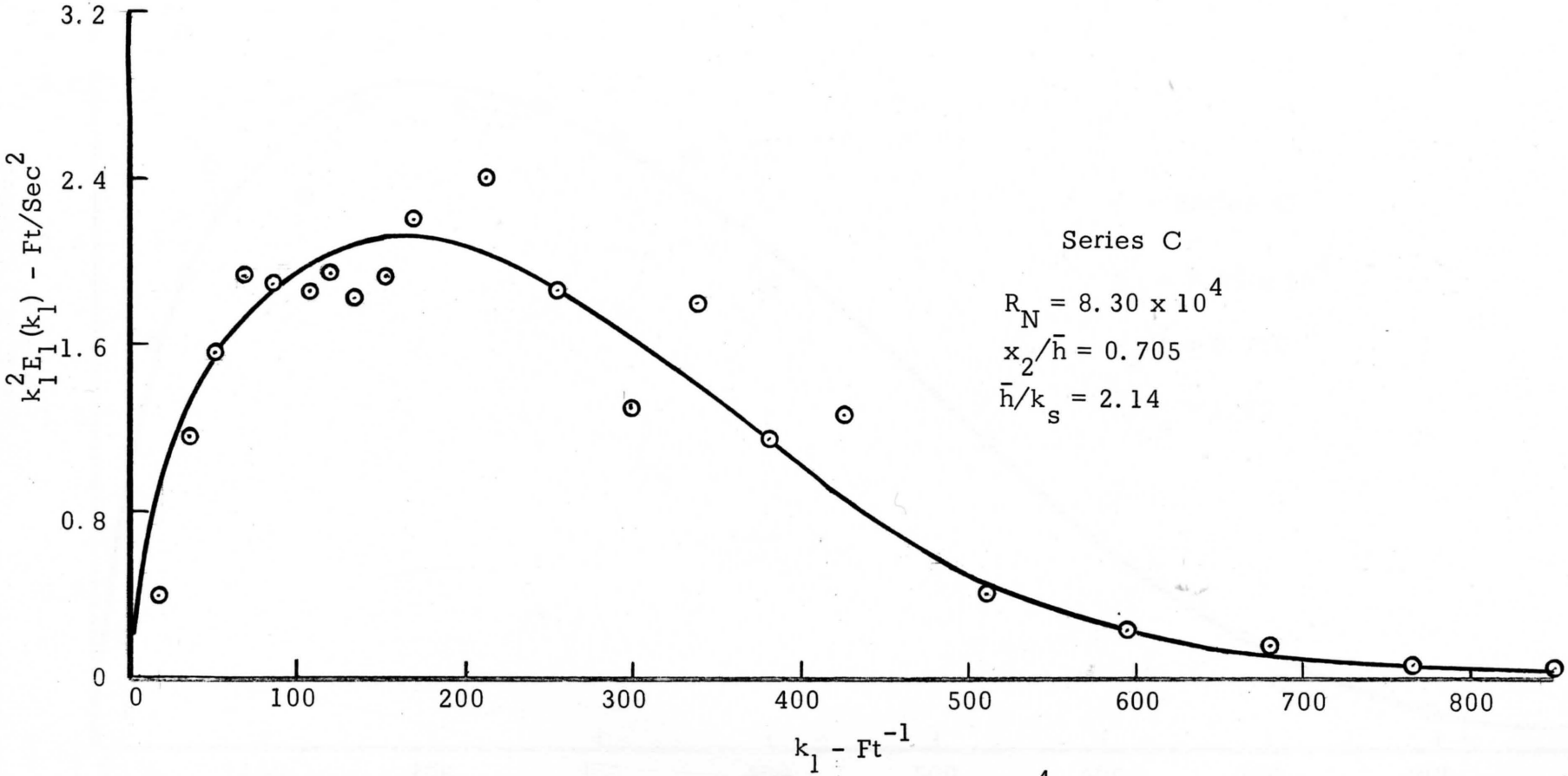

Figure 25. One-dimensional dissipation spectra at $R_N = 8.3 \times 10^4$--Series C.

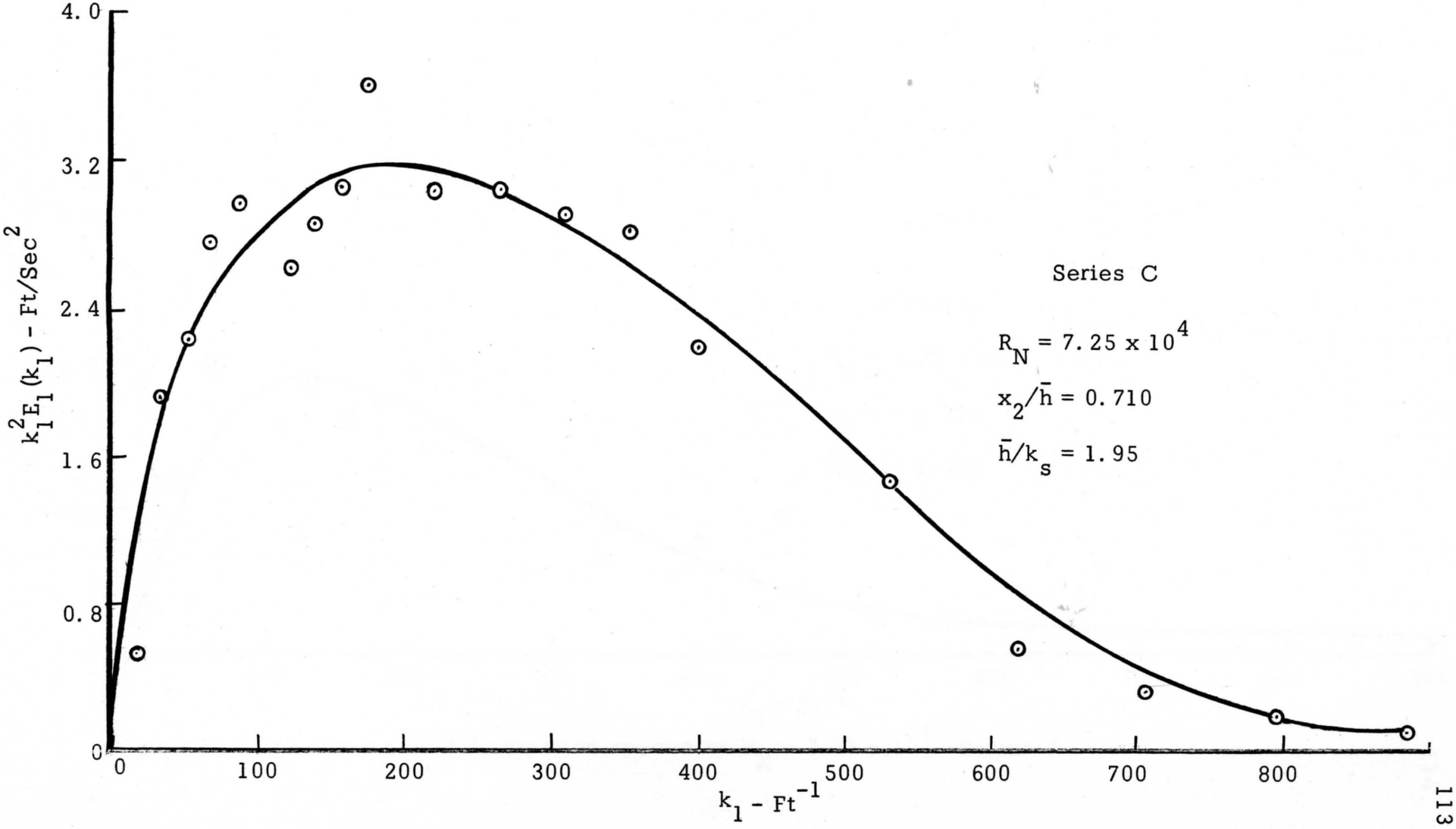

Figure 26. One-dimensional dissipation spectra at $R_N = 7.25 \times 10^4$--Series C.

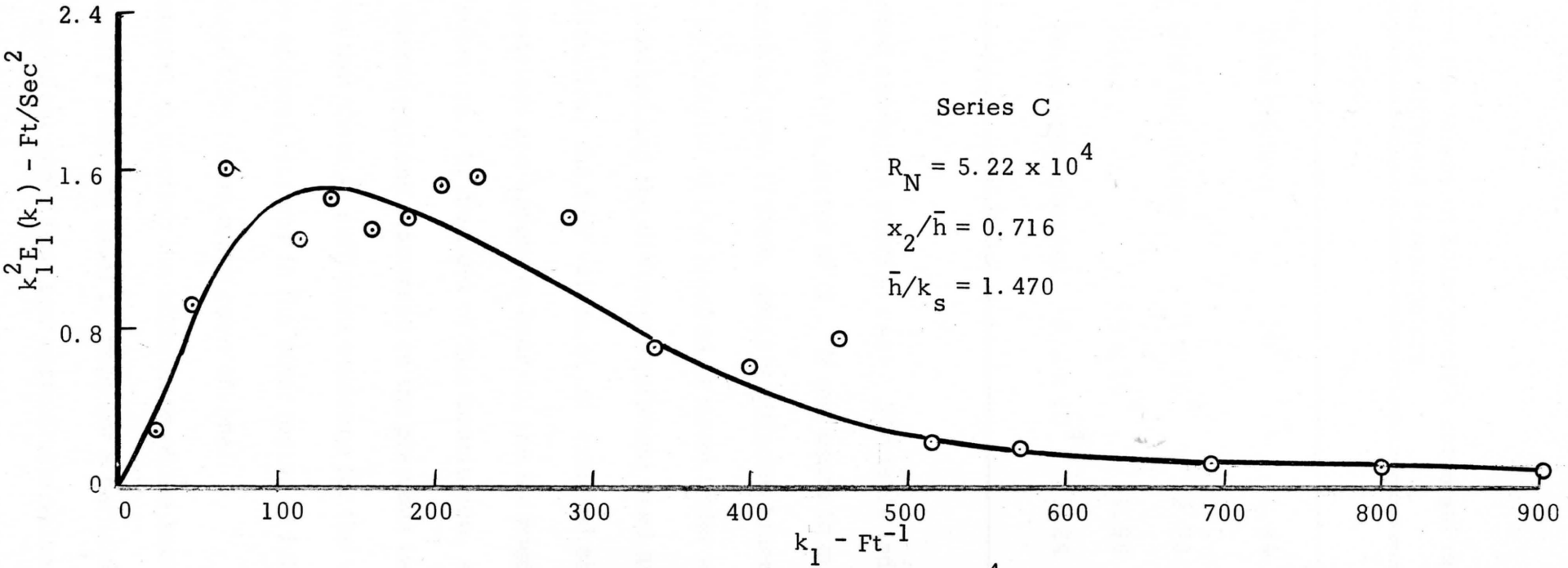

Figure 27. One-dimensional dissipation spectra at $R_N = 5.22 \times 10^4$--Series C.

Table 1. Comparison of the values of Kolmogoroff's universal constant α' evaluated by different investigators.

Author	Flow	R_N	α	α'
Grant et al. (1962)	Tidal channel	10^8	1.44	0.472
Gibson and Schwartz (1963)	Grid turbulence	1×10^4	2.70	0.885
Laufer (1954)	Pipe	5×10^4	1.96	0.642
Present work	Rough open channel	8.3×10^4	3.24	1.006

The values quoted above are average ones. The table indicates that the value of α' varies by a factor of 2. If one bears in mind the different conditions (such as type of flow, grossly different kinematic dissipation rates varying by a factor of one hundred or more) under which the data of Table 1 were obtained and the different equipment used and associated experimental difficulties, the four values of α' reported above are perhaps reasonably consistent and appear to bear out the Kolmogoroff theory for an inertial subrange. In the light of this conclusion, as well as from various other considerations discussed in the previous two subsections, it is believed that there is sufficient evidence for the validity of Kolmogoroff's theory of local isotropy in the outer region of fully-developed turbulent shear flow in the rough open channel.

It may be of interest to mention the importance of the knowledge of the validity of Kolmogoroff's theory of local isotropy for a particular region in a specified field of turbulent shear flow and approximate value of α'.

An observation of $E_1(k_1)$ at one value of k_1 permits one to evaluate ϵ, the most important single measurement in a turbulent field. Average Reynolds stress and eddy viscosity can be calculated from 'ϵ' and mean-velocity distribution provided production and dissipation of energy balance, a hypothesis quite well confirmed for regions not too close to boundary.

Test of simplified form of Heisenberg's equation

Of all the physical transfer theories that are considered in Chapter III, Heisenberg's theory received the best attention as it is based on a more sound physical basis. Hence his theory has been singled out to be tested by the data presented in Figures 14 to 22. In the region of universal equilibrium range, the turbulence energy distribution function should be a function of ϵ, ν, and k. Beyond the respective transition wave numbers, the spectral data of runs in Series A and C in the outer region of flow should be representable by one equation. The difficulty of transforming the equation of Heisenberg (equation (68)) to the corresponding equation for the longitudinal one-dimensional spectrum function is pointed out in Chapter III. The two extreme cases resulting from this equation are given by equations (69) and (70). The corresponding longitudinal one-dimensional spectrum equations are given by (71) and (72). The simplified form of Heisenberg's equation for one-dimensional spectrum function is given by

$$E_1(k_1) = \frac{9}{55}\left(\frac{8}{9}\frac{\epsilon}{k_H}\right)^{2/3} k_1^{-5/3}\left[1 + \left(\frac{9 \times 63}{55}\right)^{3/4}\frac{8}{3}\frac{\nu^3}{\epsilon k_H^2}k_1^4\right]^{-4/3} \tag{118}$$

This has the form of equation (68) with the extremes given by equations (71) and (72). This simplified Heisenberg's equation will be tested to verify whether this could represent the entire region of universal equilibrium range.

Equation (118) could be written as

$$E_1(k_1) = 0.1513\left(\frac{\epsilon}{k_H}\right)^{2/3} k_1^{-5/3}\left[1 + 2.73\,\frac{1}{\epsilon k_H^2}k_1^4\right]^{-4/3} \tag{119}$$

By rearranging equation (119)

$$\left(\frac{E_1(k_1)}{0.1513\left(\frac{\epsilon}{k_H}\right)^{2/3} k_1^{-5/3}}\right)^{-3/4} = 1 + \frac{2.73}{\epsilon k_H^2}k_1^4 \tag{120}$$

The plot of the left-hand side of equation (120) against k_1^4 should give a straight line with an intercept of unity. Such sample plots are shown in Figures 28 and 29. It is seen from these figures that the straight line correlation predicted by equation (120) is obtained. Hence it could be considered that the transition region between inertial subrange and the viscous subrange is correctly represented by the simplified form of Heisenberg's equation.

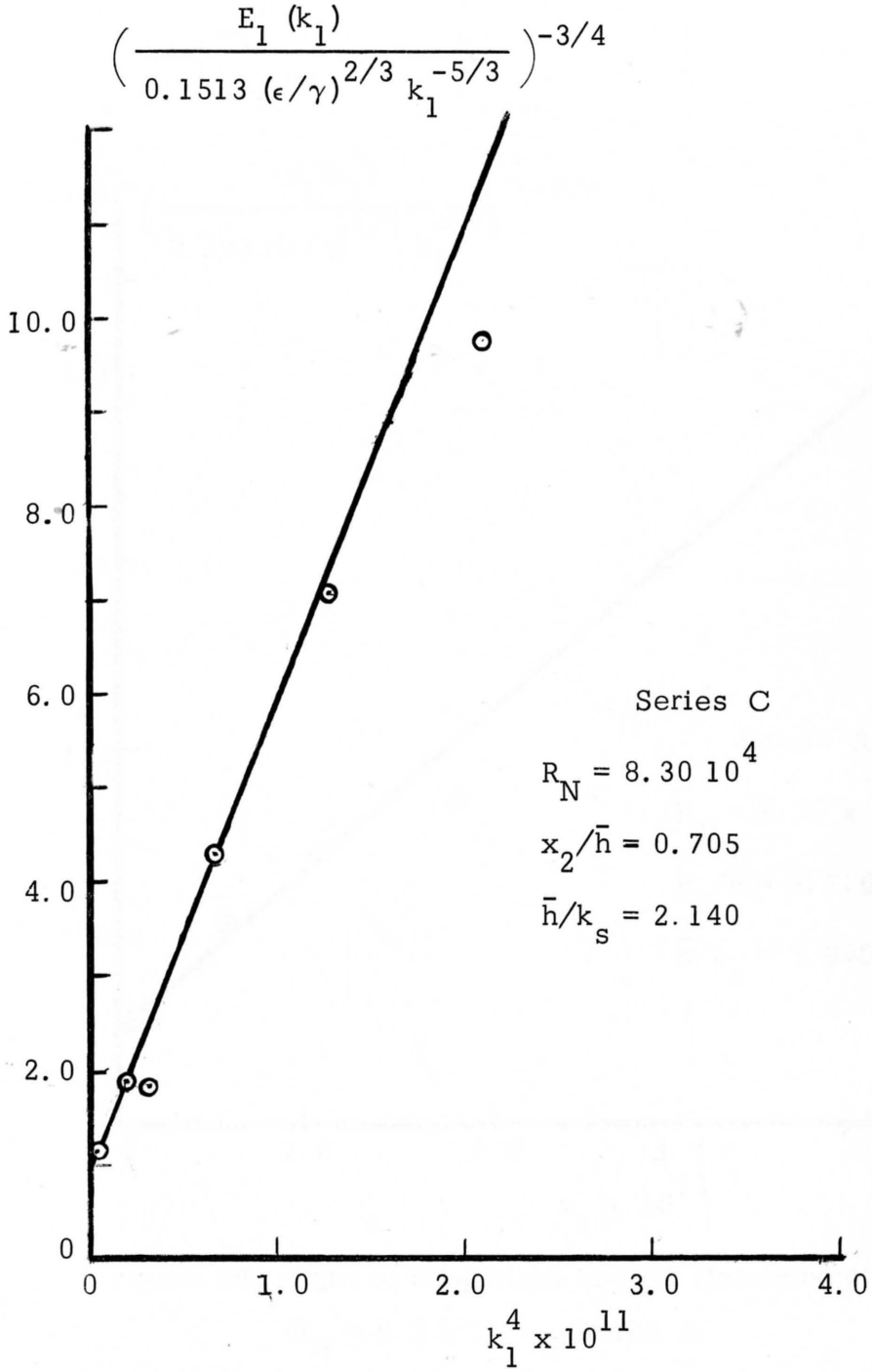

Figure 28. Test of simplified form of Heisenberg's equation at $R_N = 8.3 \times 10^4$ -- Series C.

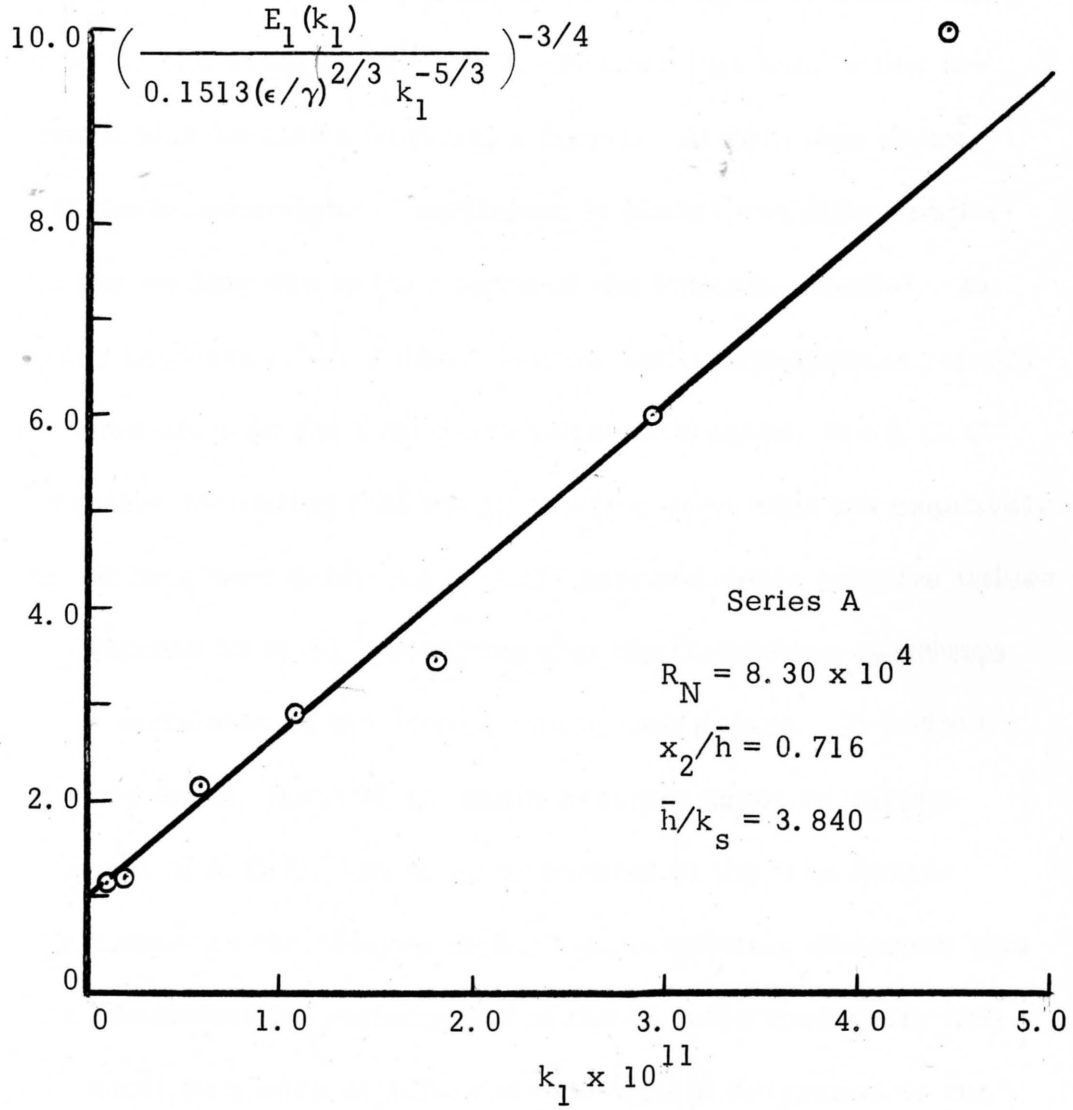

Figure 29. Test of simplified form of Heisenberg's equation at $R_N = 8.3 \times 10^4$-- Series A.

Autocorrelation Curves

Sample autocorrelation curves are shown in Figures 30 to 33. They are primarily used for calculating the average size of macroscale of turbulence as explained in Chapter V. Besides this use, a few inferences could also be drawn from these curves. At zero time delay the value of the autocorrelation coefficient is almost one (allowing for the error in the reading due to the inertia of the indicator needle). As the time delay increases, the autocorrelation coefficient reduces rapidly until it becomes zero. As the time delay further increases, the A. C. C. becomes negative indicating that the fluctuating quantities are negatively correlated. At long time delay the A. C. C. assumes again positive values as shown in Figures 30 to 33, indicating that the fluctuating quantities are positively correlated at the corresponding time delays. At further increase in time delay, the A. C. C. again assumes negative values. The measurement of A. C. C. had to be terminated at the time delays noted on the curves as the delayed signal was completely distorted; this is due to the characteristic performance of the variable time-delay network whose cutoff frequency at 3db band-width point decreases as the time delay increases. It should be mentioned, however, that this feature of time-delay network does not materially affect the measurement of the autocorrelation function as the high frequencies make little contribution to auto correlation function at large time delays.

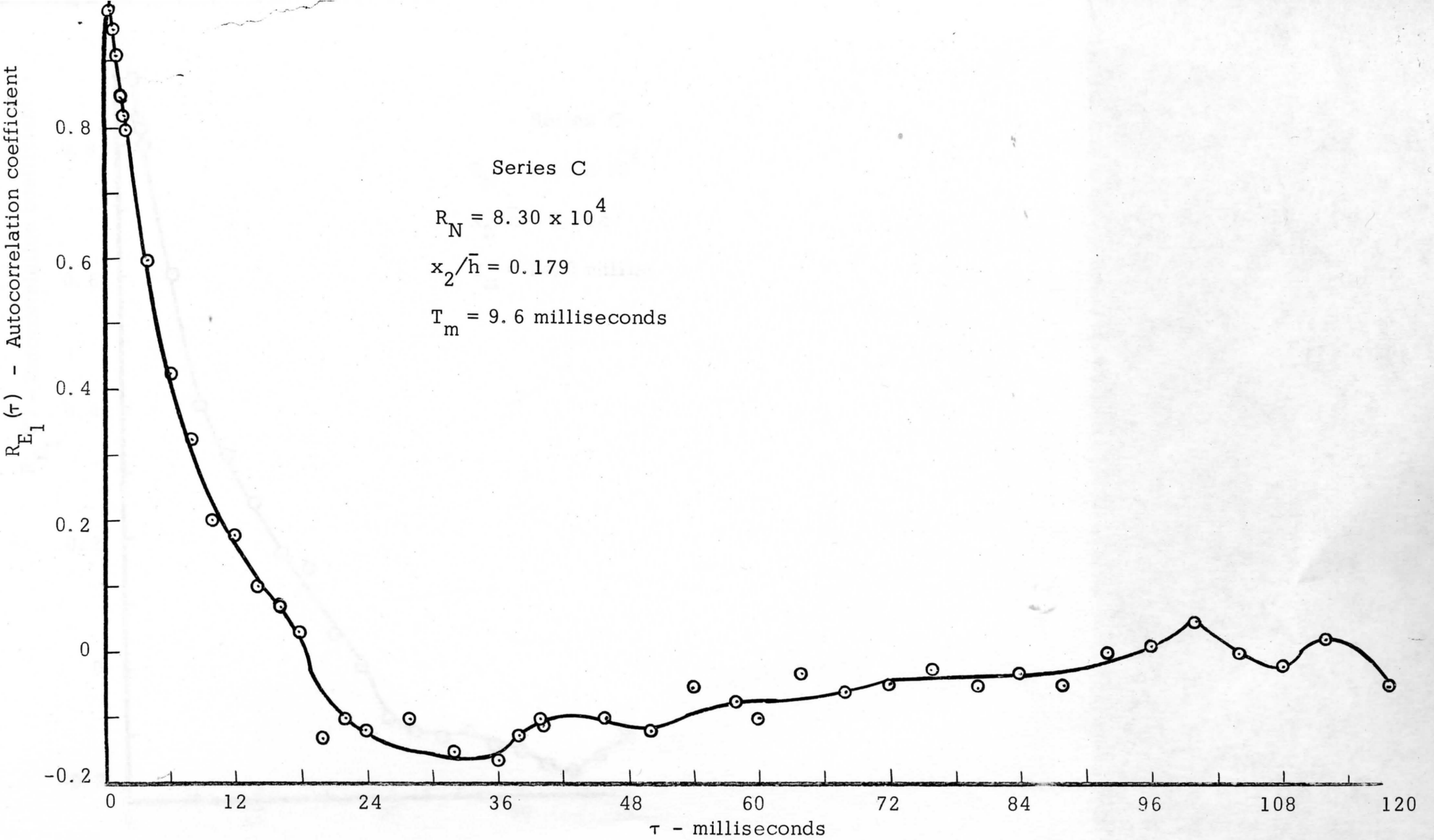

Figure 30. Autocorrelation curve at $R_N = 8.3 \times 10^4$ at a relative depth $x_2/\bar{h} = 0.179$ -- Series C

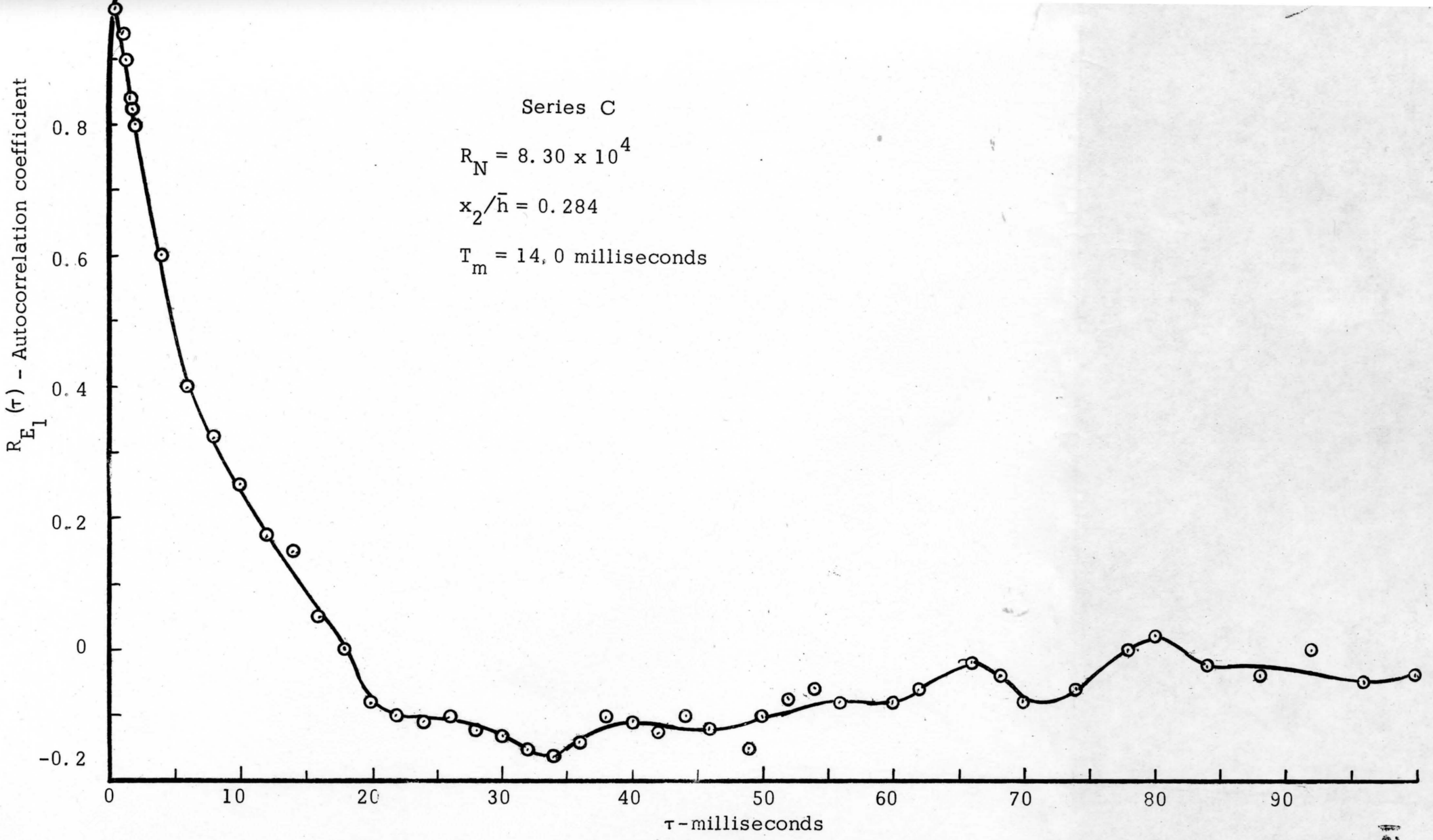

Figure 31. Autocorrelation curve at $R_N = 8.3 \times 10^4$ at a relative depth $x_2/\bar{h} = 0.284$ -- Series C.

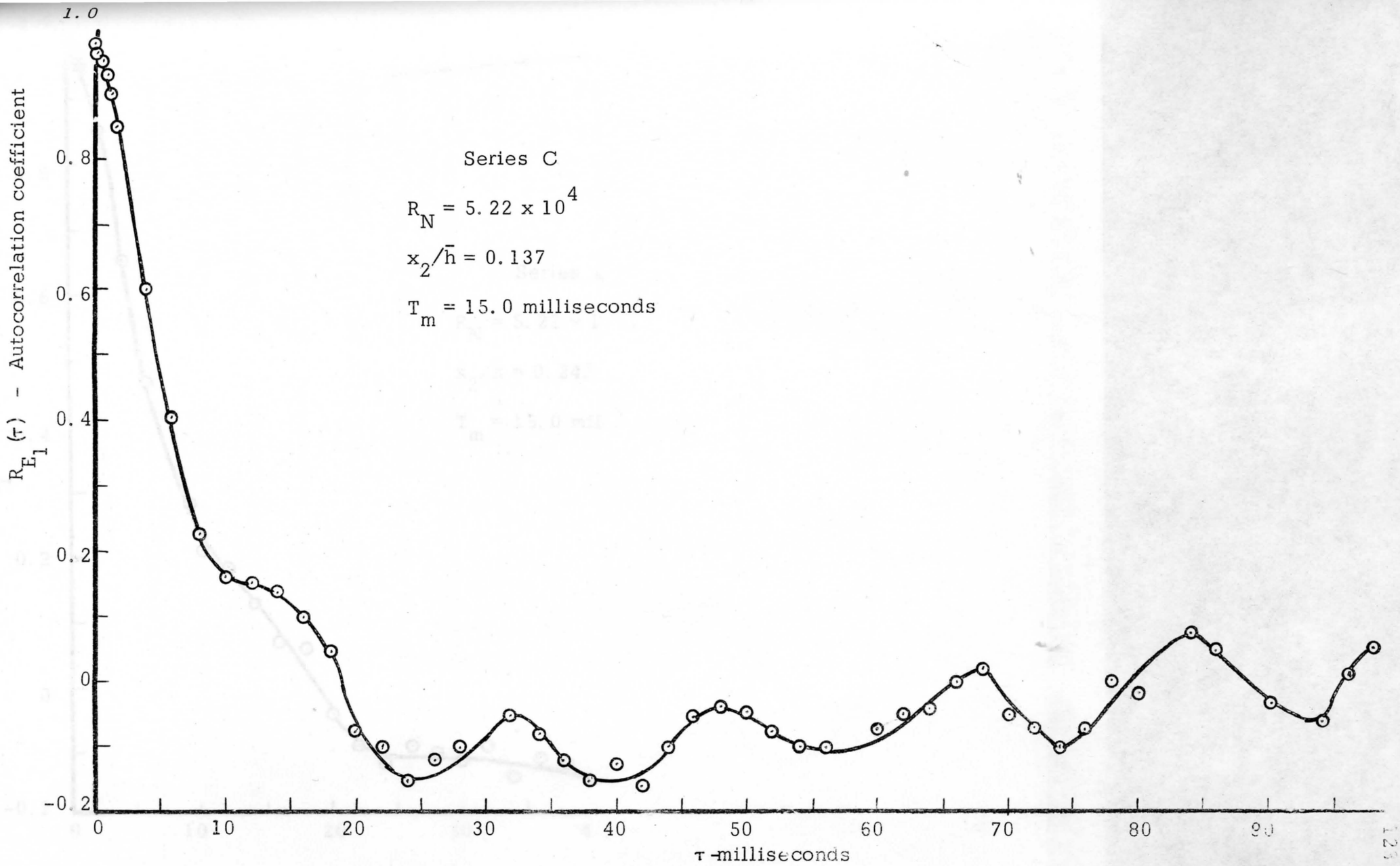

Figure 32. Autocorrelation curve at $R_N = 5.22 \times 10^4$ at a relative depth $x_2/\bar{h} = 0.137$ -- Series C.

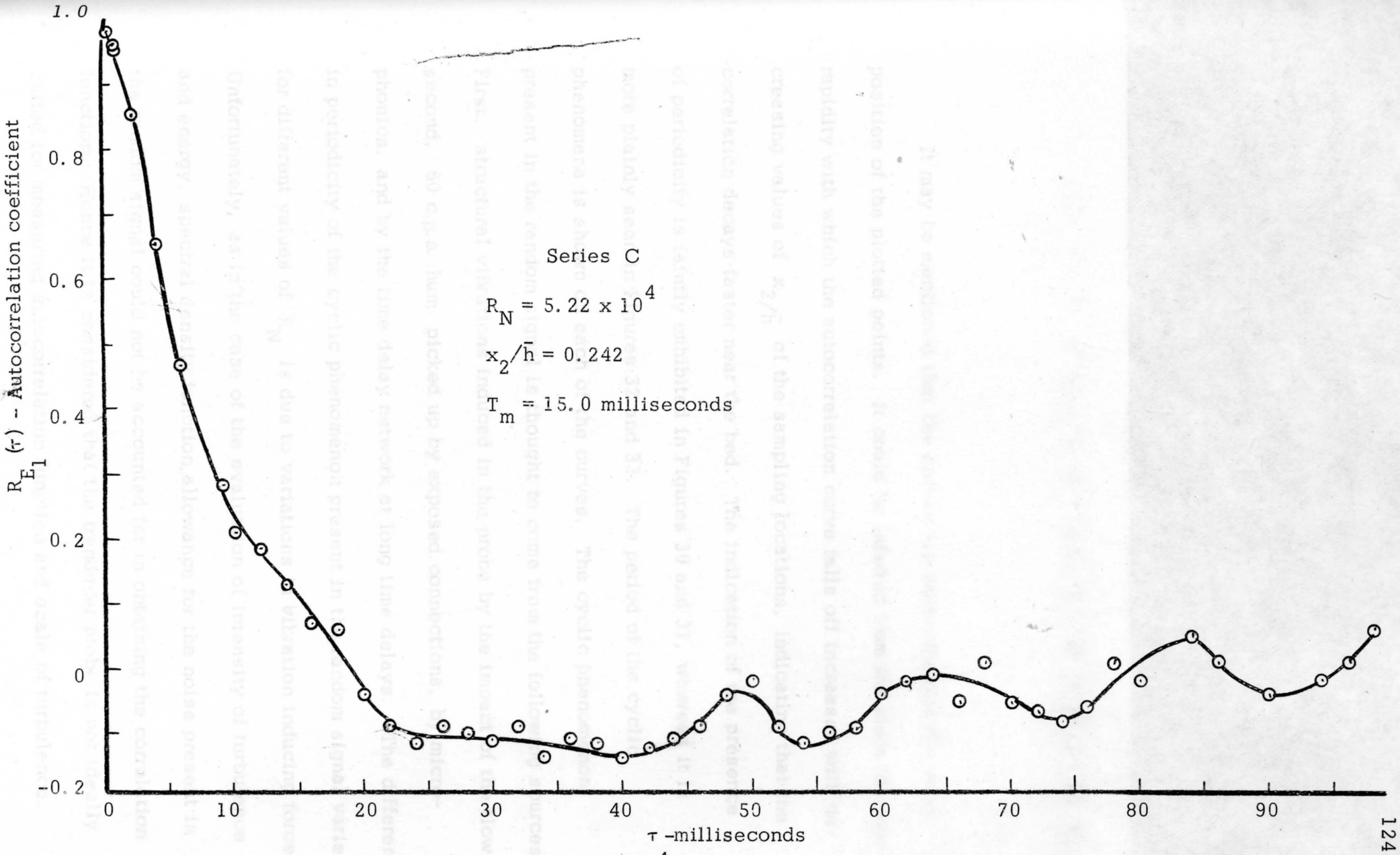

Figure 33. Autocorrelation curve at $R_N = 5.22 \times 10^4$ at a relative depth $x_2/\bar{h} = 0.242$

It may be mentioned that the curves are drawn through the mean position of the plotted points. It could be inferred from the plots that the rapidity with which the autocorrelation curve falls off increases with decreasing values of $x_{2/\bar{h}}$ of the sampling locations, indicating that the correlation decays faster near the bed. The indication of the presence of periodicity is faintly exhibited in Figures 30 and 31, whereas it is more plainly seen in Figures 32 and 33. The period of the cyclic phenomena is shown on each of the curves. The cyclic phenomenon present in the random signal is thought to come from the following sources: First, structural vibrations induced in the probe by the impact of the flow, second, 60 c.p.s. hum picked up by exposed connections, by microphonics, and by the time delay network at long time delays. The difference in periodicity of the cyclic phenomenon present in the random signal varies for different values of R_N is due to variations in vibration inducing forces. Unfortunately, as in the case of the evaluation of intensity of turbulence and energy spectral density function, allowance for the noise present in the random signal could not be accounted for in obtaining the correlation function. Hence it is considered that the tranducer probe is not ideally suited for measuring autocorrelation function and scale of turbulence.

Macroscale of Turbulence

In general the macroscale is dependent on the boundary dimensions of flow. In the case of turbulent shear flow bounded by a solid surface,

the macroscale is comparable with the scale of the variation of the mean flow, i.e., depth in an open-channel flow. No effort was made to keep the depth of flow constant in varying the value of Reynold's number of flow for different series of runs. Therefore, it is considered expedient to present the distribution of the average macroscale L_{x_1} over the depth of flow in the form of dimensionless plot, using the depth of flow as repeating parameter. Such plots are shown in Figures 34 and 35.

It is interesting to note that for all the six runs the general shape of the $\frac{L_{x_1}}{\bar{h}}$ versus $\frac{x_2}{\bar{h}}$ curve is the same. The value of $\frac{L_{x_1}}{\bar{h}}$ decreases with increasing rate as the bed of the channel is approached, and it increases with increasing distance from the bed until a maximum value is reached; and thereafter once again its value decreases as the water surface of the channel is approached. Unfortunately, due to the limitations of the size of the tranducer probe, measurements could not be made much closer than 0.1 of an inch to the bed of the channel; and due to the accoustic properties of the probe, measurement could not be extended very near to the surface of flow in the channel. Notwithstanding these limitations imposed on the measurements, it is possible to deduce important conclusions from these plots.

In Figure 34, $\frac{L_{x_1}}{\bar{h}}$ values for various Reynolds numbers and relative roughnesses are plotted against $x_{2/\bar{h}}$. All these runs correspond to fully-developed turbulent regime of flow as in each case the value of the roughness Reynolds number $\left(\frac{k_s u_*}{\nu}\right)$ far exceeds 75. Allowing for

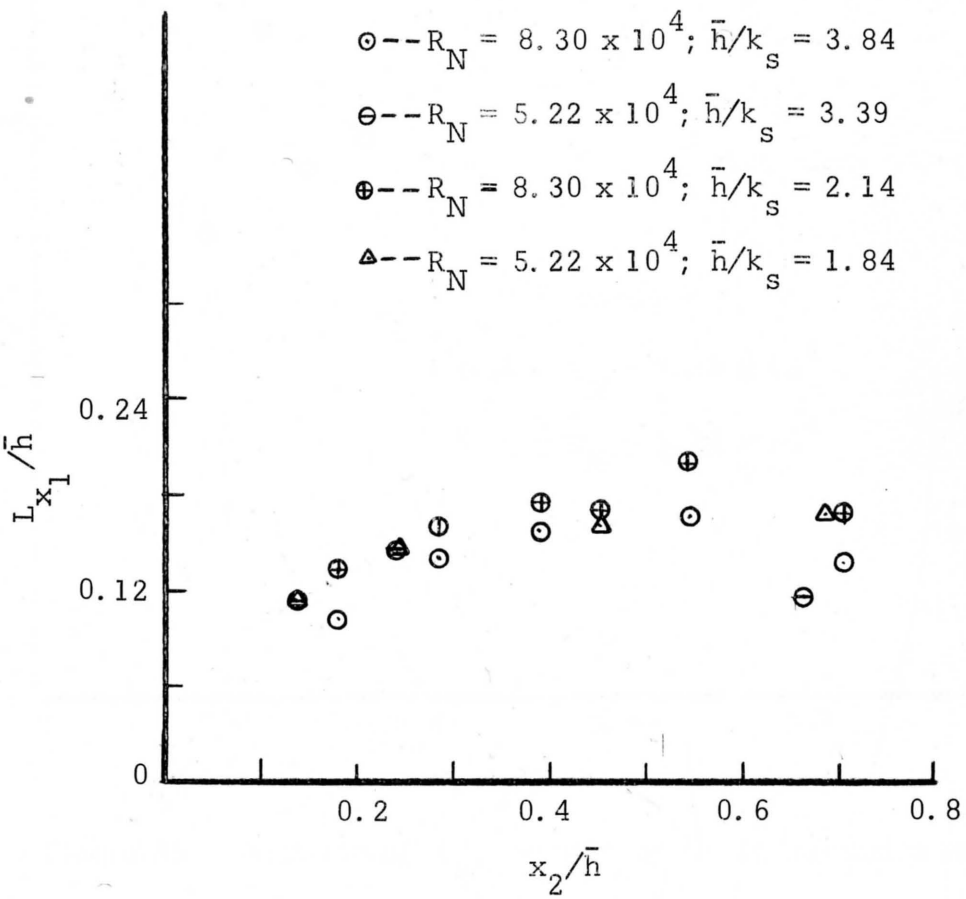

Figure 34. Variation of L_{x_1} versus $x_2/\bar{h}$ at different values of R_N and $\bar{h}/k_s$ for the case of fully developed turbulent flow.

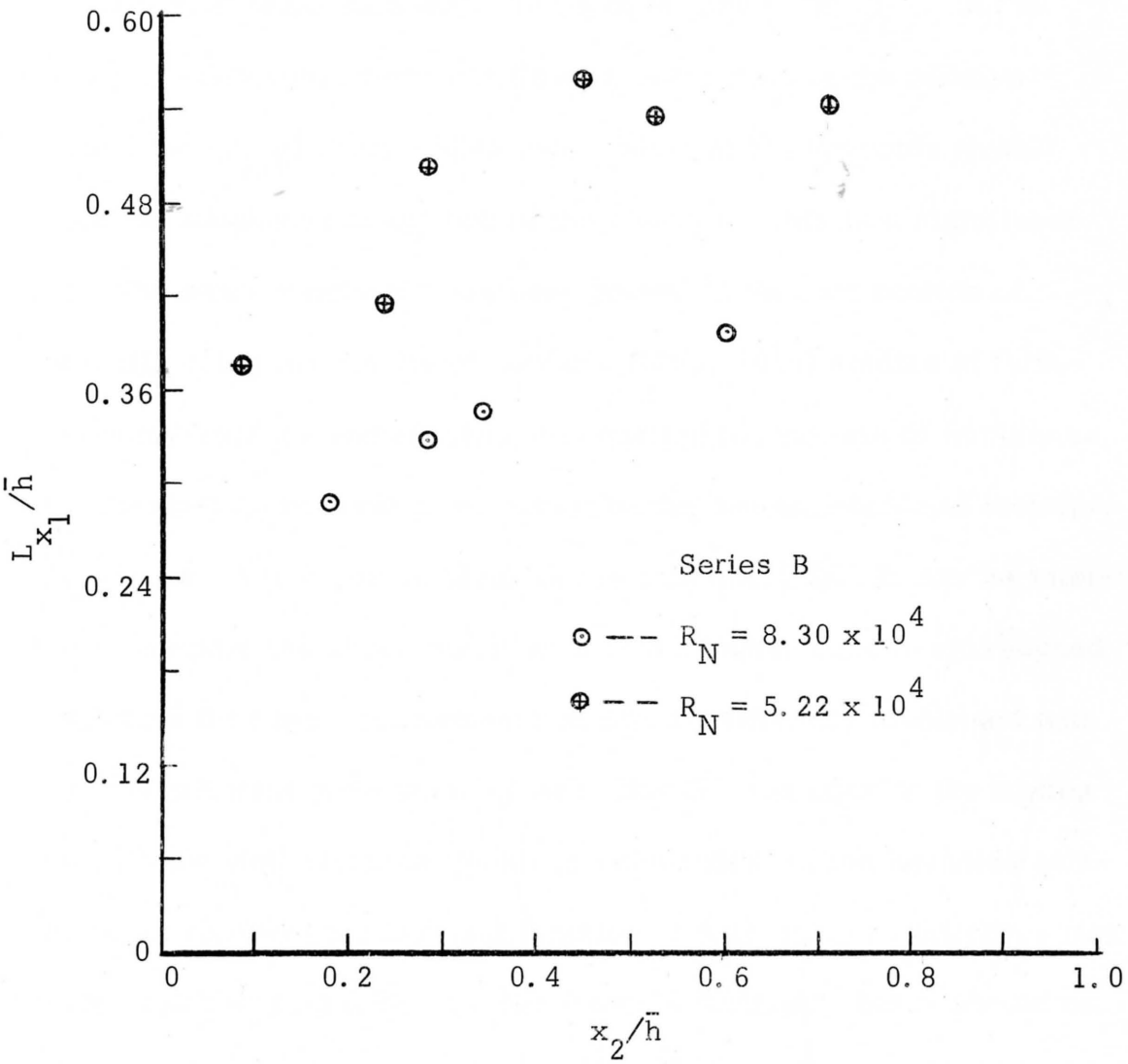

Figure 35. Variation of L_{x_1} versus $x_2/\bar{h}$ in transition regime of flow with R_N as a parameter.

slight scatter due to errors from various sources, it could be concluded from this figure that all the points fall on the same curve. Thus the variation of the macroscale with the depth of flow $\left({}^{L}x_{1}/\bar{h} \right)$, in the case of fully-developed turbulent flow, is a function of the relative depth of flow $(x_{2}/\bar{h})$ only and is independent of the Reynolds number and relative roughness of the bed of the channel. This is a significant result. The same conclusion has been proved in the last section of Chapter III, using the results of Laufer's (1951, 1954) studies of turbulence energy balance and adopting an equation for the rate of turbulence energy dissipation in shear flow similar to the one applicable to isotropic turbulent flow. The result is given in the equation (95). It may be interesting to compare the above result with an analogous conclusion reached by Nikuradse from his measurements on pipes artificially roughened with the sand of different grain size. That is that the variation of the mixing length with the wall distance (ℓ/R) is independent of the Reynolds number and wall roughnesses and is a function of only $x_{2/R}$. Reference may be made to Schlichting (1960) for Nikuradse's findings. But it should be noticed that the macroscale tends to decrease as the water surface is approached, whereas the mixing length "ℓ" increases with increasing distance from the wall indefinitely.

The variation of the values of $L_{x_1/\bar{h}}$ with the relative depth of flow in the transition regime of flow is shown in Figure 35. Figure 34 is in direct contrast with the Figure 35, as it should be. It is evident from

this Figure 35 that $L_{x_{1/\bar{h}}}$ is a function of the Reynolds number and, perhaps, relative roughness. It is also clear that at lower Reynolds numbers the values of $L_{x_{1/\bar{h}}}$ are much higher. This indicates that the turbulence has a larger scale at lower Reynolds numbers as might be expected from ideas on the origin of turbulence.

As there is much similarity among open-channel flows and boundary-layer flows and pipe flows, an effort is made to explain the trend of the variation of the macro-scale over the depth of flow making use of the results of turbulence energy balance studies of Klebanoff (1954) and Laufer (1954) in boundary-layer flow and pipe flow respectively. Reference may be made to Chapter II, where the salient features of the results of their studies are presented briefly. From the outer region of flow in the open-channel where turbulence production is negligible and diffusion is predominant, the macroscale of turbulence increases until the intermediate region is reached. In this region the rate of turbulence energy production is significant, and the energy balance is provided by production and dissipation only. This increase in macroscale in the intermediate region may be attributed to the increase in energy production. But as the bed of the channel is approached, even though the energy production becomes markedly predominant, the viscous effects tend to break the larger eddies into smaller ones. The viscous action increases rapidly in the wall region ($y^* \lesssim 30$), which accounts for the sharp decrease in the macroscale of turbulence. It may be pointed

out that in most of the runs only one measurement of the macroscale could be taken in the wall region. From this analysis it appears that the region of maximum macroscale is where the effect of viscosity is small and turbulence generation is significant enough.

It should be pointed out that the macroscale measured in this investigation is only average macroscale at different positions over the depth. In order to measure the actual macroscale at any position, it is necessary to obtain the longitudinal spatial correlation curve. As explained in Chapter IV, efforts to obtain $R_{x_1 u_1}(x_1)$ were not successful with the tranducer probes used. Difficulties in getting $R_{x_1 u_1}(x_1)$ curve even with hot-wire or film anemometer are pointed out by Hinze (1959). For this reason, perhaps, Laufer (1951) in his detailed investigation of turbulent flow in a two-dimensional channel measured only the distributions of L_{x_2} and L_{x_3} and derived the distribution of L_{x_1}, assuming that L_{x_1} is twice the value of L_{x_3}, which is strictly true only in isotropic turbulence. Even though Jordan (1963) made an intensive study of the distribution of the scale of turbulence in a pipe, he confined his study only to L_{x_2}.

Hence the results of the distribution of the average macroscale of turbulence obtained in this study can be compared only to Laufer's work with caution. He obtained distribution of L_{x_1} in a two-dimensional channel, 5 inches wide and 60 inches tall. The 5-inch width was directed along the x_2 axis. His Reynolds numbers were based on the

half-width of the channel and the maximum velocity. The trend of the variation of L_{x_1} across the width of his channel and over the depth in the open channel is significantly similar. The maximum value of L_{x_1} in his channel occurs at $x_2/d \approx 0.5$ (d corresponds to half width), whereas in this work it occurs approximately at $x_{2/\bar{h}} = 0.54$. It could also be noted that at corresponding Reynolds numbers in the transition regime $\left(5 \leq \frac{k_s u_*}{\nu} \leq 70\right)$ the ratio of the maximum value of L_{x_1} to characteristic linear dimension (in his case a 5-inch width) is nearly the same in a two-dimensional channel as well as in an open channel, irrespective of the medium of fluid. It should also be noted that the maximum value of L_{x_1} in the fully-developed turbulent regime is less than in the transition regime, even if the R_N in both cases were the same, suggesting that roughness decreases the value of L_{x_1}.

Microscale of Turbulence

The distribution of the longitudinal microscale of turbulence, also called dissipation length λ_{x_1}, as a function of the relative depth of flow with relative roughness as a parameter at three Reynolds numbers, is presented in Figures 36 to 38. The trend of the variation of λ_{x_1} seems to be unaffected by the relative roughness. The dissipation length λ_{x_1} increases from the water surface until it attains a maximum value, and thereafter it decreases rapidly as the bed of the channel is further approached. In the case of higher values of $\bar{h}/k_s$, the microscale of

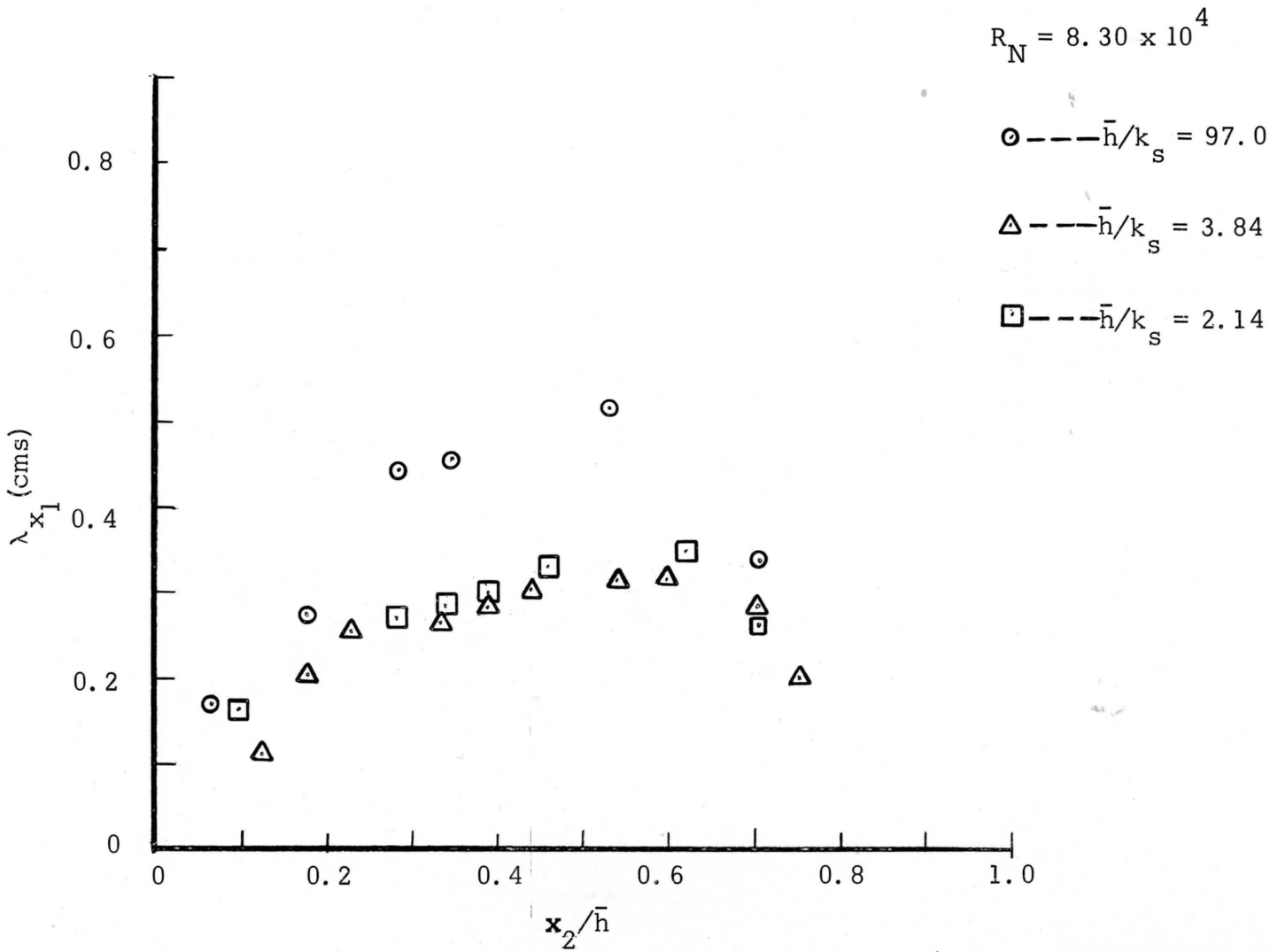

Figure 36. Variation of λ_{x_1} as a function of relative depth $x_2/\bar{h}$ with $\bar{h}/k_s$ as a parameter with $R_N = 8.30 \times 10^4$.

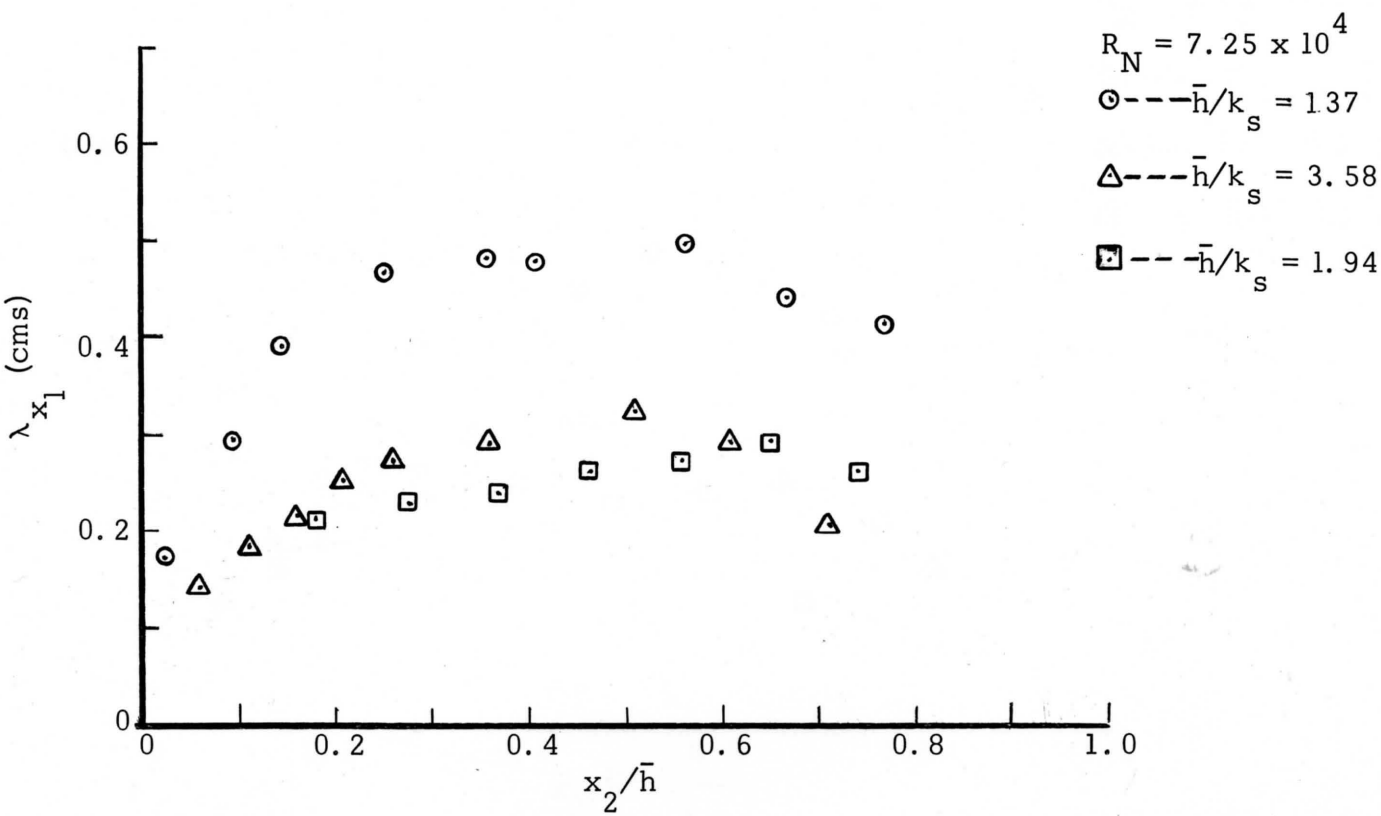

Figure 37. Variation of λ_{x_1} as a function of relative depth $x_2/\bar{h}$ with $\bar{h}/k_s$ as a parameter at $R_N = 7.25 \times 10^4$.

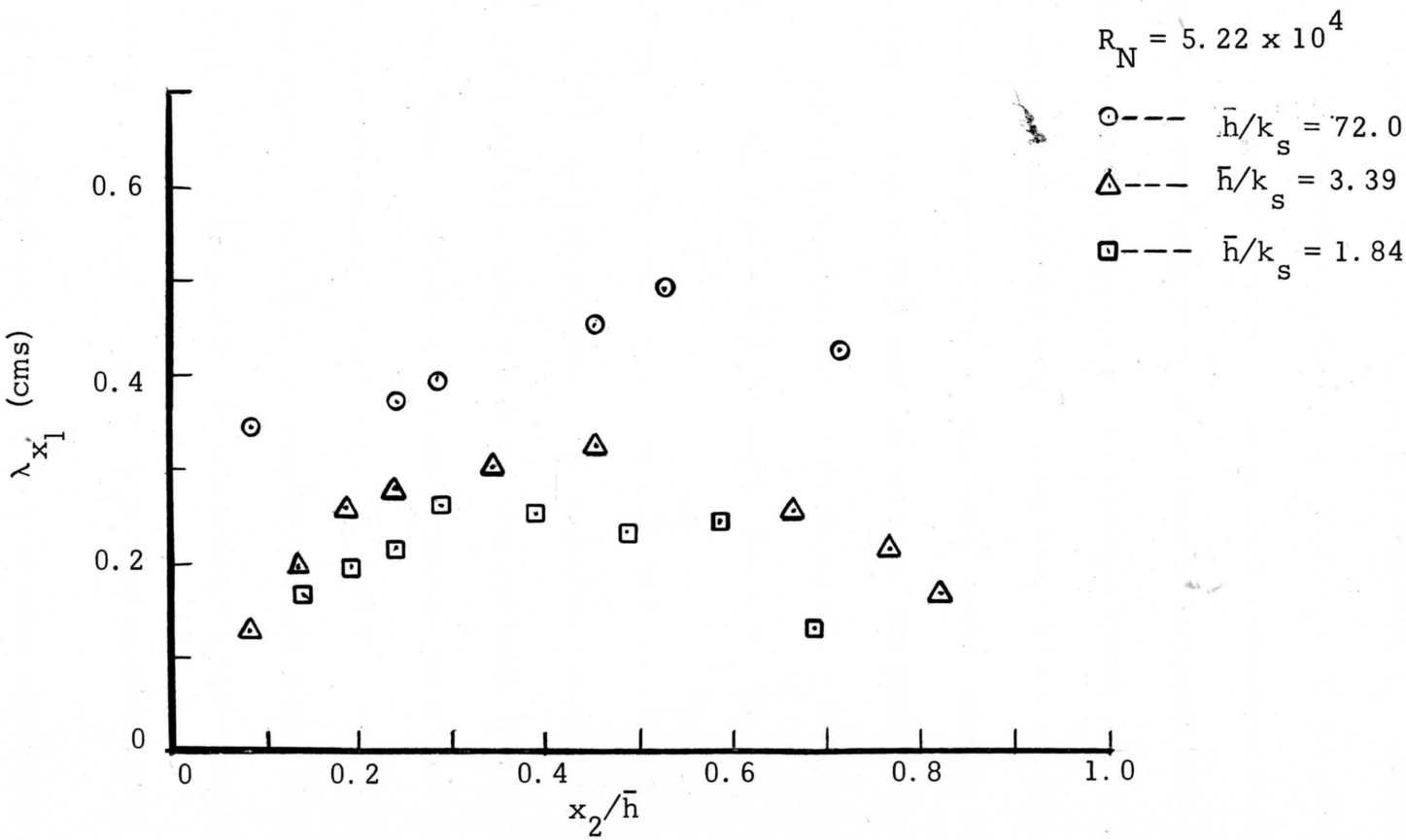

Figure 38. Variation of λ_{x_1} as a function of relative depth $x_2/\bar{h}$ with $\bar{h}/k_s$ as a parameter at $R_N = 5.22 \times 10^4$

turbulence λ_{x_1} reaches a maximum value nearer to the wall than for the cases with lower values of $\bar{h}/k_s$ for all the three Reynolds numbers. It could also be inferred that the microscale of turbulence λ_{x_1} decreases considerably with the decrease in the values of $\bar{h}/k_s$. These results could be explained in terms of what is known about turbulence energy balance in boundary layer flows from the studies of Klebanoff (See Chapter II) and the relation between the dissipation length λ_{x_1}, the rate of energy dissipation and the mean square value of the velocity fluctuation that could be considered to be similar to the equation (40).

In the outer region of flow near the surface, the production of turbulence is negligible and whatever amount of energy is diffused from the wall region into this region is dissipated. As $\epsilon \propto \frac{\overline{u_1^2}}{\lambda_{x_1}^2}$, λ_{x_1} in the outer region is small due to small values of $\overline{u_1^2}$ and ϵ. In the wall region both production and dissipation reach maximum values and are of equal importance except in a very thin layer near the wall (i. e., $y^* < 20$). No specific quantitative correlation is known between the production of turbulence and turbulent velocity fluctuation u_1. It is suspected that the mean square velocity fluctuation at a point is a few orders less in magnitude than the rate of generation of turbulence. Hence it follows from $\epsilon \propto \frac{\overline{u_1^2}}{\lambda_{x_1}^2}$ that λ_{x_1} should reduce in magnitude as the wall is approached. In the intermediate region both production and dissipation of turbulence are considerable but are of equal magnitude. Hence λ_{x_1}

has to have maximum value somewhere in the intermediate region. Not only are there no turbulence-energy-balance studies in open channel flows, but there are also no similar studies even in turbulent boundary-layer flows past rough surfaces. Hence it is very difficult to speculate on the relative magnitudes of production, diffusion and dissipation of turbulence in different zones of rough open channels. Since the value of ϵ is bound to increase for decreasing values of $\bar{h}/k_s$, it is inferred that λ_{x_1} is smaller over the entire section, for smaller values of $\bar{h}/k_s$, at all the three Reynolds numbers. It is suspected that the intermediate region is displaced a little towards the surface by the presence of bed roughness which explains, perhaps, why the maximum value of λ_{x_1} occurs farther from the wall at low values of $\bar{h}/k_s$.

In Figures 39 to 41 the variation of the longitudinal microscale of turbulence as a function of the relative depth from the bed is presented with Reynolds number as a parameter at three different relative roughnesses. It should be pointed out again that the relative roughness could not be kept absolutely constant for flows at different Reynolds numbers but the variation in $\bar{h}/k_s$ for Series A and C is small. It indicates from Figure 39 that the dissipation length λ_{x_1} remains constant over the relative depth of flow for the range of Reynolds numbers 5.22×10^4 to 8.30×10^4. But for the little scatter either due to the nonconstancy in $\bar{h}/k_s$ or experimental errors, one arrives at the same conclusion from the Figures 40 and 41. The only explanation that could be offered is that the range

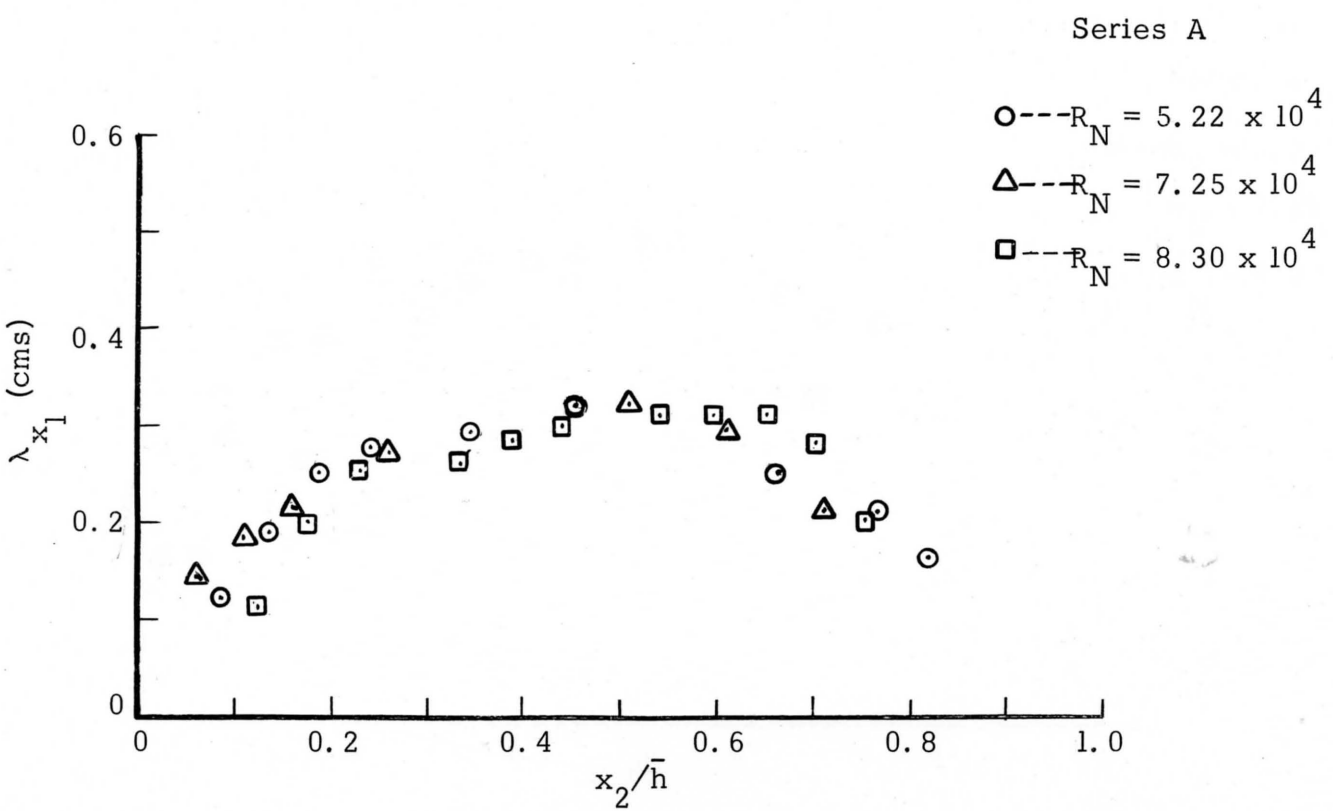

Figure 39. Variation of λ_{x_1} as a function of relative depth $x_2/\bar{h}$ with R_N as a parameter -- Series A.

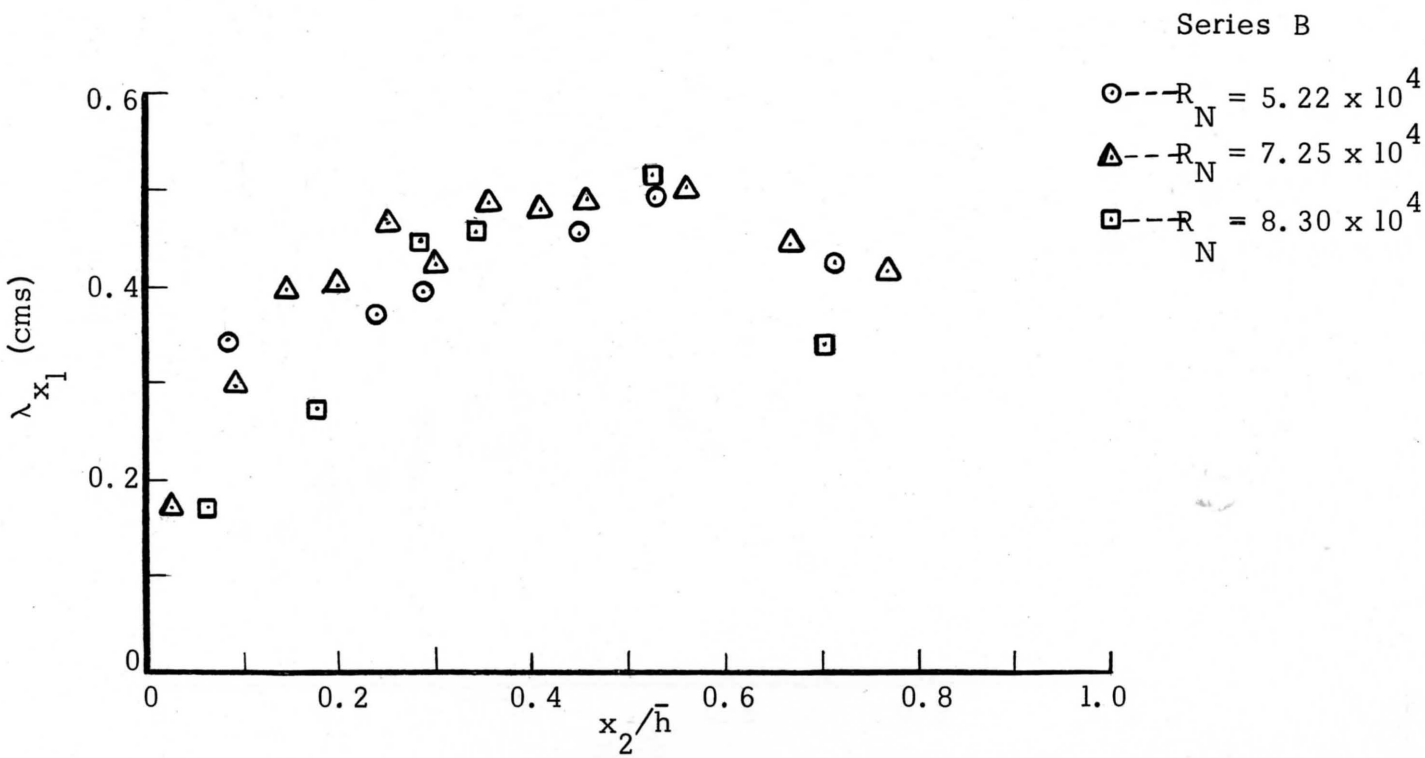

Figure 40. Variation of λ_{x_1} as a function of relative depth $x_2/\bar{h}$ with R_N as a parameter -- Series B.

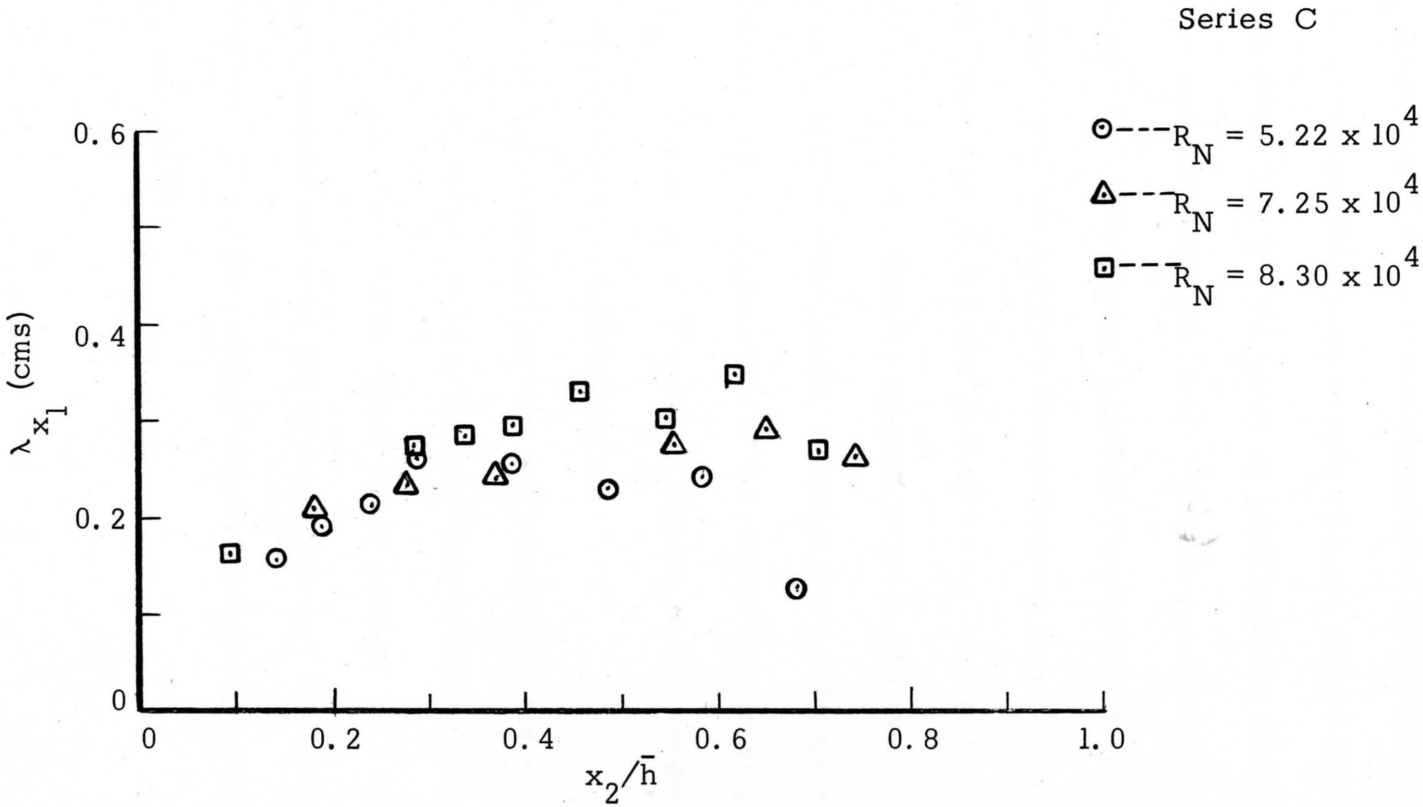

Figure 41. Variation of λ_{x_1} as a function of relative depth $x_2/\bar{h}$ with R_N as a parameter -- Series C.

of Reynolds numbers investigated is too small to show marked distinct trends.

Similar distributions of the dissipation length were obtained by Laufer (1951) in a 5-inch wide, two-dimensional channel and by Jordan (1963) and Brookshire (1961) in a 5-inch diameter pipe with the maximum occurring at different distances from the wall. The ranges of values of the dissipation length λ_{x_1} from Laufer's two-dimensional channel investigation and Jordan's and Brookshire's investigations in a pipe are 0.198 cms to 0.685 cms and 0.127 cms to 0.456 cms respectively. The range of values of λ_{x_1} from this investigation is 0.120 cms to 0.51 cms. It may be mentioned that Laufer's values were obtained at lower Reynolds numbers, and it might explain the reason for his slightly higher values of λ_{x_1}. The range of Reynolds numbers in this investigation is comparable to that of Jordan and Brookshire.

It should be strongly emphasized that the tranducer probe cannot be accurately sensitive to eddies smaller than the diameter of the barium titanate crystal (1/16 inch). Hence the actual lower limit of λ_{x_1} could not be ascertained accurately but only the average value of the lower limit of λ_{x_1} is obtained. The important influence of roughness is to extend further the lower limit of λ_{x_1}.

Correlation of Turbulence Properties

In the last section of Chapter III, two important relations (equations (90) and (95)) connecting the statistical properties of turbulence are presented, and it is indicated that such relationships may be of some use in solving practical problems. The left-hand side of the equation (90) is actually a dimensionless grouping of the three statistical characteristics of turbulence and fluid property. This dimensionless grouping should have a constant value at different positions over the depth of flow at any given values of Reynolds number and relative roughness. In Table 2, the calculated values of the equation (90) are presented for four different Reynolds numbers and relative roughnesses. The values of the expression in the last three columns are reasonably constant if one keeps in mind the experimental errors involved in determining especially the values of L_{x_1} and λ_{x_1} and the approximate assumptions made in deriving that equation. In the first two columns the values are spread more, and the cause could be attributed to experimental errors only.

Regarding equation (95), it has already been proved experimentally (See Figure 34) that $L_{x_1}/\bar{h}$ is a function of relative depth of flow only in the case of fully-developed turbulent flow. Laufer (1954) showed that u_1'/u_* is a function of relative depth only in the outer region of flow.

Table 2. Values of the dimensionless quantity in equation (90) at various relative depths, Reynolds numbers, and relative roughnesses.

Series A $R_N = 5.22 \times 10^4$ $\bar{h}/k_s = 3.39$		Series B $R_N = 8.3 \times 10^4$ $\bar{h}/k_s = 97.0$		Series B $R_N = 5.22 \times 10^4$ $\bar{h}/k_s = 72.0$		Series B $R_N = 4.06 \times 10^4$ $\bar{h}/k_s = 65.70$		Series C $R_N = 8.3 \times 10^4$ $\bar{h}/k_s = 2.14$	
$\frac{x_2}{\bar{h}}$	$\frac{\lambda^2 x_1 u'_1}{\nu L_{x_1}}$	$\frac{x_2}{\bar{h}}$	$\frac{\lambda^2 x_1 u'_1}{\nu L_{x_1}}$	$\frac{x_2}{\bar{h}}$	$\frac{\lambda^2 x_1 u'_1}{\nu L_{x_1}}$	$\frac{x_2}{\bar{h}}$	$\frac{\lambda^2 x_1 u'_1}{\nu L_{x_1}}$	$\frac{x_2}{\bar{h}}$	$\frac{\lambda^2 x_1 u'_1}{\nu L_{x_1}}$
0.137	78.40	0.179	84.30	0.084	159.0	0.065	73.0	0.179	64.80
0.242	121.0	0.284	181.50	0.242	134.0	0.242	97.40	0.284	79.50
0.452	108.0	0.344	172.50	0.284	122.0	0.344	94.50	0.390	78.60
				0.452	117.0	0.530	72.60		
0.663	76.80	0.705	64.70	0.530	110.8			0.546	61.60
				0.716	94.0	0.716	103.60	0.705	47.40

These experimental results could form a basis for the approximate estimation of L_{x_1}, λ_{x_1}, u'_1 and perhaps ϵ for a given boundary shear flow problem. The mean flow quantities such as Reynolds number of flow, shear velocity, relative roughness, and relative depth can easily be estimated. If the shear flow problem, for example, is a flow in an energy dissipator, then at any relative depth of flow (preferably in the outer region of flow) the corresponding value of L_{x_1} can be found from the Figure 34, since the flow in energy dissipators is usually fully-developed turbulent flow. At the same relative depth, using Laufer's plot, the value of u'_1 can be obtained from the known value of the shear velocity. If the tabulated values of the expression on the left-hand side of the equation (90) are available for extensive range of Reynolds numbers and relative roughnesses, the value corresponding to the known values of R_N and $\bar{h}/k_s$ for the problem at hand can be evaluated by interpolation. As L_{x_1}, u'_1 are already known, the value of λ_{x_1} can be determined. If the value of ϵ is required in the outer region of flow, where local isotropy can be expected to exist, it could be evaluated using the equation (40) as the knowledge of every quantity in that equation can be determined as explained above.

CHAPTER VII

CONCLUSIONS

From the experimental investigation and the subsequent interpretation and discussion of results, the following conclusions can be made concerning the structure of shear turbulence in rough open channels.

1. The relative intensity of turbulence over the entire depth of flow decreases with increase in R_N at a constant bed roughness and increases with decrease in the value of $\bar{h}/k_s$ at a constant value of R_N. It seems to attain a maximum value in the constant stress layer where the production of turbulence is also maximum.
2. The influence of roughness on the relative intensity of turbulence is markedly pronounced near the bed, and the trend in the variation of $u_1' / \overline{U}_1$ is not affected by roughness.
3. In the outer region of fully-developed turbulent flow in the rough open channel, the wave number at which the transition between locally isotropic turbulence and anisotropic turbulence occurs, is independent of the Reynolds' number, but varies inversely with the depth of flow. This is in complete agreement with the picture of the mechanism of the generation, transfer, and dissipation of turbulent energy as proposed by

Kolmogoroff. It has been verified that both the inertial and viscous subranges of the universal equilibrium range (local isotropy) can be expected to exist in the energy spectrum of turbulence in the wave number space.

4. The longitudinal one-dimensional energy spectrum function (equation 118) for the entire region of universal equilibrium range, obtained by combining equations (69) and (70) for the two extremes (inertial subrange and viscous subrange), a simplified form of Heisenberg equation (68), describes satisfactorily the transition between inertial and viscous subranges.

5. It is concluded that local isotropy cannot exist in the wave number space in turbulent shear flow in the open channel near the bed due to the presence of steep mean velocity gradients.

6. The contribution to turbulence energy in the entire wave number range increases as the bed of the channel is approached.

7. The concept of local isotropy is inadequate for obtaining the distribution of the rate of dissipation of turbulent energy in turbulent shear flow even though it could be made use of in the outer region to evaluate the local rate of energy dissipation.

8. The rapidity with which the autocorrelation falls off increases with decreasing values of the relative depth measured from the bed at the sampling locations. Thus the correlation decays faster near the bed.

9. The longitudinal average macroscale of turbulence decreases as the bed of the channel is approached and it increases with increasing distance from the bed until a maximum value is reached; and thereafter it begins to decrease as the water surface is approached. The macroscale is maximum in the intermediate region where the viscous action is negligible and turbulence generation is considerable; it is approximately located at $x_{2/\bar{h}} = 0.54$.

10. In the case of fully-developed turbulent flow, $L_{x_1}/\bar{h}$ is a function of relative depth of flow $(x_{2/\bar{h}})$ only, and independent of Reynolds' number and relative roughness of the bed of the channel. In the transition regime of flow, $L_{x_1}/\bar{h}$ is a function of Reynolds' number as well as relative roughness and the turbulence has larger scale (L_{x_1}) at lower Reynolds numbers.

11. The longitudinal microscale of turbulence, λ_{x_1}, increases from the liquid surface until it attains a maximum value at a relative distance from the bed around $x_{2/\bar{h}} = 0.55$ and then it decreases rapidly as the bed of the channel is further approached. The position of the maximum value of λ_{x_1} shifts towards the

surface as the relative roughness $\bar{h}/k_s$ decreases. The influence of roughness on the shape of the distribution of λ_{x_1} is negligible.

12. At a constant value of R_N, the value of λ_{x_1} decreases over the entire depth of flow as the relative roughness $\bar{h}/k_s$ decreases. Then λ_{x_1} remains constant over the relative depth of flow for the range of Reynolds numbers in this investigation at a constant relative roughness $\bar{h}/k_s$.

13. Equation (90) is proved to be valid for a set of values of R_N and $\bar{h}/k_s$. A procedure for estimating important statistical characteristics of turbulence such as L_{x_1}, λ_{x_1}, u_1' and ϵ in fully-developed turbulent shear flow in channels on the basis of the knowledge of mean flow quantities like R_N, u_*, $\bar{h}/k_s$, and $x_{2/\bar{h}}$ is suggested.

14. The presence of artificial roughness on the bed of the channel has an indirect influence on the structure of turbulence in open-channel flows by transforming the flow into fully-developed turbulent flow at a lower Reynolds number.

15. Due to the acoustical properties of the tranducer probe, it is considered that it is not ideally suited for measuring auto-correlation function and scales of turbulence.

CHAPTER VIII

SUGGESTIONS FOR FURTHER RESEARCH

As pointed out in Chapters IV and VI, due to the limitations of the tranducer probe, complete information on the structure of shear turbulence in open-channels could not be obtained. On the basis of the experience gained in this investigation, it is believed that improvements can be made in organizing measurement of data. Besides, prior to this work, there have been very few turbulence measurements in open channels and no measurements in rough open channels so far as the author knows. Hence, it is felt that there is sufficent need to pursue this study much more intensively as well as extensively. With this view in mind, a few suggestions are offered below to extend the present author's research with the hope that they may be of some use to someone else.

1. Measurements should be made of relative intensity of turbulence over a wider range of values of R_N with $\bar{h}/k_s$ as a parameter and over a wider range of $\bar{h}/k_s$ with R_N as a parameter, keeping the geometrical similarity of the roughness constant.
2. Attempts should be made to make measurements within the constant stress layer extending to the laminar sublayer possibly using a device such as the hot-film anemometer with highly viscous fluid and uniform sand-grain roughness

on the bed. At present no mean or turbulence energy balance studies have been made either in the vicinity of a rough wall or in open channels. This study may also be used to substantiate or refute the speculation that turbulence energy moves from the outer region to the inner region by the action of pressure forces which compensate for greater dissipation within the region of $y^* < 20$.

3. It is necessary to use a device such as the hot-film annemometer (which can measure lateral velocity fluctuations) if further turbulence measurements are to yield a more complete picture of the structure of shear turbulence.

   a. As no conclusive studies have been made yet about the validity of Kolmogoroff's concept of local isotropy for spectra of lateral velocity fluctuations, it will be of great interest to obtain cross-spectra. Besides, such data can be made use of in conjunction with equation (115) in applying a further check on the existence of local isotropy in spectra of longitudinal velocity fluctuations. Furthermore, measurements of spectra of shear stress and shear correlation coefficient can be made and can also be used as additional checks on the occurrence of local isotropy in spectra of u_1.

b. Measurements of space correlations and their associated macroscales and microscales could not be made in this study. It may be pointed out that measurements of $R_{x_{u_1}}(x_1)$ and associated L_{x_1} have not been made in any kind of wall shear flow. No turbulence study is complete without measuring these quantities.

4. It may be interesting to measure the distribution of λ_{x_1} over the relative depth taking $\bar{h}/k_s$ as a parameter over a range of constant values of R_N and to repeat the same taking R_N as a parameter over a range of constant values of $\bar{h}/k_s$, keeping the geometry of bed roughness similar.

5. It will be useful to check the validity of the equation (90) over a wider range of R_N and $\bar{h}/k_s$.

6. The possibility of replacing the Lagrangian correlation with Eulerian space-time correlation is worth investigating. If such a substitution were possible, it paves the way for the direct determination of the Lagrangian correlation coefficient and associated mean scales of the eddies participating in the diffusion process. This simplified procedure for the determination of the Lagrangian scales of eddies could be used to determine a functional expression for the diffusion coefficient in turbulent shear flow on the basis of Kolmogoroff's theory and to evaluate the extent of influence of the relative roughness of the bed on the diffusion coefficient.

LITERATURE CITED

Bass, J. 1949. "Sur les bases mathematiques de la théorie de la turbulence d' Hei senberg." Comptes Rendus des Séances De L' Académie des Sciences, Paris. 228:228.

Batchelor, G. K. 1946. "The theory of axisymetric turbulence." Proceedings Royal Society, Series A. 186:480.

Batchelor, G. K. 1948. "Energy decay and self-preserving correlation functions in isotropic turbulence." Quarterly of Applied Mathematics. 6:97.

Batchelor, G. K. 1953. "The theory of homogeneous turbulence." Cambridge University Press, Cambridge, Great Britain. 197 p.

Brookshire, W. A. 1961. "A study of the structure of turbulent shear flow in pipes." Unpublished Ph. D. dissertation in Chemical Engineering. Louisiana State University, Baton Rouge, Louisiana.

Burgers, J. N. and M. Mitchner. 1953. "On homogeneous nonisotropic turbulence connected with a mean motion having a constant velocity gradient." Proceedings Kon. Ned. AKad. Van. Wet. B., 56(3) and 56(4). (Original not seen; abstracted in J. O. Hinze. 1959. "Turbulence" McGraw-Hill Book Company, Inc., New York. 586 p.)

Chandrasekhar, S. 1949. "On Heisenberg's elementary theory of turbulence." Proceedings of the Royal Society of London, Series A. 200:20.

Chandrasekhar, S. 1950a. "The theory of axisymmetric turbulence." Philosophical Transactions of the Royal Society of London, Series A. 242:557.

Chandrasekhar, S. 1950b. "The decay of axisymmetric turbulence." Proceedings of the Royal Society of London, Series A. 203:358.

Clyde, Calvin G. 1961. "Fluctuations of total head near a smooth wall in a turbulent open channel flow." Unpublished Ph. D. dissertation in civil engineering. University of California, Berkeley, California.

Corrison, S. 1949. "An experimental verification of local isotropy." Journal of Aeronautical Science. 16:757.

Corrison, S. 1961. "Turbulent flow." American Scientist. 49:(3); 300-325.

Craya, A. 1957a. "Sur les Corrélations triples entrois points en turbulence homogène." Comptes Rendus des Sciences De L' Academie des Sciences, Paris. 244:560-562.

Craya, A. 1957b. "Une méthode d'investigation des corrélations doubles pour la turbulence homoge ne en présence de vitesses moyennes." Comptes Rendus des Sciences De L'Academie des Sciences, Paris. 244:1448-1450.

Craya, A. 1957c. "Sur les équations de la turbulence homoge'ne en présence d'un champ de vitesse moyenne." Comptes Rendus des Séances De L'Academie des Sciences, Paris. 244:847-848.

Craya, A. 1957d. "Sur la structure des corrélations triples en turbulence homoge'ne associée a' unchamp de vitesses moyennes." Comptes Rendus des Sciences De L'Academie des Sciences, Paris. 244:1609-1611.

Deissler, R. G. 1958. "On the decay of homogeneous turbulence before the final period." The Physics of Fluids, 1(2):111-121.

Deissler, R. G. 1960. "A theory of decaying homogeneous turbulence." The Physics of Fluids. 3(2):176-187.

Deissler, R. G. 1961. "Effects of inhomogeneity and of shear flow in weak turbulent fields." The Physics of Fluids. 4(10):1187-1198.

Deissler, R. G. 1962. "Pressure fluctuations in a weak turbulent field with a uniform transverse velocity gradient." The Physics of Fluids. 5(9):1124-1125.

Dryden, H. L. and A. M. Kuethe. 1929. "Effect of turbulence in wind tunnel measurements." National Advisory Committee for Aeronautics, Report Number 342.

Dryden, H. L. 1938. "Turbulence investigations at the National Bureau of Standards." Proceedings of the Fifth International Congress of Applied Mechanics. p. 362.

Eagleson, P. S., C. J. Huval, and F. E. Perkins. 1961. "Turbulence in the early wake of a fixed flat plate." Massachusetts Institute of Technology Hydrodynamics Laboratory, Technical Report No. 46.

Fox, J. 1964. "Velocity Correlations in weak turbulent shear flow." The Physics of Fluids. 7(4):562-564.

Frenkiel, F. N. 1958. "Statistical study of turbulence-spectral functions and correlation coefficients." National Advisory Committee for Aeronautics, Technical Memorandum 1436.

Gibson, M. M. 1962. "Spectrum of turbulence at high Reynolds number." Nature. 195:1281-1283.

Gibson, M. M. 1963. "Spectra of turbulence in a round jet." Journal of Fluid Mechanics. Part II. 15:161-173.

Gibson, C. H. and W. H. Schwarz. 1963. "The universal equilibrium spectra of turbulent velocity and scalar fields." Journal of Fluid Mechanics. 16:365-384.

Goldstein, S. 1938. "Modern developments in fluid dynamics." Oxford University Press, London. Volume 1.

Grant, H. L., A. Moilliet, and R. W. Stewart. 1959. "A spectrum of turbulence at very high Reynolds number." Nature. 184:808-810.

Grant, H. L., R. W. Stewart, and A. Moilliet. 1962. "Turbulence spectra from a tidal channel." Journal of Fluid Mechanics. 12:241-263.

Halbronn. 1954. Discussion of "Turbulent boundary layer on steep slopes" by W. J. Bauer. Transactions of the American Society of Civil Engineers. 119:1238.

Heisenberg, W. 1948. "On the theory of statistical and isotropic turbulence." Proceedings of the Royal Society of London. Series A. 195:402-406.

Heisenberg, W. 1958. "Zur Statistischen theorie der turbulence." Z. Phys. Vol. 124. pp. 628-657. (1948). English translation available as National Advisory Committee for Aeronautics, Technical Memorandum 1431 (1958).

Hino, M. 1959. Discussion of paper, "Eddy diffusion in homogeneous turbulence." by Orlob, G. T. Proceedings of the American Society of Civil Engineers. 85:HY9.

Hinze, J. O. 1959. "Turbulence" McGraw-Hill Book Company, Inc., New York. 586 p.

Hueter, T. F. and R. H. Bolt. 1955. "Sonics." John Wiley and Sons, Inc., New York. 456 p.

Ippen, A. T., R. S. Tonkin, and F. Raichlen. 1955. "Turbulence measurements in free surface flow with an impact tube-pressure tranducer combination." Massachusetts Institute of Technology Hydrodynamics Laboratory, Technical Report Number 20.

Ippen, A. T. and F. Raichlen. 1957. "Turbulence in civil engineering: Measurement in free surface streams." Proceedings of the American Society of Civil Engineers. 83:HY5 pp. 1392-1-1392-27.

Jordon, H. B. 1963. "A study of the scale of turbulence in a circular channel." Unpublished Ph. D. Dissertation in Chemical Engineering. Louisiana State University, Baton Rouge, Louisiana.

Kampè, de Feriet, J. 1948. "Le tenseur spectral de la turbulence homogene nonisotrope dans un fluide incompressible." Proceedings of the Seventh International Congress of Applied Mechanics. p. 6-26.

Karman, Von. 1931. "Mechanishe Ähnlichkeit und turbulenz." English translation available as National Advisory Committee for Aeronautics Technical Memorandum 611.

Karman, Von. 1937. "The fundamentals of the statistical theory of turbulence." Journal of the Aeronautical Sciences. 4(4):131-138.

Karman, Von and L. Howarth. 1938. "On the statistical theory of isotropic turbulence." Proceedings of the Royal Society of London. Series A. 164:192-215.

Karman, Von. 1948. "Progress in the statistical theory of turbulence." Proceedings of the National Acadamy of Sciences, Washington. 34:530.

Lumley, J. L. 1964. "Spectral budget in wall turbulence." The Physics of Fluids. 7(2):190-196.

Lumley, J. L. and H. A. Panofsky. 1964. "The structure of atmospheric turbulence." Interscience Publishers, New York. 239 p.

Neubert, H. K. P. 1963. "Instrument tranducers: An introduction to their performance and design." Oxford University Press, London. 390 p.

Obukhoff, A. M. "On the distribution of energy in the spectrum of turbulent flow." C. R. Acad. Sci. U. R. S. S. 32:19. (Translation issued by Minister of Supply, England as P. 21452T).

Ogura, Y. 1962a. "Energy transfer in a normally distributed and isotropic turbulent velocity field in two dimensions." The Physics of Fluids. 5(4):395-401.

Ogura, Y. 1962b. "Energy transfer in an isotropic turbulent flow." Journal of Geophysical Research 67(8):3143-3149.

Onsager, L. 1945. "The distribution of energy in turbulence." The Physical Review. 68:286.

Pai, S. E. 1957. "Viscous flow theory -- Turbulent flow." D. Van Nostrand Company, Inc., Princeton, New Jersey. Volume II.

Perkins, F. E. and P. S. Eagleson. 1959. "The development of a total head tube for high frequency pressure fluctuations in water." Massachusetts Institute of Technology Hydrodynamics Laboratory, Technical note number 5.

Pond, S., R. W. Stewart and R. W. Burling. 1963. "Turbulence spectra in the wind over waves." Journal of the Atmospheric Sciences. 20:319-324.

Prandtl, L. 1926. "Uber die ausgebildete turbulenz;" Proceedings of the Second International Congress of Applied Mechanics, Zurich.

Proudman, I. and W. H. Reid. 1954. "On the decay of a normally distributed and homogeneous turbulent velocity field." Philosophical Transactions of the Royal Society of London, Series A. 247:163-189.

Reis, F. B. 1952. "Studies of correlation and spectra in homogeneous turbulence." Unpublished Ph. D. Dissertation. Department of Mathematics. Massachusetts Institute of Technology, Cambridge, Massachusetts.

Reynolds, Osborne, 1894. "On the dynamical theory of incompressible viscous fluids and the determination of the criterion." Proceedings of the Royal Society of London, Series A. 56:40-45.

Robertson, H. P. 1940. "The invariant theory of isotropic turbulence." Proceedings of the Cambridge Philosophical Society. 36:209.

Romano, J. E. 1954. "Spectrum of turbulence in axisymmetric flow." Unpublished Ph. D. Dissertation in Chemical Engineering, University of Illinois, Urbana, Illinois.

Roshko, A. 1954. "On the development of turbulent wakes from vortex streets." National Advisory Committee for Aeronautics, Technical Report Number 1191.

Rouse, H. (ed.) 1959. "Advanced mechanics of fluids." John Wiley and Sons, New York. 444 p.

Schubauer, G. B. 1954. "Turbulent processes as observed in boundary-layer and pipe flow." Journal of Applied Physics. 25(2):188-196.

Simmons, L. F. G. and C. Salter. 1938. "An experimental determination of the spectrum of turbulence." Proceedings of the Royal Society of London, Series A. 165:73.

Tatsumi, T. 1957. "The theory of decay process of incompressible, isotropic turbulence." Proceedings of the Royal Society of London, Series A. 239:16-45.

Taylor, G. I. 1915. "Eddy motion in the atmosphere." Philosophical Transactions of the Royal Society of London, Series A. 215:1-26.

Taylor, G. I. 1921. "Diffusion by continuous movements." Proceedings of the London Mathematical Society, Series 2., 20:196-211.

Taylor, G. I. 1932. "The transport of vorticity and heat through fluids in turbulent motion." Proceedings of the Royal Society of London, Series A. 135. p. 685.

Taylor, G. I. 1935. "Statistical theory of turbulence Parts I-IV." Proceedings of the Royal Society of London, Series A. 151: 421-478.

Taylor, G. I. 1938. "The spectrum of turbulence." Proceedings of the Royal Society of London, Series A. 164:476-490.

Tachen, C. M. 1953. "On the spectrun of energy in turbulent shear flow." Journal of Research, National Bureau of Standards, 50:51-62.

Townsend, A. A. 1947. "Measurements in the turbulent wake of a cylinder." Proceedings of the Royal Society of London, Series A. 190:551-561.

Townsend, A. A. 1947. "Measurement of double and tripple correlation derivatives in isotropic turbulence." Proceedings of the Cambridge Philosophical Society. 43:560-570.

Townsend, A. A. 1956. "The structure of turbulent shear flow." Cambridge University Press, Cambridge, Great Britain. 315 p.

LIST OF SYMBOLS AND DEFINITIONS

Symbol	Definition	Dimension
A	Cross sectional area	(L^2)
B_1, B_2	Constants in the equation (91)	
C	Tranducer probe sensitivity in millivolts per pound per square inch of pressure change	$\left(\frac{m \cdot V \times L^2}{F}\right)$
C_1	Constant in the equation (88)	
C_2	Constant in the equation (89)	
E	Turbulent kinetic energy per unit volume of fluid	(M/LT^2)
E(k)	Heisenberg's turbulence energy spectral density function	(L^5/T^2)
$E_{i,j}(\vec{k})$	Spectrum tensor of turbulence kinetic energy	(L^5/T^2)
$E_1(n)$	Longitudinal one-dimensional turbulence energy spectrum function in frequency domain	(L^2/T)
$E_1(k_1)$	Longitudinal one-dimensional turbulence energy spectrum function in wave number domain	(L^3/T^2)
$e = -\frac{\partial}{\partial x_1}(P + \gamma\bar{h})$		(F/L^3)
$F_1(N)$	Normalized longitudinal one-dimensional turbulence energy-spectrum function in frequency domain	(T)
$F_1(k_1)$	Normalized longitudinal one-dimensional turbulence energy-spectrum function in wave number domain	(L)
$f(x_1)$, f(n)	Coefficient of spatial longitudinal-velocity correlation	(N)

g	Acceleration due to gravity	(L/T^2)
$g(r)$	Coefficient of spatial lateral velocity correlation	(N)
H	Instantaneous value of total head	(L)
$\bar{H}$	Mean value of total head	(L)
H'	Deviation of instantaneous total head from its mean value	(L)
$\bar{h}$	Mean depth of flow	(L)
h'	Deviation of the instantaneous depth from the mean value	(L)
$h(r)$	Coefficient of spatial triple velocity correlation	(L)
i, j, k	Subscripts in index notation and refer to cartesian coordinates. They take on values of 1, 2 and 3	
κ	Von Karman's Universal constant in the equation (87)	
$\vec{k}$	Wave number vector	(1/L)
k_i	Component of wave number vector	(1/L)
k_1	$\frac{2\pi n}{\bar{U}_1}$ Longitudinal component of wave number vector	(1/L)
k_e	Wave number range of energy containing eddies	(1/L)
k_d	Wave number range of main dissipation	(1/L)
Δk_1	Effective band width established by the analyzer in wave number	(1/L)
k_H	Numerical constant of order unity in equation (64)	

k_s	Nikuradse's equivalent sand-grain roughness	(L)
$k(r)$	Coefficient of spatial triple velocity correlation	
L	Loitsianskii's invariant	(L^2/T^2)
L_{x_1}	Eulerian average integral or macroscale of turbulence in x_1 direction	(L)
L_{x_2}	Eulerian average integral or macroscale of turbulence in x_2 direction	(L)
L_{x_3}	Eulerian average integral or macroscale of turbulence in x_3 direction	(L)
M	Coefficient in the equation (74)	$\left(\frac{L^{4/3}}{T^2}\right)$
n	Frequency in cycles per second	(1/T)
Δn	Effective band width established by the analyzer in cycles per second	(1/T)
P	Coefficient defined by the equation (74)	(T^2)
P_i	Instantaneous pressure	(F/L^2)
$\bar{P}$	Temporal mean pressure	(F/L^2)
p	Deviation of the instantaneous pressure from its mean	(F/L^2)
$q(r)$	Coefficient of spatial triple velocity correlation	(N)
$R_{ij}(\vec{r})$	Double-velocity correlation tensor	(L^2/T^2)
$R_{E_1}(\tau)$	Coefficient of Eulerian time correlation of longitudinal fluctuation velocity	(N)
R_{x_2}	Coefficient of spatial lateral velocity correlation	(N)
$R_{L_{V_1}}(\tau)$	Coefficient of Lagrangian longitudinal velocity correlation	(N)

$R_{x_1 u_1}$	Coefficient of spatial correlation of longitudinal velocity u_1 separated by a distance x_1 .	
$R_{x_2 u_1}$	Coefficient of spatial correlation of longitudinal velocity u_1 separated by a distance x_2 .	
$R_{x_3 u_1}$	Coefficient of spatial correlation of longitudinal velocity u_1 separated by a distance x_3 .	
$R_{\lambda x_1} = u_1' \lambda_{x_1} / \nu$		
$R_{\lambda x_2} = u_1' \lambda_{x_2} / \nu$		
r	Ratio of root mean square value of u_1 to the product of the r.m.s value of its time derivative and a selective time constant in the equation (97)	
r	Separation between two points in the longitudinal direction	(L)
$R_{ll}(\vec{r})$, $R_{22}(\vec{r})$	Longitudinal and lateral components of second order velocity correlation tensor	(L^2/T^2)
S_o	Slope of the channel bed	(N)
T	Averaging time	(T)
$T_{ij}(r)$	Scalar function obtained by averaging the correlation tensor over all the directions in space	(L^2/T^2)
$T_{ij,k}(\vec{r})$	Third order two point velocity correlation tensor	(L^3/T^3)
Δt	Averaging time of u_i	(T)
$U_i(t)$	Instantaneous velocity at a point and at time t	(L/T)
$\overline{U}_i$	Temporal mean velocity at a point	(L/T)
$u_i(t)$	Deviation of the instantaneous velocity from its mean value	(L/T)
$\overline{U}_1$, $\overline{U}_2$ and $\overline{U}_3$	Components of $\overline{U}_i$ along x_1, x_2 and x_3 axes	(L/T)

u_1, u_2, u_3	Components of u_i along x_1, x_2 and x_3 axes	(L/T)
u'_i, u'_1	Root-mean-square of velocity fluctuation	(L/T)
$\overline{u^2}$	Mean square value of velocity fluctuation	(L^2/T^2)
u_*	Friction velocity	(L/T)
V'_T	Root-mean-square value of the total tranducer probe output in volts	(volts)
V'_R	Root-mean-square value of the real turbulence signal of the probe	(volts)
V'_N	Root-mean-square value of the noise	(volts)
V_T	Instantaneous value of the total tranducer probe output in volts	(volts)
V_R	Instantaneous value of the real turbulence signal of the probe	(volts)
V_N	Instantaneous value of the noise	(volts)
$W(k)$	Transfer function giving the amount of energy from wave numbers less than k flowing to those greater than k	(L^5/T^3)
$\vec{x}$	Position vector	(L)
x_1, x_2 and x_3	Cartesian coordinate axes	(L)

$$y^* = \frac{x_2 u_*}{\nu}$$

α	Absolute constant in the equations (61) and (75)
α'	Absolute constant in the equation (62)
β, β'	Constants in the equation (78)
γ, γ'	Constants in the equation (78)

γ	Unit weight of fluid	(M/L^2T^2)
λ	Eulerian microscale or dissipation length	(L)
λ_{x_1}	Eulerian microscale or dissipation length along x_1 axis	(L)
λ_{x_2}	Eulerian microscale or dissipation length along x_2 axis	(L)
ϵ_o	Rate of turbulent energy dissipation per unit volume of fluid	(ML/T^3)
ϵ'	Rate of turbulent energy dissipation per unit volume of flow	(ML/T^3)
ϵ	Rate of turbulent energy dissipation per unit mass	(L^2/T^3)
$\epsilon(k, t)$	$= 2\pi k^2 \left[2(E_{1,2})_{A \cdot V} - \left(K_1 \frac{\partial E_{i,i}}{\partial k_2} \right) \cdot AV \right]$	(L^3/T^2)
ρ	Density of fluid	(M/L^3)
τ	Time interval	(T)
τ	Preselected time constant in determining microscale with the correlator	(T)
τ	Turbulent shear stress at a point in the flow	(M/LT^2)
τ_o	Shear stress at the bed	(M/LT^2)
τ	Time delay	(T)
τ_c	Time corresponding to the point on time axis at which autocorrelation curve intersects τ-axis	(T)
μ	Dynamic viscosity of fluid	(M/LT)
$\Psi_{ij}(k)$	Scalar function obtained by averaging the spectrum tensor over all directions in wave number space	(L^5/T^2)

η	Kolmogoroff's length scale in the viscous subrange	(L)
ν	Kinematic viscosity	(L^2/T)
$\nu_t(k)$	Heisenberg's turbulence viscosity associated with wave number 'k'	(L^2/T)

APPENDIXES

Appendix A

Theory of operation of the tranducer probe

The instantaneous total head acting at the tip of the probe can be expressed as

$$H = \bar{H} + H' = (\bar{h} + h') + \left(\frac{\bar{P}}{W} + \frac{p}{W}\right) + \left(\frac{\bar{U}_1 + u_1}{2g}\right)^2 \qquad (1)$$

where $\bar{H}$, $\bar{P}$ and $\bar{U}_1$ are the mean values and H', p, and u_1 are the turbulent fluctuations about the temporal means. Since the tranducer used is insensitive to the mean quantities because of its low frequency response as shown by Perkins and Eagleson (1959) and Eagleson et al. (1961), $\bar{H}$ does not contribute to the probe output. Therefore, the effective total head to which the probe responds is given by

$$H' = h' + \frac{p}{W} + \frac{2\bar{U}_1 u_1}{2g} + \frac{u_1^2}{2g} \qquad (2)$$

In this study the fluctuations of depth h' are negligibly small. Experimental studies of Townsend (1947) and Roshko (1954) indicate that the ratio $u_1'/\bar{U}_1$ is substantially less than 0.1 except in the immediate vicinity of flow boundary. Consequently the term $u_1^2/2g$ may be neglected in comparison to $\frac{\bar{U}_1 u_1}{g}$. As indicated by Ippen (1957) the terms p/W and $u_1^2/2g$ are of the same order of magnitude and are

generally out of phase. Therefore, p/W can also be neglected. Hence the effective fluctuating head acting at the tip of the probe may be approximated by

$$H' = \frac{\bar{U}_1 u_1}{g} \tag{3}$$

The probe responds to the above fluctuating head, and the time history of total head would appear much the same as that for longitudinal fluctuating velocity component with the only difference being the scale factor $\bar{U}_1/g$. Great care should be exercised in interpreting the results if the analysis of the signal indicates a very high turbulence level (i.e., $u'_1 > 0.1\ \bar{U}_1$). Ippen et al. (1955) estimated an error of 11 percent in determination of u'_I when $u'_1/\bar{U}_1 = 0.1$ and an error of 22 percent when $u'_1/\bar{U}_1 = 0.2$.

If V'_R is the tranducer output in volts due to H' acting on the probe, and C is the calibration constant in volts per foot of head

$$V'_R = C\ \frac{\bar{U}_1 u'_1}{g} \tag{4}$$

Hence

$$u'_1 = \frac{g\ V'_R}{C\ \bar{U}_1} \tag{5}$$

This equation was used for calculating u'_I from the measurements of the r. m. s. voltmeter of the random signal indicator and correlator to which the signal from the amplifier output terminal was fed.

Care should be taken in interpreting the turbulence data obtained with the tranducer probe because not only the probe responds indiscriminately to pressure fluctuations of acoustical origin, but also to free or forced vibrations. Besides, the natural frequency of the probe itself might interfere with the energy spectrum measurements in indicating an abrupt peak at the natural frequency irrespective of the turbulence characteristics being measured. As the spectrum measurements were made in this study at frequencies much below the resonant frequency (80 K. C.), peaks were not observed in the spectrum measurements.

Appendix B

Calibration of the tranducer probe

Frequency response. The details pertaining to the computation of the low frequency relative response of the tranducer probe can be found in the publications of Perkins and Eagleson (1959) and Hueter and Bolt (1955). The experimental set up used for the determination of low frequency response of the probe is shown in Figure 42. At a constant amplitude a series of tests was run at frequencies from 2 to 16.7 c. p. s. It was found that by 14 c. p. s. the sensitivity of the probe had reached a constant limiting value. This value was assigned to represent a relative response of 1.0 and the relative response at lower frequencies was computed from the experimental data. The plot of relative response against frequency is shown in Figure 43. The estimated low frequency response curve is superimposed on the measured points. The agreement between estimated and measured low frequency response of the probe is seen to be good. This result indicates that the probe may be used to measure fluctuations of as low frequency as 4 c. p. s. with sufficient accuracy.

The high frequency response of the probe in water could not be determined due to the limitation imposed by the mechanical system to generate high frequency pressure fluctuations in the pressure chamber. Neubert (1963) pointed out that the useful frequency range of a piezoelectric tranducer is one-fifth of the frequency interval between zero and

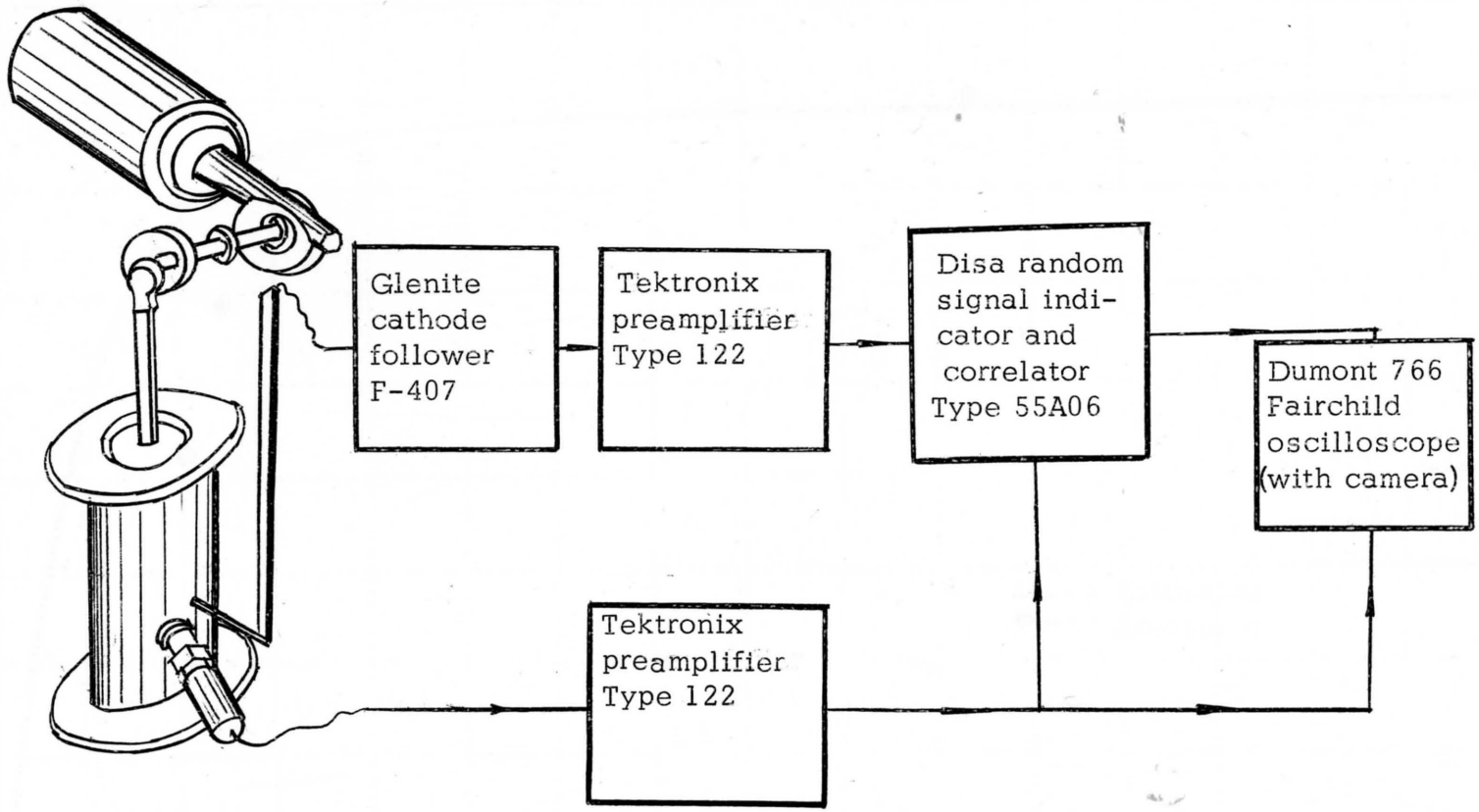

Figure 42. Experimental set-up for calibration of the tranducer probe at low frequency range.

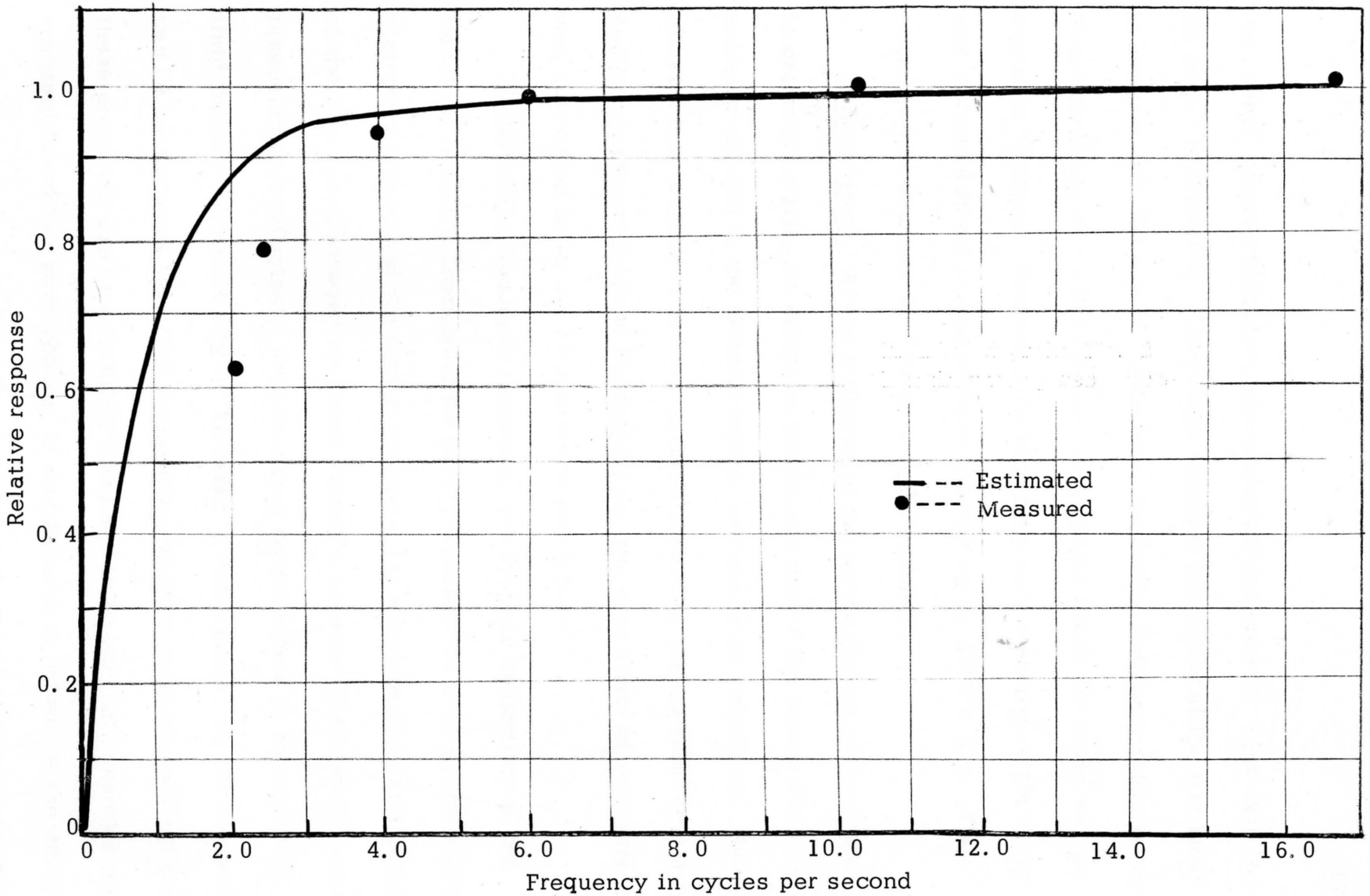

Figure 43. Low frequency response of tranducer probe number 2.

the lowest resonant frequency if a magnification error of 4 per cent in its output is tolerated. The lowest resonant frequency of the tranducer in water is 80,000 c. p. s. Therefore, its useful frequency range is much above the frequencies of turbulent fluctuations which the probe was required to measure. However, the high frequency response of the probe was measured in air in an anechoic chamber up to 1000 c. p. s. The response was found to be flat up to that frequency.

Sensitivity. As the stiffness of the tip diaphragm of the probe is extremely small, its effect on the attenuation of the stress which is actually induced in the ceramic crystal can easily be neglected. Using the physical properties of the crystal furnished by the manufacturer and neglecting the stiffness of the diaphragm, the sensitivity of the probe was calculated to be 19.15 millivolts per p. s. i.

Unlike the frequency response, the dynamic sensitivity of the tranducer is only a function of its physical properties such as the relative dielectric constant of the crystal material, the absolute dielectric constant of the free space between its faces, Young's modulus of elasticity and the piezoelectric coefficient. Thus it makes no difference in what kind of fluid medium the sensitivity of the probe is determined. As the pressures can be generated at very high frequencies by ordinary loud speakers and these pressures can be accurately measured in an anechoic chamber with standard laboratory microphones, it was decided to determine the sensitivity of the probe in the anechoic chamber of the electrical engineering department.

The block diagram of the experimental arrangement used in the anechoic chamber is shown in Figure 44. The standard precision microphone and the probe were mounted before the speaker system at the same distance and elevation side by side. At a particular frequency a sinusoidally varying sound pressure wave was generated using audiogenerator and speaker system. The signals from both the microphone and probe were fed to the inputs of the two channel oscilloscope for visual inspection of the response of the probe and microphone. The output of the microphone was measured with vacuum tube voltmeter and the output of the tranducer probe was measured with r. m. s. voltmeter of the random signal indicator and correlator which was used in turbulence measurements.

At a constant frequency the amplitude was varied over a range corresponding to preselected readings of microphone output expressed in db of pressure level and the corresponding outputs of the probe were measured simultaneously. The same procedure was repeated by isolating the probe from contact with the pressure fluctuations in order to measure the noise due to hum and possible structural vibration. The two steps outlined above were repeated at different frequencies to make sure the high frequency response of the probe is flat.

From the readings of the microphone output, absolute values of the pressure changes acted on the probe were calculated in p. s. i. Corresponding actual outputs of the probe, after allowance for noise, were calculated in millivolts at a preamplifier gain of 100. Plots of

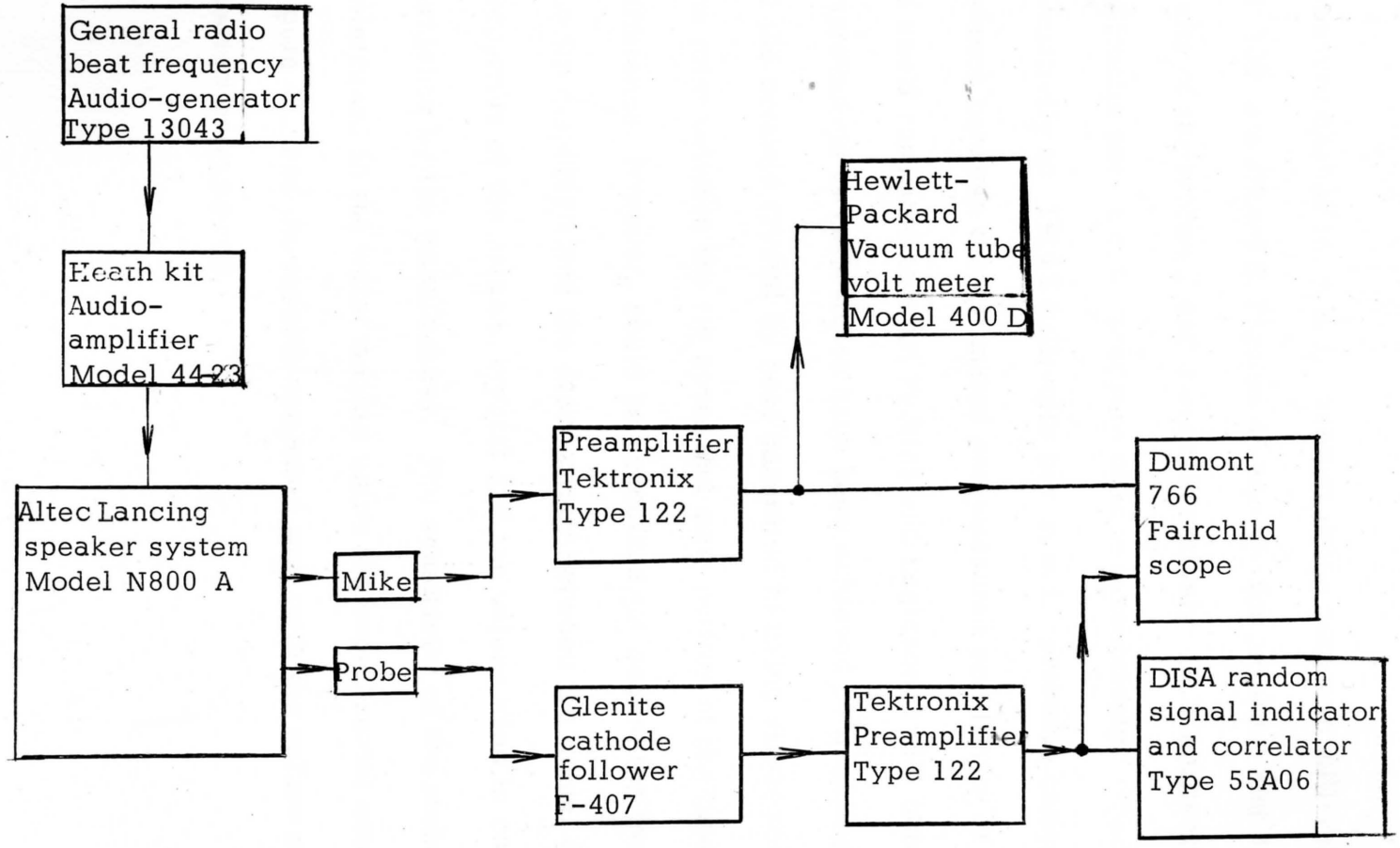

Figure 44. Block diagram of the experimental set-up for calibration of the tranducer probe in anechoic chamber.

pressure change in p. s. i. against probe output in millivolts at a gain of 100 are shown in Figures 45 and 46 for probes 2 and 3. The sensitivity of the probes 2 and 3 are respectively 16. 5 millivolts and 14. 0 millivolts per p. s. i. pressure change respectively. Their estimated sensitivity is 19. 15 millivolts per p. s. i. pressure change. The difference between the estimated and measured sensitivity of the probes is small compared to what Perkins and Eagleson (1959) obtained and this improvement is believed to have been achieved by avoiding depolarization of the ceramic crystal by heat generated in using silver soldering to seal the joint between the tip cover and main portion of the tube. The small difference, however, could be accounted for neglecting the stiffness of the tip diaphragm and the discrepancy between the actual dimensions and properties of the ceramic crystal and the values used in computation as furnished by the manufacturer. The sensitivity of the probes was also determined in the water medium using the experimental setup shown in Figure 42, and the results compared well with the values obtained in air medium as expected.

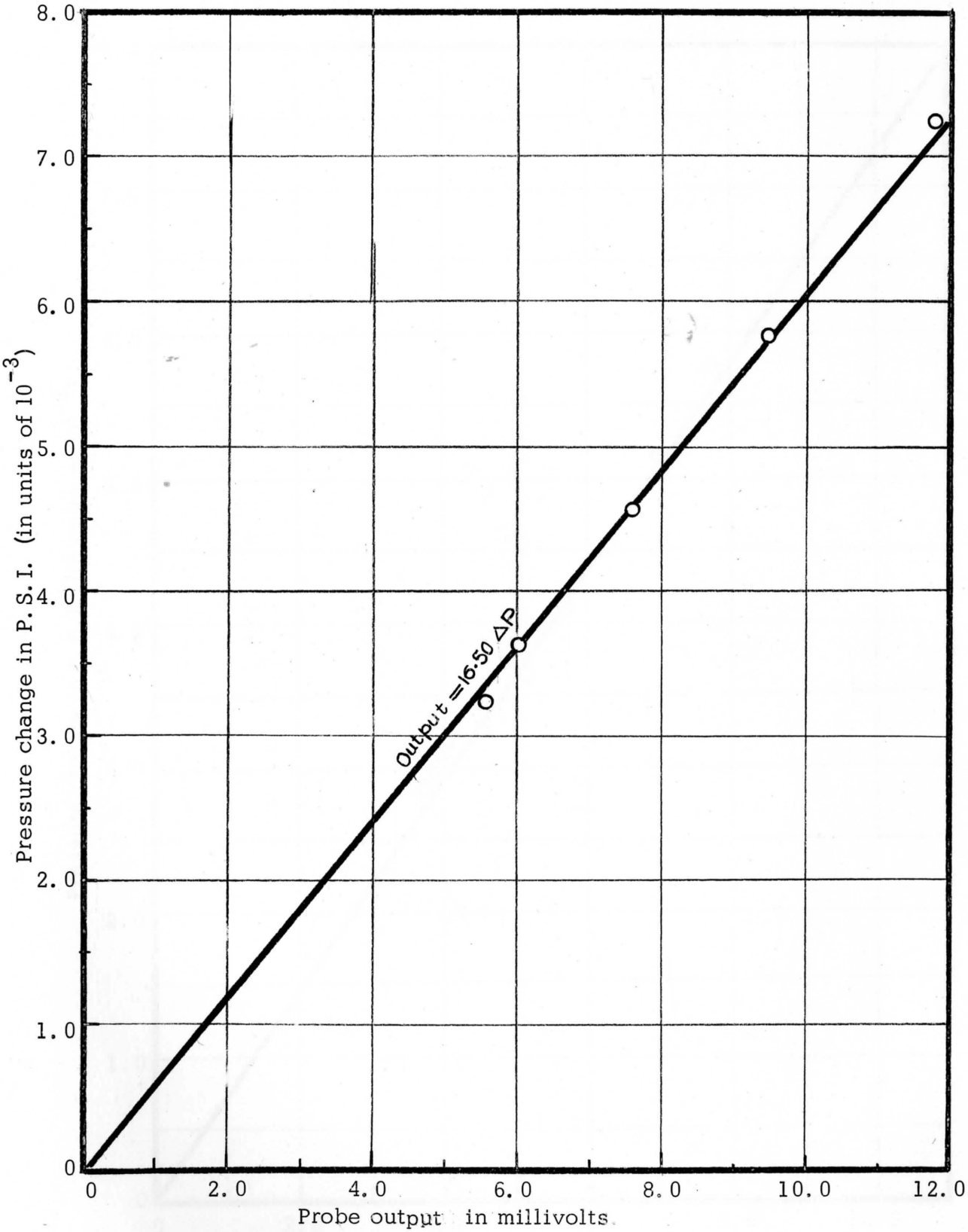

Figure 45. Pressure sensitivity of the tranducer probe No. 2.

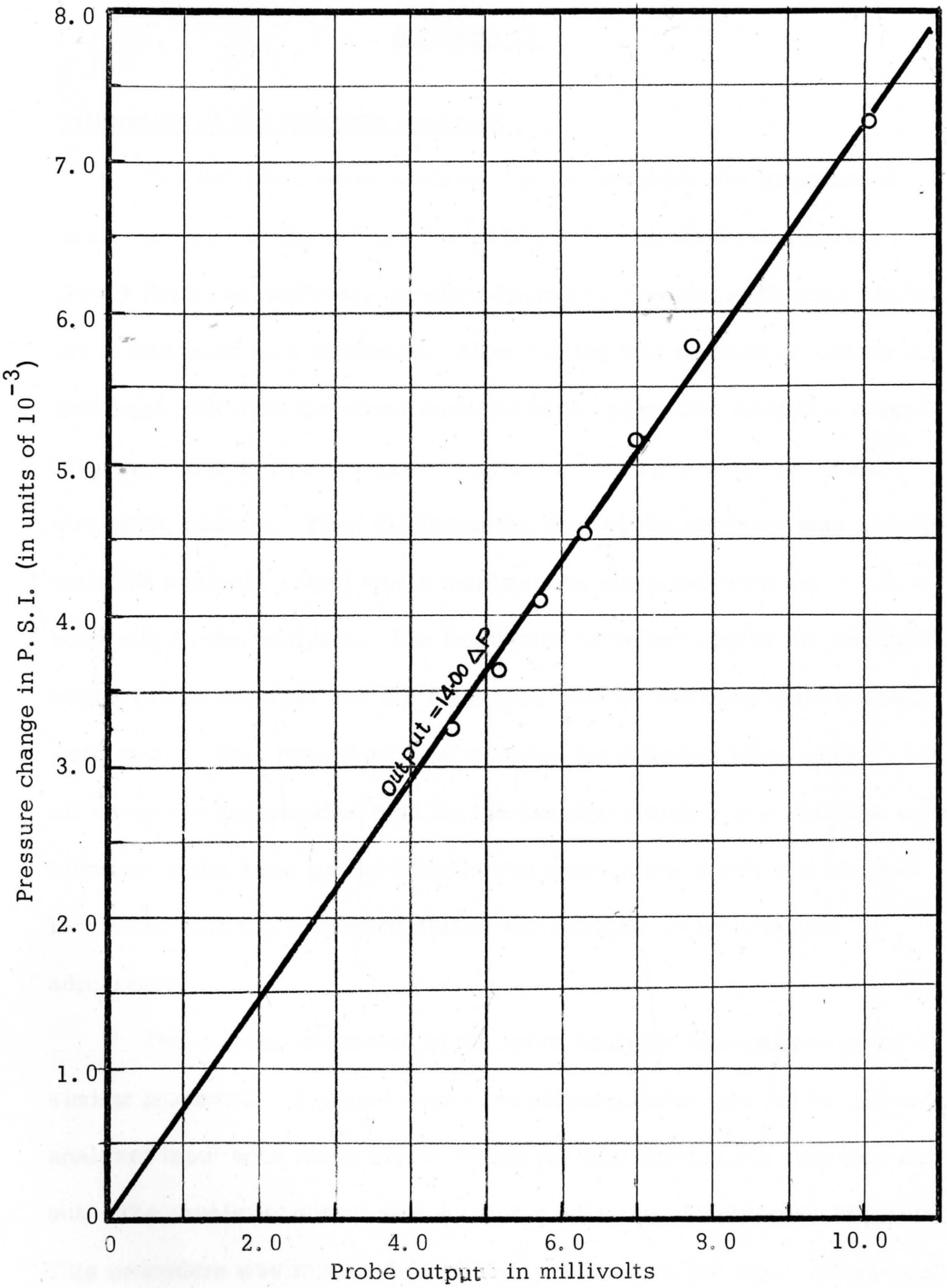

Figure 46. Pressure sensitivity of the tranducer probe No. 3.

Appendix C

Calibration of the spectrum analyzer

The harmonic wave analyzer used to measure the spectrum of turbulence was a Quan-Tech Model 303. To calibrate the frequency dial of the wave analyzer, Hewlett-Packard's Electronic Counter Model 522B was used as a reference. After nulling was done by adjusting the zero beat following the steps outlined in the operation manual a signal from the audiooscillator was fed to the inputs of the analyzer and the electronic counter. Then the frequency dial of the analyzer was adjusted until the analyzer output was a maximum as measured with the r. m. s. voltmeter of the analyzer. The frequency corresponding to the maximum output of the analyzer and the frequency read by the electronic counter were noted. This procedure was repeated for different frequencies. In all cases the frequencies read on the frequency dial of the analyzer were identically the same as the frequencies read on the electronic counter indicating that the frequency dial of the analyzer is in complete adjustment.

The r. m. s. voltmeter in the wave analyzer was calibrated by a similar procedure. A signal from the audiooscillator was fed to the wave analyzer input with the analyzer frequency dial set to give maximum output. The analyzer output was measured with the vacuum-tube voltmeter. This procedure was repeated for different values of the input voltage and

frequency. It was found that the readings of the r. m. s. voltmeter and the vacuum-tube voltmeter were identically the same indicating the r. m. s. voltmeter of the analyzer reads accurately enough.

Spectrum measurements were made with the wave analyzer with a fixed nominal band width of 30 c. p. s. The effective band width is defined as the rectangular band width having the same area as the area under the experimentally determined band shape. To determine the band shape, a signal from the audiooscillator was fed to the input of the analyzer with the analyzer frequency dial set to a preselected value; say 500 c. p. s. The gain control of the analyzer was adjusted until the r. m. s. voltmeter read a maximum which was then taken as a reference value. Then the frequency dial of the analyzer was adjusted such that the r. m. s. voltmeter read 0. 8, 0. 6 . . . 0. 01 times the reference value. The corresponding frequencies were read on the electronic counter. A plot of the output of the analyzer versus the frequency was drawn and shown in Figure 47. A rectangle having the same area as the area under the curve is fitted and the width of the rectangle, or in other words, the effective band width was found to be 59. 00 c. p. s.

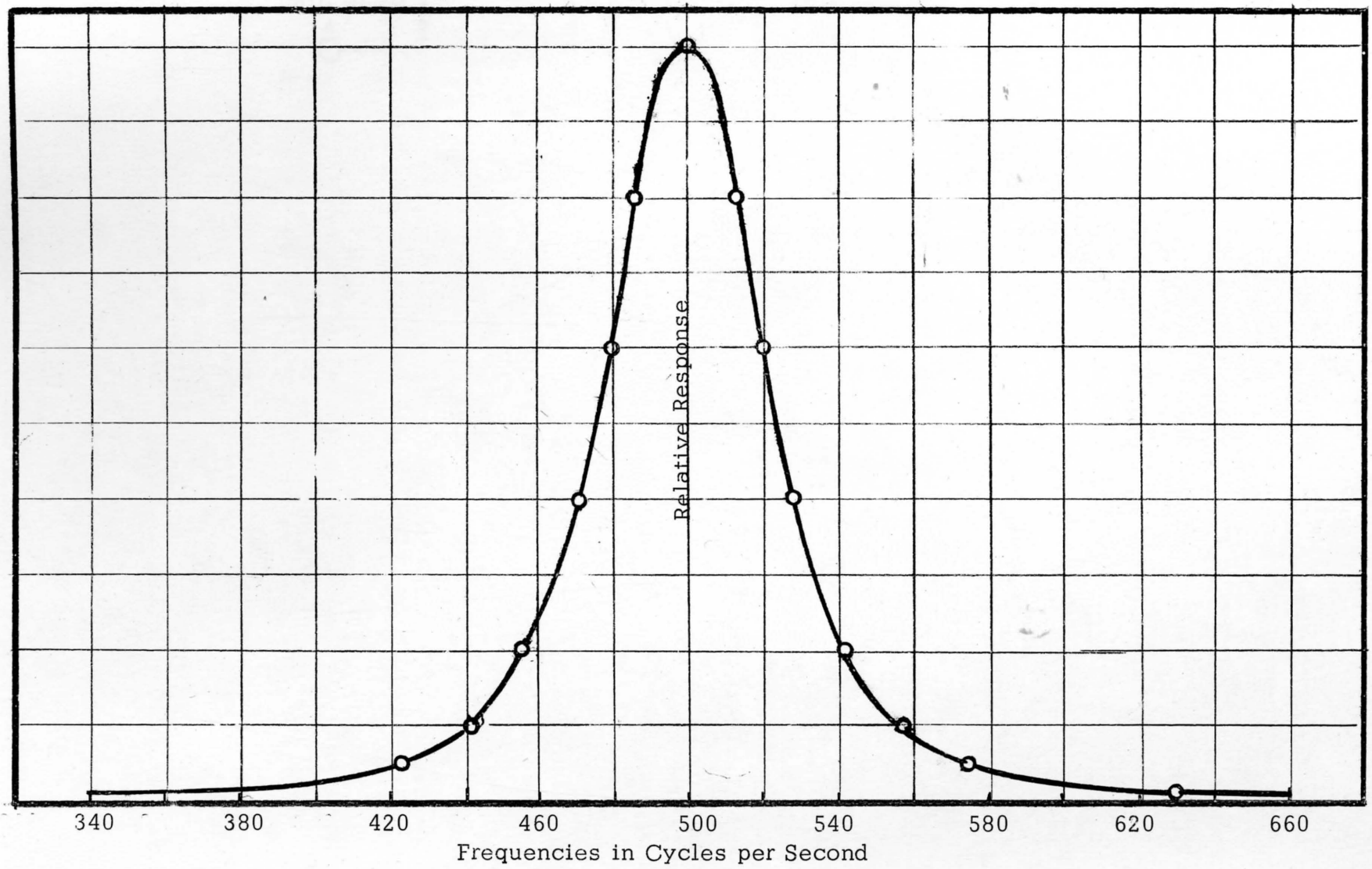

Figure 47. Response curve of spectrum analyzer.

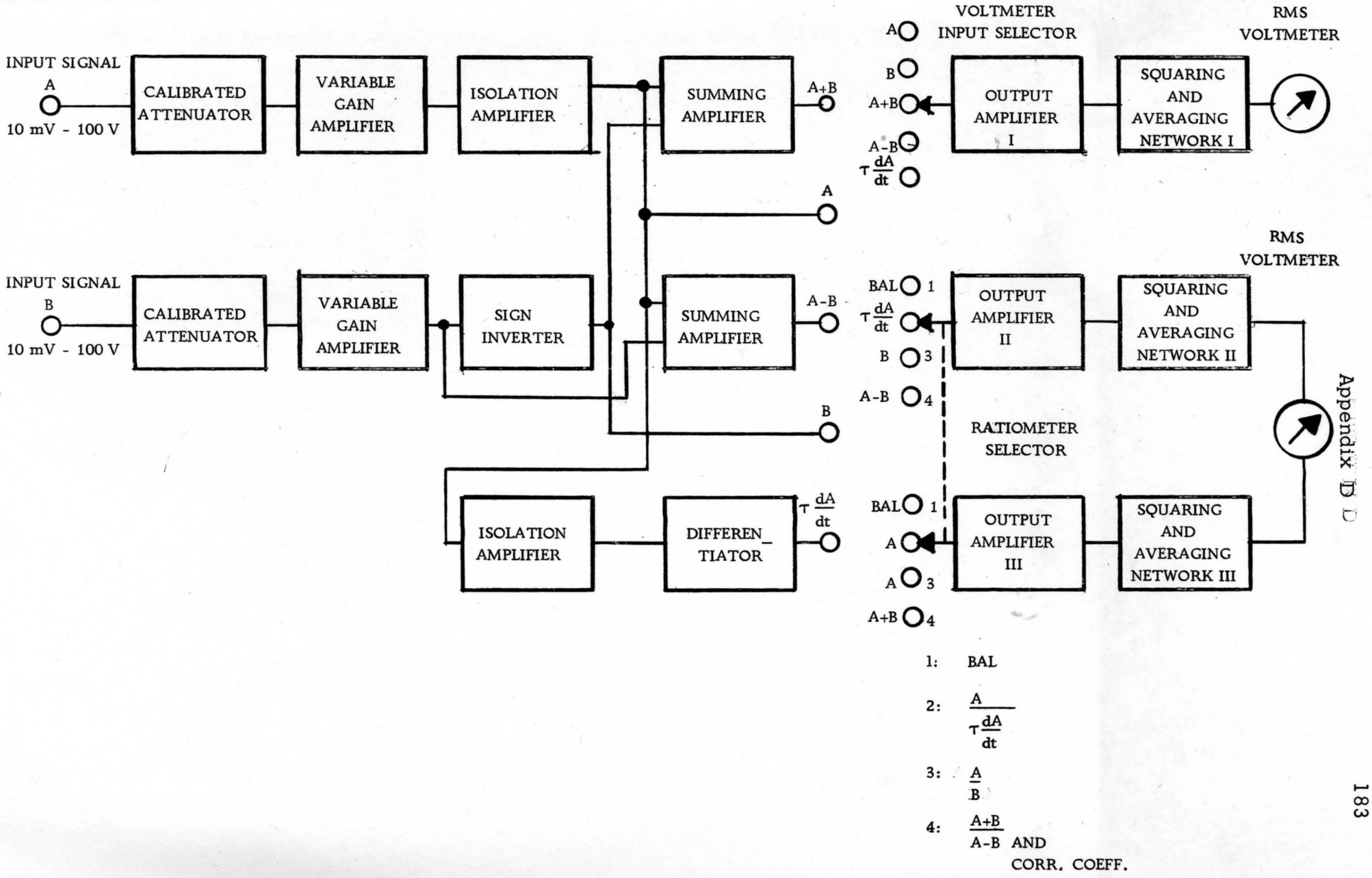

Figure 48. Block diagram of the internal circuit of the random signal indicator and correlator